Multidisciplinary Design Optimization and Industry Review of a 2010 Strut-Braced Wing Transonic Transport

By

J. F. Gundlach IV, A. Naghshineh-Pour, F. Gern, P.-A. Tetrault,

A. Ko, J. A. Schetz, W. H. Mason, R. K. Kapania, B. Grossman,

R. T. Haftka (University of Florida)

MAD 99-06-03

June 1999

Multidisciplinary Analysis and Design Center for Advanced Vehicles

Department of Aerospace and Ocean Engineering

Virginia Polytechnic Institute and State University

Blacksburg, VA 24061-0203

Multidisciplinary Design Optimization and Industry Review of a 2010 Strut-Braced Wing Transonic Transport

John F. Gundlach IV

(ABSTRACT)

Recent transonic airliner designs have generally converged upon a common cantilever low-wing configuration. It is unlikely that further large strides in performance are possible without a significant departure from the present design paradigm. One such alternative configuration is the strut-braced wing, which uses a strut for wing bending load alleviation, allowing increased aspect ratio and reduced wing thickness to increase the lift to drag ratio. The thinner wing has less transonic wave drag, permitting the wing to unsweep for increased areas of natural laminar flow and further structural weight savings. High aerodynamic efficiency translates into reduced fuel consumption and smaller, quieter, less expensive engines with lower noise pollution. A Multidisciplinary Design Optimization (MDO) approach is essential to understand the full potential of this synergistic configuration due to the strong interdependency of structures, aerodynamics and propulsion. NASA defined a need for a 325-passenger transport capable of flying 7500 nautical miles at Mach 0.85 for a 2010 date of entry into service. Lockheed Martin Aeronautical systems (LMAS), our industry partner, placed great emphasis on realistic constraints, projected technology levels, manufacturing and certification issues. Numerous design challenges specific to the strut-braced wing became apparent through the interactions with LMAS, and modifications had to be made to the Virginia Tech code to reflect these concerns, thus contributing realism to the MDO results. The SBW configuration is 9.2-17.4% lighter, burns 16.2-19.3% less fuel, requires 21.5-31.6% smaller engines and costs 3.8-7.2% less than equivalent cantilever wing aircraft.

Acknowledgements

This research would not be possible without support, advice, data and other contributions from a number of people and organizations. NASA deserves much credit for having the vision to pursue bold yet promising technologies with the hope of revolutionizing air transportation. Lockheed Martin Aeronautical Systems provided valuable contributions in data, design methods and advice borne from hard-won experience. The SBW team faculty advisors and members of the MAD center have guided the research and offered direction throughout the duration. I would especially like to thank faculty members Dr. Joseph Schetz, Dr. William Mason, Dr. Bernard Grossman, Dr. Rafael Haftka, Dr. Rakesh Kapania, and Dr. Frank Gern for providing guidance in my efforts. My predecessor, Joel Grasmeyer, provided an excellent code, which was thoughtfully documented and free of clutter. I learned a great deal about programming from studying his work. Other members of the SBW team, Amir Naghshineh-Pour, Phillipe-Andre Tetrault, Andy Ko, Mike Libeau and Erwin Sulaeman, have made large contributions to the research and have been very cooperative and generous with their time. I appreciate the friendly work environment and productive atmosphere made possible by the SBW team student members and advisors. Last, but definitely not least, I wish to thank my wife and best friend, Katie Gundlach, for unselfishly giving her loving support.

Contents

List of Figures

List of Tables

Nomenclature

$Angle_{Scrape}$	Angle of Attack for Tail Scrape, deg
AR_{HT}	Horizontal Tail Aspect Ratio
AR_{VT}	Vertical Tail Aspect Ratio
AR_{W}	Wing Aspect Ratio
AR_{Weff}	Effective Wing Aspect Ratio in Ground Effect
BFL	Balanced Field Length, ft
b_{HT}	Horizontal Tail Span, ft
BPR	Bypass Ratio
b_{rudder}	Rudder Span, ft
b_{VT}	Vertical Tail Span, ft
b_{w}	Wing Span, ft
$c\ bar$	Average Wing Chord, ft
C_{Df}	Flat Plate Friction Drag Coefficient
$C_{DGround}$	Ground Roll Drag Coefficient
C_{Dm}	Minimum Drag Coefficient
$C_{DmFactor}$	Minimum Drag Coefficient Factor
$C_{DoApproach}$	Landing Approach Zero-Lift Drag Coefficient
C_{Dp}	Profile Drag Coefficient
C_{dwave}	Wave Drag Coefficient of Strip
C_{HTroot}	Horizontal Tail Root Chord, ft
C_{HTtip}	Horizontal Tail Tip Chord, ft
C_{l}	2-D Section Lift Coefficient
C_{L}	Total Lift Coefficient
C_{Lbreak}	Lift Dependent Profile Drag Constant
$Clearance$	Average Ground Clearance, ft
$C_{LGround}$	Lift Coefficient in Ground Effect
C_{Lm}	Lift Coefficient of Minimum Drag Coefficient
$C_{LScrape}$	Scrape Angle Lift Coefficient
$C_{L\alpha}$	Lift Curve Slope
$C_{L\alpha Ground}$	Lift Curve Slope in Ground Effect
C_{L2}	Second Segment Climb Lift Coefficient
$C_{n\ req}$	Required Yawing Moment Coefficient
C_{rudder}	Rudder Average Chord, ft
C_{VTroot}	Vertical Tail Root Chord, ft
C_{VTtip}	Vertical Tail Tip Chord, ft
C_{Wbreak}	Wing Break Chord, ft
C_{Wroot}	Wing Root Chord, ft
C_{Wtip}	Wing Tip Chord, ft
D	Drag, lbs
D_{E}	Drag of Inoperable Engine, lbs
D_{Engine}	Engine Diameter, ft
$D_{Fuselage}$	Fuselage Diameter, ft
dx_htail	Distance from CG to AC of Horizontal Tail, ft
dx_vtail	Distance from CG to AC of Vertical Tail, ft
f	Wingtip Engine Induced Drag Factor
$f_{Approach}$	Landing Approach Drag Factor
f_{Break}	Lift Dependent Profile Drag Constant

FF	Form Factor
$F_{Initial}$	Initial Braking Force, lbs
F_m	Mean Braking Force, lbs
F_{static}	Static Braking Force, lbs
f_6	Wingtip Engine Induced Drag Factor, $AR_W = 6$
f_{12}	Wingtip Engine Induced Drag Factor, $AR_W = 12$
g	Acceleration of Gravity (32.2 ft/sec^2)
h_f	Landing Obstacle Height, ft
h_{Pylon}	Pylon Height, ft
h_{TO}	Height of Object to Clear at Take-Off, ft
k	Lift Dependent Drag Factor
K_{Brake}	Braking Factor
k_{Break}	Lift Dependent Drag Factor
L/D	Lift to Drag Ratio
$L_{WLE,HTLE}$	Streamwise Distance from Wing LE to Horizontal Tail LE, ft
$L_{WLE,VTLE}$	Streamwise Distance from Wing LE to Vertical Tail LE, ft
m	Chordwise Distance from LE of Wing Root to LE of Segment MAC, ft
M	Mach Number
MAC	Mean Aerodynamic Chord, ft
MAC_{HT}	Horizontal Tail Mean Aerodynamic Chord, ft
MAC_{VT}	Vertical Tail Mean Aerodynamic Chord, ft
MAC_W	Wing Mean Aerodynamic Chord, ft
$Margin_{Scrape}$	Tail Scrape Angle Safety Margin, deg
M_{crit}	Critical Mach Number
M_{dd}	Drag Divergent Mach Number
$M_{Landing}$	Landing Mach Number
n	Number of g's
$Offset$	Wing/Strut Aerodynamic Offset, ft
q	Dynamic Pressure, lb/ft^2
R/C	Rate of Climb, ft/sec
$R/C_{CruiseInitial}$	Rate of Climb at Initial Cruise Altitude, ft/sec
$Reserve$	Reserve Range, nmi
s	Chordwise Distance from LE of Segment Root to LE of Segment Tip, ft
S	Wetted Area of Component
S_A	Landing Air Distance, ft
S_B	Landing Braking Distance, ft
S_{FR}	Landing Free Roll Distance, ft
S_{HT}	Horizontal Tail Area, ft^2
S_{ref}	Reference Area (Usually S_w), ft^2
S_{strip}	Planform Area of Strip, ft^2
S_{VT}	Vertical Tail Area, ft^2
S_w	Wing Planform Area, ft^2
S_{wet}	Aircraft Wetted Area, ft^2
sfc	Specific Fuel Consumption at Altitude
sfc_{Static}	Static Fuel Consumption
t/c	Thickness to Chord Ratio
T	Thrust at Given Altitude and Mach number,lbs
$T\ bar$	Mean Thrust of Take-Off Run, lbs
$t/c_{Average}$	Average Thickness to Chord Ratio
t/c_{Break}	Breakpoint Thickness to Chord Ratio

t/c_{Root}	Root Chord Thickness to Chord Ratio
t/c_{Tip}	Tip Chord Thickness to Chord Ratio
T_E	Thrust of Good Engine at Engine-Out Condition, lbs
$Temp$	Temperature at Altitude
$Temp_{SL}$	Temperature at Sea Level
t_{FR}	Time of Landing Free Roll, sec
$T_{SL,static}$	Sea Level Static Thrust, lbs
TVC_{HT}	Horizontal Tail Volume Coefficient
TVC_{vT}	Vertical Tail Volume Coefficient
T/W	Aircraft Thrust to Weight Ratio
V_{TD}	Touch-Down Velocity, ft/sec or kts
W	Aircraft Weight, lbs
$W_{BodyMax}$	Maximum Body and Contents Weight, lbs
$W_{BodyMax,in}$	Input Maximum Body and Contents Weight, lbs
$W_{EconCruise}$	Economic Mission Average Cruise Weight, lbs
$W_{FuelEcon}$	Economic Mission Fuel Weight, lbs
W_{Fuse}	Fuselage Weight, lbs
W_i	Initial Cruise Weight, lbs
$W_{Landing}$	Landing Weight, lbs
W_o	Final Cruise Weight, lbs
W_{TO}	Take-Off Weight, lbs
W_{Wing}	Wing Weight, lbs
$W_{Wing,in}$	Input Wing Weight, lbs
W_{ZF}	Zero Fuel Weight, lbs
$W_{ZF,in}$	Input Zero Fuel Weight, lbs
$X_{Nose,WLE}$	Streamwise Distance from Nose the Wing Root LE, ft
Y_{Eng}	Spanwise Distance to Engine, ft
$\Delta C_{D,CL}$	Additional Profile Drag Due to Lift
ΔS_{TO}	Take-Off Inertia Distance, ft
$\Delta W_{ZF,Econ}$	Change in Zero-Fuel Weight for Econ. Mission, lbs
$\Delta\gamma_2$	Second Segment Climb Gradient Above Minimum
κ_a	Airfoil Technology Factor
γ	Landing Glide Slope
γ_2	Second Segment Climb Gradient
η_{break}	Percentage Semispan of Wing Breakpoint
μ_{Brake}	Braking Coefficient
λ_{HT}	Horizontal Tail Taper Ratio
λ_{VT}	Vertical Tail Taper Ratio
Λ	Sweep Angle
$\Lambda_{HT,LE}$	Horizontal Tail Leading Edge Sweep Angle
$\Lambda_{VT,LE}$	Vertical Tail Leading Edge Sweep Angle
$\Lambda_{W,c/2}$	Wing Half-Chord Sweep Angle
$\Lambda_{W,LE}$	Wing Leading Edge Sweep Angle
ρ	Air Density at Altitude
ρ_{SL}	Air Density at Sea Level
σ'	Ground Effect Drag Factor
$\%b_{\text{rudder}}$	Percentage Vertical Tail Span of Rudder Span
$\%C_{\text{rudder}}$	Percentage Average Vertical Tail Chord of Rudder Chord

Chapter 1

Introduction

Over the last half-century, transonic transport aircraft have converged upon what appears to be two common solutions. Very few aircraft divert from a low cantilever wing with either underwing or fuselage-mounted engines. Within the cantilever wing with underwing engines arrangement (Figure 1.1), a highly trained eye is required to discern an Airbus from a Boeing airliner, or the various models from within a single airframe manufacturer. While subtle differences such as high lift device and control system alternatives distinguish the various aircraft, it is unlikely that large strides in performance will be possible without a significant change of vehicle configuration.

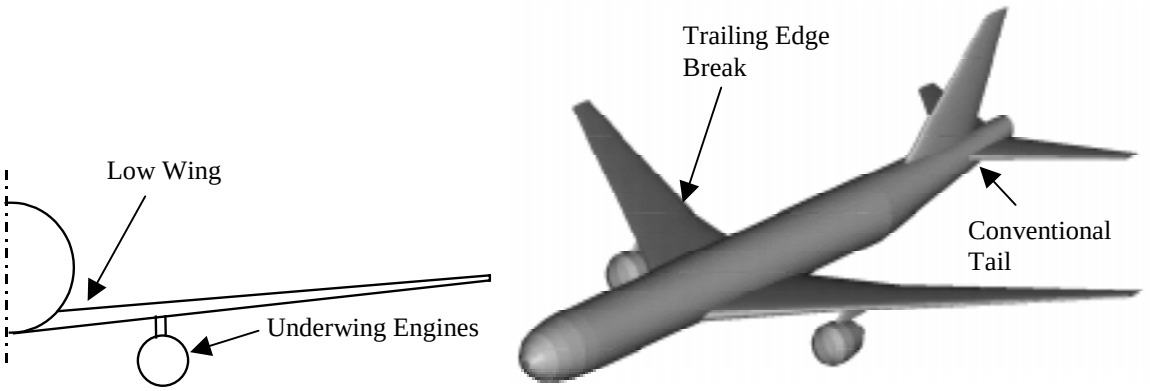

Figure 1.1. Conventional Cantilever Configuration.

Numerous alternative configuration concepts have been introduced over the years to challenge the cantilever wing design paradigm. These include the joined wing [Wolkovitch (1985)], blended wing body [Liebeck et. al. (1998)], twin fuselage [Spearman (1997)], C-wing [Mcmasters et. al. (1999)] and the strut-braced wing, to name a few. This study compares the strut-braced wing (SBW) to the cantilever wing. No attempt has been made to directly compare the strut-braced wing to other alternative configurations. Rather, the cantilever wing configuration is used for reference

The SBW configurations (Figures 1.2-1.4) have the potential for higher aerodynamic efficiency and lower weight than a cantilever wing as a result of favorable interactions between structures, aerodynamics and propulsion. Figure 1.5 shows schematic shear force and bending moment diagrams for a strut-braced wing. The vertical force of the strut produces a shear force

discontinuity along the span. This shear force discontinuity creates a break in the bending moment slope, which reduces the bending moment inboard of the strut. Also, the strut vertical offset provides a favorable moment that creates a spanwise bending moment curve discontinuity. This discontinuity further reduces the bending moment inboard of the strut. A decrease in bending moment means that the weight of the material required to counter that moment will be reduced. The strut provides bending load alleviation to the wing, allowing a thickness to chord ratio (*t/c*) decrease, a span increase, and usually a wing weight reduction. Reduced wing thickness decreases the transonic wave drag and parasite drag, which in turn increases the aerodynamic efficiency. These favorable drag effects allow the wing to unsweep for increased regions of natural laminar flow and further wing structural weight savings. Decreased weight, along with increased aerodynamic efficiency permits engine size to be reduced. The strong synergism offers potential for significant increases in performance over the cantilever wing. A Multidisciplinary Design Optimization (MDO) approach is necessary to fully exploit the interdependencies of various design disciplines. Overall, several facets of the analysis favorably interact to produce a highly synergistic design.

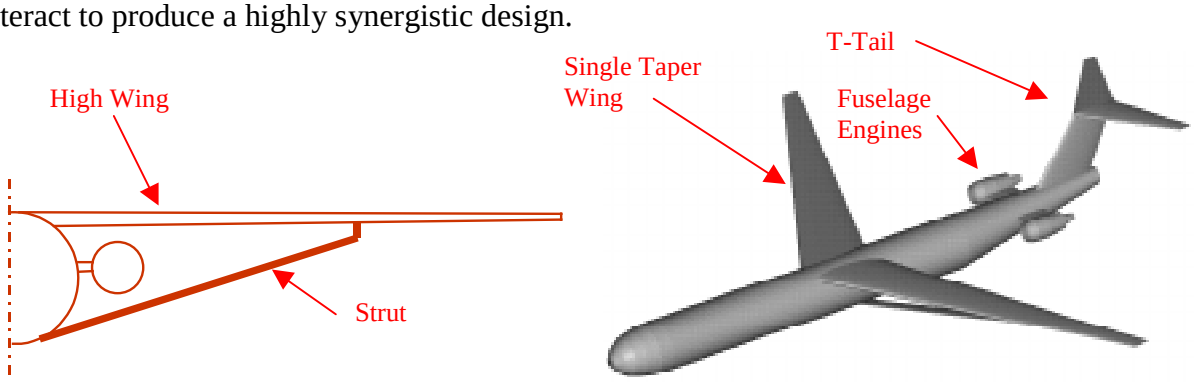

Figure 1.2. Strut-Braced Wing with Fuselage-Mounted Engines.

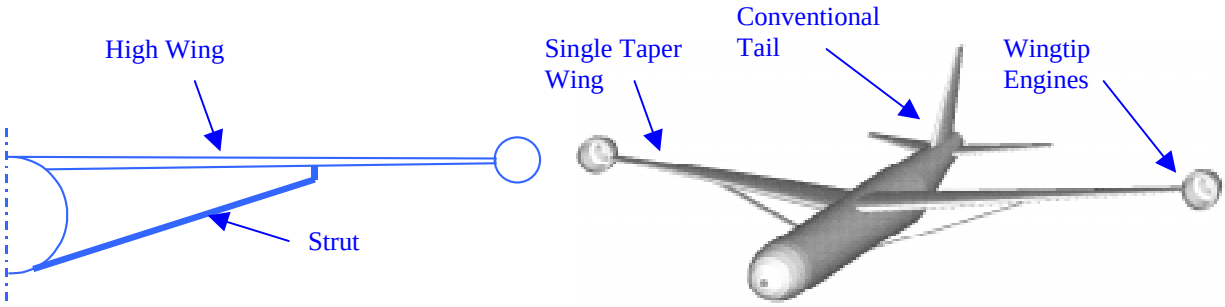

Figure 1.3. Strut-Braced Wing with Tip-Mounted Engines.

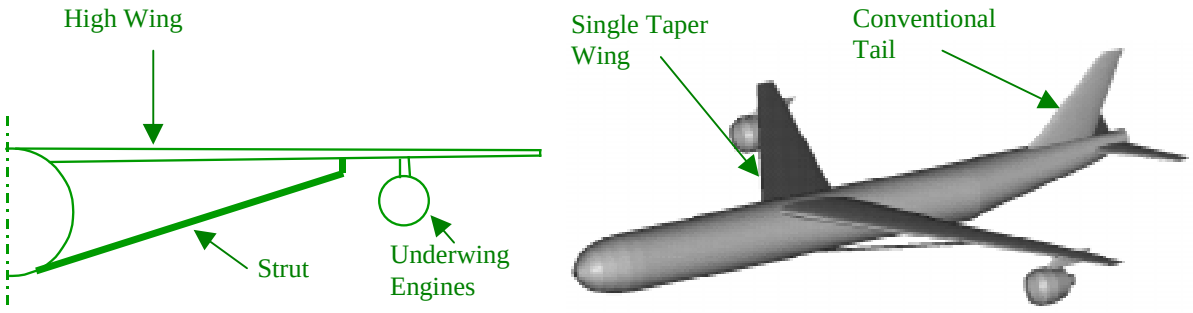

Figure 1.4. Strut-Braced Wing with Underwing Engines.

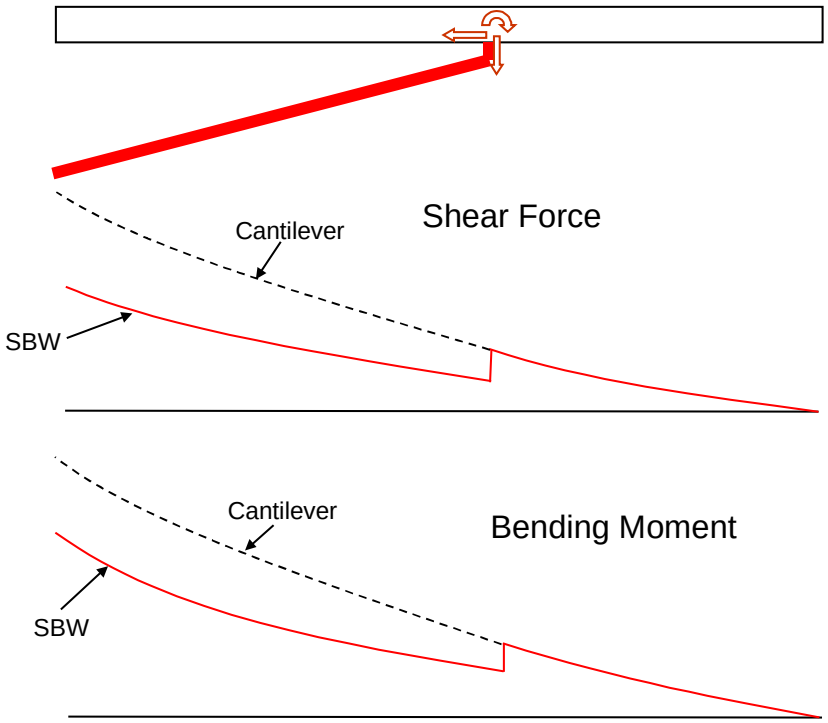

Figure 1.5. Strut-Braced Wing Shear Force and Bending Moment Diagrams.

Werner Pfenninger (1954) originated the idea of using a Truss-Braced Wing (TBW) configuration for a transonic transport at Northrop in the early 1950s (Figure 1.5). The SBW can be considered a subset of the TBW configuration. Pfenninger remained an avid proponent of the concept until his recent retirement from NASA. Several SBW design studies have been performed in the past [Pfenninger (1954), Park (1978), Kulfan et. al. (1978), Jobe et. al. (1978), Turriziani et. al. (1980), Smith et. al. (1981)], though not with a full MDO approach until quite recently [Grasmeyer (1998A,B), Martin et. al. (1998)]. Dennis Bushnell, the Chief Scientist as NASA Langley, tasked the Virginia Tech Multidisciplinary Analysis and Design (MAD) Center

to perform MDO analysis of the SBW concept [Grasmeyer (1998A,B)]. Table 1.1 summarizes the major strut braced wing design studies prior to the Virginia Tech work.

Figure 1.5. Werner Pfenninger SBW Concept (NASA Photo).

Table 1.1. Summary of Past Truss-Braced Wing Studies.

Authors/Sponsor Organization	Study Year	Type of Aircraft	Improvements	Comments
Pfenninger, W./ Northrop	1954	Long-Range, Transonic Tranport		
Dollyhigh et. al./ NASA	1977	Mach 0.60-2.86 Fighter	28% Reduction in Zero-Lift Wave Drag	Several Strut Arrangements, Allowed t/c Reduction
Park	1978	Short Haul Transport	Little Improvement	Aerolasticity Effects Considered
Kulfan et. al. and Jobe et. al./ Boeing	1978	Long Range, Large Military Transport,	Higher TOGW than Equivalent Cantilver	Wingspan = 440 ft., Laminar Flow Control
Turriziani et. al./ NASA	1980	Subsonic Business Jet	20% Fuel Savings over Cantilever	Aspect Ratio = 25
Smith et. al./ NASA	1981	High-Altitude Manned Research Aircraft	5% Increase in Range over Cantilever	

This study was funded by NASA with Lockheed Martin Aeronautical Systems (LMAS) as an industry partner. The primary role of the interactions with LMAS was to add practical industry experience to the vehicle study. This was achieved by calibrating the Virginia Tech MDO code to the LMAS MDO code for baseline 1995 and 2010 technology level cantilever wing transports. The details of the baseline cantilever aircraft were provided by LMAS. LMAS also reviewed aspects of the Virginia Tech design methods specific to the strut-braced wing [Martin et. al. (1998)]. The author worked on location at LMAS to upgrade, calibrate and validate the Virginia Tech MDO code before proceeding with optimizations of conventional cantilever and strut-braced wing aircraft.

Performance may be determined from numerous perspectives. Certainly range and passenger load are important. Life cycle cost, take-off gross weight (TOGW), overall size, noise pollution, and fuel consumption are all candidate figures of merit. Other factors such as passenger and aircrew acceptance and certifiability are less easy to quantify but may determine the fate of a potential configuration.

A technology impact study is used to further understand the differences between 1995 and 2010 technology level aircraft, and to see how the SBW and cantilever configurations exploit these technologies. If the SBW can better harness technologies groups, then greater emphasis must be placed on these. Also, synergy in technology interactions will become apparent if the overall difference in 1995 and 2010 design TOGW is greater than the sum of the TOGW differences for the individual technology groups.

The SBW may have wingtip engines, under-wing engines inboard and outboard of the strut, or fuselage-mounted engines with a T-tail. Underwing and wingtip engines use blowing on the vertical tail from the APU to counteract the engine-out yawing moment. Landing gear is on the fuselage in partially protruding pods for SBW cases. The strut intersects the pods at the landing gear bulkhead and wing at the strut offset.

The baseline cantilever aircraft (Figure 1.1) has the engines mounted under a low wing and has a conventional tail. The landing gear is stowed in the wing between the wing box and kick spar. This study uses cantilever configuration optima, rather than a fixed cantilever wing geometry, so direct comparisons with the SBW configurations can be made. The differences in T-tail fuselage-mounted engine and underwing engine cantilever designs is small, so detailed results for only the underwing engine cantilever aircraft are presented here.

Chapter 2

Problem Statement

The primary mission of interest is a 325-passenger, 7500 nautical mile range, Mach 0.85 transport (See Figure 2.1). Reserve fuel sufficient for an extra 500 nautical miles of flight is included, and fixed fuel mass fractions are used for all non-cruise flight segments. An economic mission aircraft that has reduced passenger load and a 4000 nautical mile range, while still capable of fulfilling the full mission, is also considered. Range effects on TOGW and fuel consumption are investigated. Additional goals are to determine the relative benefits of the strut-braced wing configurations over the cantilever configuration at various ranges and to find the sensitivity of all configurations to various technology groups. The selected objective functions are minimum-TOGW, minimum-fuel weight, and maximum range. The technology impact study and range investigations use minimum-TOGW as the objective function.

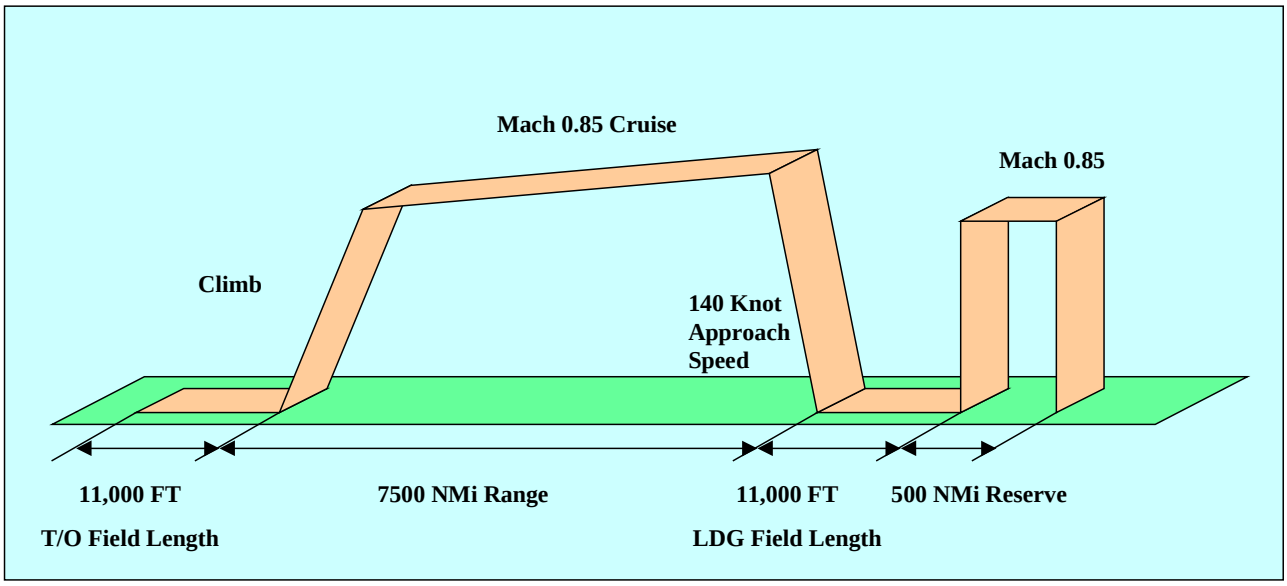

Figure 2.1. Baseline Mission Profile.

Chapter 3

Methodology

3.1 General

The Virginia Tech Truss Braced Wing (TBW) optimization code models aerodynamics, structures/weights, performance, and stability and control of both cantilever and strut-braced wing configurations. Design Optimization Tools (DOT) software by Vanderplatts R&D (1995) optimizes the vehicles with the method of feasible directions. Between 15 and 26 user selected design variables are used in a typical optimization. These include several geometric variables such as wing span, chords, thickness to chord ratios, strut geometry and engine location, plus several additional variables including engine maximum thrust and average cruising altitude (Table 3.1). As many as 17 inequality constraints may be used, including constraints for range, fuel volume, weights convergence, engine-out yawing moment, cruise section C_l limit, balanced field length, second segment climb gradient and approach velocity (Table 3.2). There are also two side constraints to bound each design variable, and each design variable is scaled between 0 and 1 at the lower and upper limits, respectively. Take-off gross-weight, economic mission take-off gross weight, fuel weight and maximum range are important examples among the many possible objective functions that can be minimized.

Some new design variables and constraints presented here were not used by Grasmeyer (1998A,B). New design variables include the wing/strut vertical aerodynamic offset, required thrust, economic mission fuel weight and economic mission average cruise altitude. The wing/strut aerodynamic offset is a surface protruding vertically downwards as shown in Figure 3.1. The required engine thrust is the thrust needed to meet a number of constraints. The engine thrust constraints will be described in more detail later in the text. The economic mission fuel weight is the fuel needed to fly the 4000 nautical mile economic mission, and the economic cruise altitude is the average cruising altitude for the economic mission.

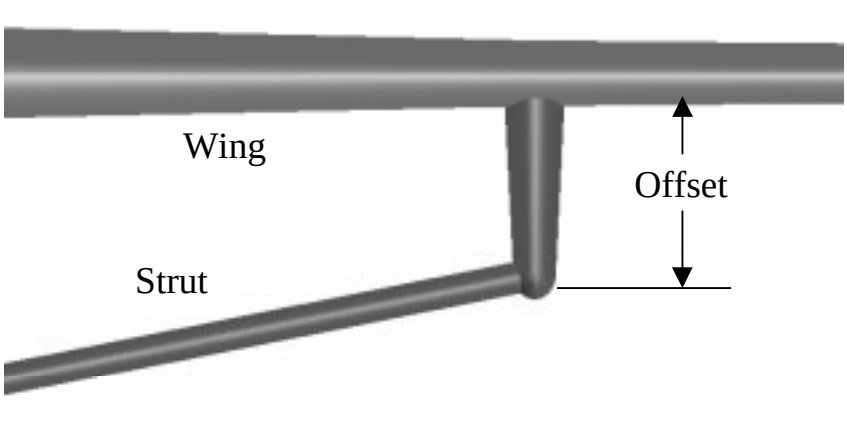

Figure 3.1. Wing/Strut Aerodynamic Offset. (LMAS Figure)

Table 3.1. Design Variables.

1.	Semi-Span of Wing/Strut Intersection
2.	Wing Span
3.	Wing Inboard ¼ Chord Sweep
4.	Wing Outboard ¼ Chord Sweep
5.	Wing Dihedral
6.	Strut ¼ Chord Sweep
7.	Strut Chordwise Offset
8.	*Strut Vertical Aerodynamic Offset
9.	Wing Centerline Chord
10.	Wing Break Chord
11.	Wing Tip Chord
12.	Strut Chord
13.	Wing Thickness to Chord Ratio at Centerline
14.	*Wing Thickness to Chord Ratio at Break
15.	Wing Thickness to Chord Ratio at Tip
16.	Strut Thickness to Chord ratio
17.	Wing Skin Thickness at Centerline
18.	Strut Tension Force
19.	Vertical Tail Scaling Factor
20.	Fuel Weight
21.	Zero Fuel Weight
22.	*Required Thrust
23.	Semispan Location of Engine
24.	Average Cruise Altitude
25.	*Econ. Mission Fuel Weight
26.	*Econ. Mission Average Cruise Altitude

*New Design Variable

Table 3.2 shows that the number of constraints has more than doubled after the research performed by Grasmeyer (1998A,B). New constraints include the climb rate available at the initial cruise altitude, wing weight convergence, maximum body and contents weight convergence, balanced field length, second segment climb, missed approach climb gradient, landing distance, economic mission range, maximum economic mission section lift coefficient and thrust at altitude. The maximum body and contents weight convergence and wing weight convergence constraints are usually turned off when the lagging variable method is used to calculate the corresponding weights. Further details on the weights convergence constraints and the lagging variable method will be given in the structures and weights section. Grasmeyer (1998A,B) calculated the required thrust of the engine by setting the engine thrust equal to the drag at the average cruise condition. In the present code the field performance and rate of climb at initial cruise altitude frequently dictate the required thrust so the thrust at altitude must be met as a constraint.

Table 3.2. Constraints.

1.	Zero Fuel Weight Convergence
2.	Range Calculated >7500 nmi
3.	*Initial Cruise Rate of Climb > 500 ft/min
4.	Cruise Section C_l Limit< 0.7
5.	Fuel Weight < Fuel Capacity
6.	C_n Available > C_n Engine-Out Condition
7.	Wing Tip Deflection < Max Wing Tip Deflection at Taxi Bump Conditions (25 feet)
8.	*Wing Weight Convergence
9.	*Max. Body and Contents Weight Convergence
10.	*Second Segment Climb Gradient > 2.4%
11.	*Balanced Field Length < 11,000 ft
12.	Approach Velocity < 140 kts.
13.	*Missed Approach Climb Gradient > 2.1%
14.	*Landing Distance < 11,000 ft
15.	*Econ. Mission Range Calculated > 4000 nmi
16.	*Econ. Mission Section C_l Limit< 0.7
17.	*Thrust at Altitude > Drag at Altitude

*New Constraint

Each constraint now has a constraint flag in the input file that turns the constraint on if the flag is set to 1 or off if the flag is set to 0. The user now has the option of selectively turning off any constraints by setting the corresponding constraint flag equal to zero, without the need to recompile the code.

Active and violated constraints are now printed during run time. Constraints that are not active or violated are not printed. This feature is very useful, because the code user can observe aspects of the optimization path and determine why the initial guess may not be a feasible design. By witnessing the violated constraints, the user can terminate the current run, modify the input file, attempt a new optimization and find a feasible design from the new inputs.

The MDO code architecture is configured in a modular fashion such that the analysis consists of subroutines representing various design disciplines. The primary analysis modules include: aerodynamics, wing bending material weight, total aircraft weight, stability and control, propulsion, flight performance and field performance. Figure 3.2 is a flow diagram of the MDO code. Initial design variables and parameters are read from an input file. The MDO code manipulates the geometry based on these inputs and passes the information on to the structural optimization and aerodynamics subroutines. The drag is calculated by induced drag, friction and form drag, wave drag, and interference drag subroutines. Additionally, the induced drag subroutine calculates the wing loads. The wing loads are passed to the structural optimization subroutines, which then calculate the aircraft structural weight. The wing bending material weight is calculated in WING.F. Other components of the aircraft structural weights are calculated in FLIPS.F, the weight estimation subroutine modified from FLOPS [McCullers] with LMAS equations. The propulsion analysis calculates the specific fuel consumption at the cruise condition. The specific fuel consumption, L/D, and aircraft weight are passed to the performance module, which calculates the range of the aircraft. The stability and control subroutine determines the engine-out yawing moment and the available yawing moment. The field performance subroutine, FIELD.F, calculates the take-off and landing performance. All constraints and the objective function are evaluated and passed to the optimizer. The optimizer manipulates the design variables until the objective function is optimized and all the constraints are not violated. Details of the analysis will be discussed in further depth in the following sections.

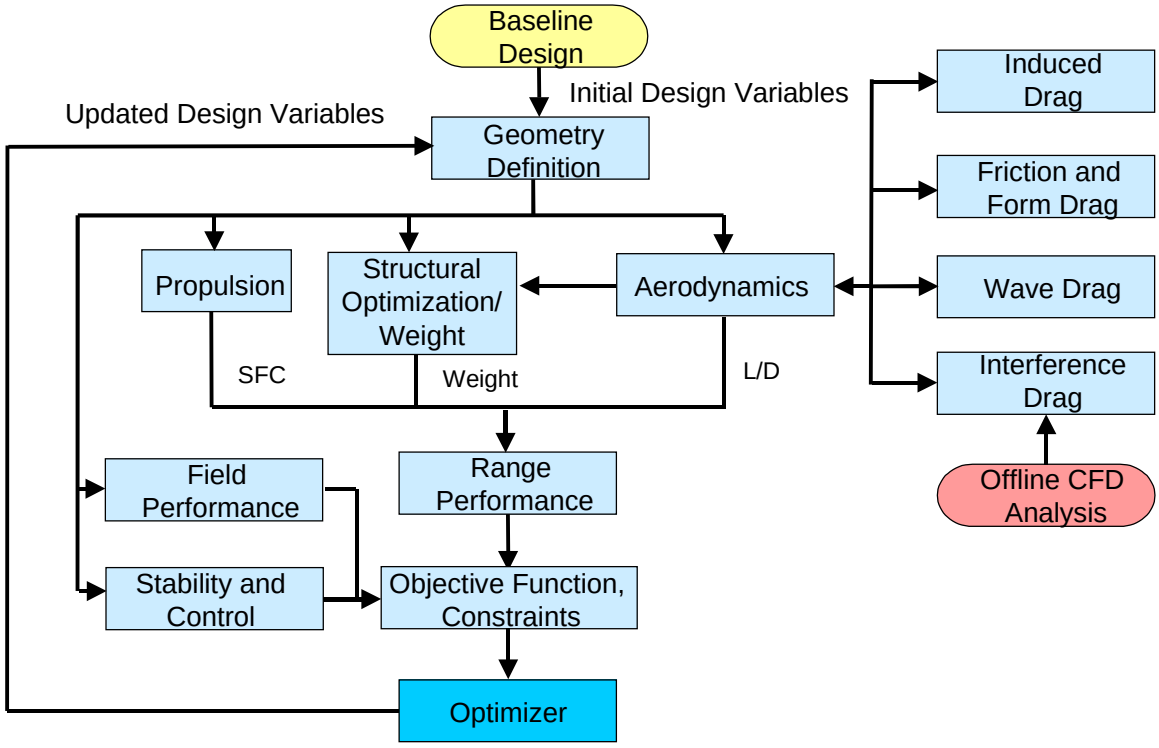

Figure 3.2. MDO Code Architecture.

Differences between the analysis and parameters of cantilever and SBW configurations are present in the design code, as is necessary for such dissimilar vehicles. The primary difference is in the analysis of the wing bending material weight, as discussed in the structures and weights section. The strut has parasite drag and interference drag at the intersections with the fuselage and wing. Also, some geometry differences are justified, such as setting the minimum root chord for the cantilever wing to 52 feet to make room for wing-mounted landing gear and kick spar. The SBW, devoid of any need for a double taper, has the chord linearly interpolated from root to tip. The SBW has a high wing and fuselage mounted gear. It is important to note that, even though the external geometry of the fuselage is identical for all cases, the fuselage weights will generally be different. This is because the fuselage weight is a function of the overall aircraft weight, tail weights, and engine and landing gear placement, all of which vary within a given configuration and from one configuration to another.

3.2 Objective Functions

The baseline mission requires that the aircraft carry 325-passengers for 7500 nautical miles at Mach 0.85. An economic mission of 4000 nautical miles with a reduced passenger load is also of interest, because commercial aircraft seldom operate at their design mission. The economic mission take-off gross weight is minimized for a minimum-economic mission TOGW case, and sometimes evaluated for the minimum-TOGW case. Range effects on take-off gross weight are investigated. A minimum-fuel objective function is also considered.

The economic mission is a 4000 nautical mile range, reduced passenger load flight profile for an aircraft also capable of flying the full 7500 nautical mile, full passenger load mission. The economic mission may be evaluated in two ways. In the first case, the objective function is minimum economic mission TOGW, and the full mission weights must converge and meet all constraints. In the second case, the economic mission TOGW is evaluated for the full mission minimum-TOGW aircraft. The economic fuel weight and economic cruise altitude are selected by the optimizer such that the economic take-off gross weight is minimized, while meeting all of the appropriate constraints.

In the first case, the aircraft geometry, weights, altitude and other variables are allowed to vary as with any other optimization. In addition to these variables, the economic fuel weight and economic cruise altitude are also design variables. Economic range and economic maximum section lift coefficient at cruise constraints are added to the usual constraints.

In the second case, all design variables are now fixed at the minimum-TOGW optimum values. All constraints except for the economic range and economic cruise altitude are turned off. Now the only two design variables are economic cruise altitude and economic fuel weight, and the two constraints are economic range and economic maximum section lift coefficient at cruise.

The economic cruise section C_l limit is the same value as the full mission maximum section C_l. However, it is important to have two separate constraints, because the two mission profiles tend to have different average cruise altitudes. The maximum allowable economic section lift coefficient typically limits the economic average cruise altitude.

The economic flight profile is analyzed at economic cruise weight, which is given by:

$$W_{EconCruise} = W_{ZF} - \Delta W_{ZF,Econ} + \frac{1}{2} \cdot W_{FuelEcon}$$

and at the economic average cruise altitude. The change in economic zero-fuel weight due to reduced passenger and baggage load, $\Delta W_{ZF,Econ}$, was provided by LMAS. The aerodynamics subroutine is called to find the *L/D*, and other terms such as the specific fuel consumption at this condition are determined. Then the Breguet range equation is used to find the calculated range.

The technology impact study investigates the relative benefits of several technology groups when applied to baseline 1995 technology level aircraft. A 1995 aircraft represents the current technology level similar to that of the Boeing 777. Each case is optimized for minimum-TOGW. A technology factor of 1 is associated with a metallic 1995 aircraft benchmark. LMAS prepared several factors to be applied to various vehicle component weights, tail volume coefficients, specific fuel consumption, induced drag, and constants for wave drag and laminar flow. Groupings were made in the following categories: natural laminar flow, other aerodynamics, systems, structural weights and propulsion.

The natural laminar flow group allows laminar flow on the wing, strut, tails, fuselage and nacelles.

Table 3.3. Natural Laminar Flow Technology Group.

1995	2010
No Laminar Flow	Transition *x/c* Calculated on Wings, Strut, and Tails as a Function of Sweep and Mach Number. Transition Reynolds Number on Fuselage and Engine Nacelles Set to 2.5×10^6. Laminar Tech Factor Applied

The other aerodynamics group includes the effects of riblets on the fuselage and nacelles, active load management for induced drag reduction, all moving control surfaces and supercritical airfoils.

Table 3.4. Other Aerodynamics Technology Group.

1995	2010
Low Airfoil Tech Factor Applied (For Wave Drag Korn Equation) Other Aerodynamic Tech Factors = 1.	High Airfoil Tech Factor Applied Induced Drag Tech Factor Applied Fuselage Turbulent Drag Tech Factor Applied

Systems technologies include integrated modular flight controls, fly-by-light and power-by-light, simple high-lift devices, and advanced flight management systems.

Table 3.5. Systems Technology Group.

1995	2010
1995 Horizontal Tail Volume Coefficient All Systems Tech Factors = 1.	Horizontal Tail Volume Coefficient Reduction Controls Weight Tech Factor Applied Hydraulics Weight Tech Factor Applied Avionics Weight Tech Factor Applied Furnishings and Equipment Weight Tech Factor Applied

Airframe technologies reflect composite wing and tails and integrally stiffened fuselage skins.

Table 3.6. Structures Technology Group.

1995	2010
Weights Tech Factors = 1.	Wing Weight Tech Factor Applied Horizontal Tail Weight Tech Factor Applied Vertical Tail Weight Tech Factor Applied Body Weight Tech Factor Applied

The propulsion technology is reflected in reduced specific fuel consumption.

Table 3.7. Propulsion Technology Group.

1995	2010
Specific Fuel Consumption Tech Factor = 1.	Specific Fuel Tech Factor Applied

3.3 Geometry Changes

Previous work by Grasmeyer (1998A,B) used a constant wing thickness to chord ratio, *t/c*, on the outboard panel and an average *t/c* for the inboard section. Calibrations with LMAS baseline designs proved troublesome with this formulation, so the actual *t/c* values at the root, breakpoint and tip are now separately defined to be more consistent.

Changing the formulation introduced some complications. Although WING.F, the wing bending material weight subroutine, requires *t/c* inputs for these three locations, it assumes that

the tip *t/c* and break *t/c* are identical. WING.F was modified to correct this. Andy Ko modified the *t/c* interpolation such that the thickness and chord are interpolated linearly rather than linearly interpolating the *t/c*. This ensures that the wing contours remain conic sections, and the new formulation better reflects reality. Figure 3.3 shows the new and old t/c formulations.

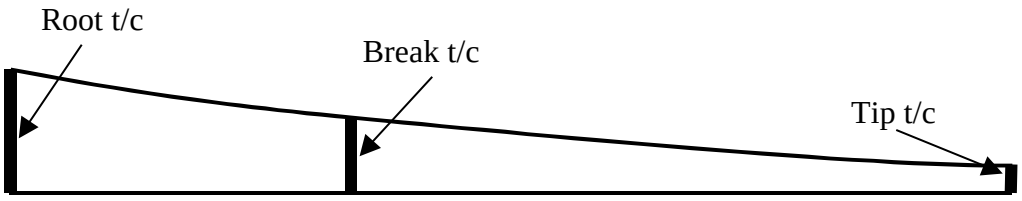

a) New Definition.

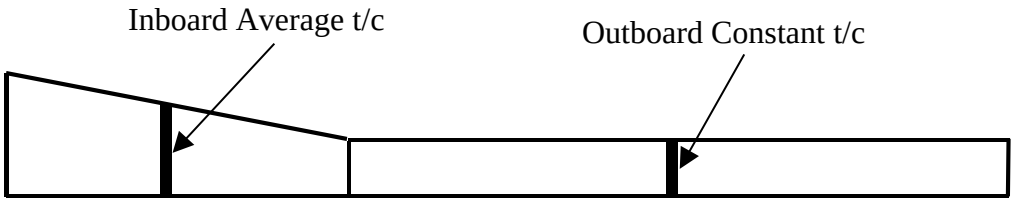

b) Old Definition.

Figure 3.3. *t/c* Definitions.

For a strut-braced wing configuration, the wing has a single taper and the strut has no taper. There is a series of if-then statements in subroutine CONVERT that will automatically interpolate the wing breakpoint chord and set the strut tip chord equal to the strut root chord. The wing breakpoint chord is calculated in this way so that the wing outboard panel is not permitted to have excessive taper (taper ratio > 1). The strut chord is held constant, because the wing/strut intersection interference drag is no longer a function of strut tip chord. Compounding the problem, the strut-offset thickness is increased when the strut tip chord is increased. An increase in strut offset thickness is lighter for a given bending load, because the moment of inertia is higher. These effects combine to produce taper ratios well in excess of 1.0 if the taper ratio is not constrained.

FLIPS.F and FLOPS [McCullers] use different average wing thickness conventions. The original FLOPS uses:

$$t/c_{Average} = \frac{4 \cdot t/c_{Root} + 5 \cdot t/c_{Break} + t/c_{Tip}}{10}$$

and FLIPS.F uses the convention:

$$t/c_{Average} = \frac{4 \cdot t/c_{Root} + t/c_{Tip}}{5}$$

The SBW code originally did not account for the engine moment arm for fuselage mounted engines. The lateral distance from the aircraft centerline to the center of a fuselage-mounted engine is now calculated as:

$$Y_{Engine} = \frac{1}{2} \cdot D_{fuselage} + \frac{1}{2} \cdot D_{Engine} + h_{Pylon}$$

and this value is substituted for the wing-mounted engine Y_{Engine} value normally used for the required yawing moment coefficient calculation.

3.4 Aerodynamics

Numerous iterations of both the Virginia Tech TBW code and Lockheed's version of FLOPS [McCullers] were made so that drag polars produced by each code are consistent at reference design conditions. The drag components considered in the Virginia Tech MDO tool are parasite, induced, interference and wave drag. Unless specified otherwise, the drag model is identical to previous Virginia Tech SBW studies [Grasmeyer (1998A,B)]

To calculate the parasite drag, form factors are applied to the equivalent flat plate skin friction drag of all exposed surfaces on the aircraft. The amounts of laminar flow on the wing and tails are estimated by interpolating Reynolds number vs. sweep data for F-14 and 757 glove experiments [Braslow et. al. (1990)]. Transition locations of the horizontal and vertical tails now follow the same procedures as for the wing and strut, whereas they were considered fully turbulent in previous studies [Grasmeyer (1998A,B)]. The fuselage, nacelle, and pylon transition locations are estimated by an input transition Reynolds number of 2.5 million. Laminar and turbulent flat-plate skin friction form factors are calculated by a hybrid formulation using Lockheed's Modular Drag (MODRAG) formulas and the FRICTION algorithm [Mason] in the Virginia Tech TBW code. The wing, tail surfaces, nacelle and fuselage wetted areas and form factors for friction drag calculations now use the LMAS formulation. The wing thickness distribution for the form/friction drag is found from the new thickness calculation procedure. The engine equivalent length/diameter ratio used for the form drag is modified. The old formulation has identical form factor formulas for both the nacelle and fuselage, but the LMAS

procedure has two distinct formulas. Previously, the pylon drag was greater for the wing-mounted engines than for fuselage-mounted engines, but now the drags are equal. The form drag multiplying factor is now the same for both underwing and fuselage-mounted engines. The parasite drag of a component is found by:

$$C_{D_p} = C_{D_f} \cdot FF \cdot \frac{S}{S_{ref}}$$

The induced drag module [Grasmeyer (1997)] uses a discreet vortex method to calculate the induced drag in the Trefftz plane. Given an arbitrary, non-coplanar wing/truss configuration, it provides the optimum load distribution corresponding to the minimum induced drag. This load distribution is then passed to the wing structural design subroutine, WING.F. Induced drag reductions are employed on the wingtip-mounted engine case [Grasmeyer (1998A,B), Patterson et. al. (1987), Miranda et. al. (1986)], with the relative benefits wingtip engines decreasing as the aspect ratio increases (Figure 3.4). The field performance section gives more detail on the wingtip-mounted engine drag reduction.

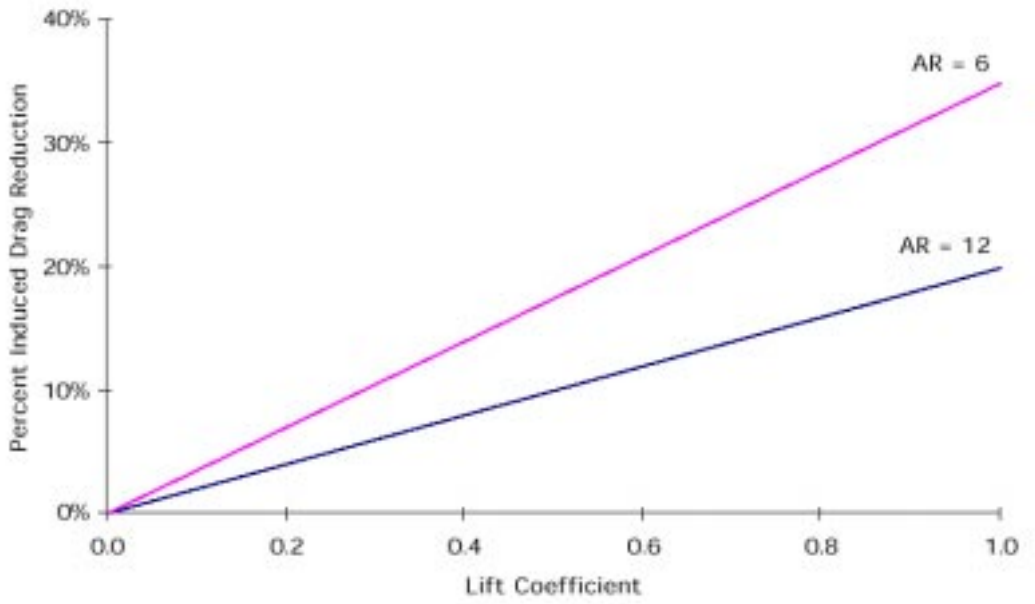

Figure 3.4. Wingtip-Mounted Engine Induced Drag Reduction. [Grasmeyer (1998A,B)]

An additional profile drag due to lift term was added to help correlate the LMAS and VPI drag polars at off-design conditions. The equation is:

$$\Delta C_{D,CL} = \left(\frac{1}{f_{break}} - 1 \right) \cdot \frac{\left(C_L - C_{Lbreak} \right)^2}{\pi \cdot AR_W}$$

where f_{break} and C_{Lbreak} are constant inputs determined from correlation with LMAS drag polars. The overall effect of this drag component at design conditions is small, because C_L is close to C_{Lbreak}.

The interference drag between the wing-fuselage and strut-fuselage intersections are estimated using Hoerner (1965) equations based on subsonic wind tunnel tests. The wing-strut interference drag is based on Virginia Tech CFD results [Tetrault (1998)], and is found to be:

$$C_D = \frac{18}{Offset} \quad \text{(Counts)}$$

Tetrault (1998) used the USM3D CFD code with VGRIDns unstructured grid generator for this analysis. Figure 3.5 shows the correlation between the CFD results and the interference drag equation. A hyperbola is used to fit the data because the interference drag is expected to greatly increase with decreasing arch radii.

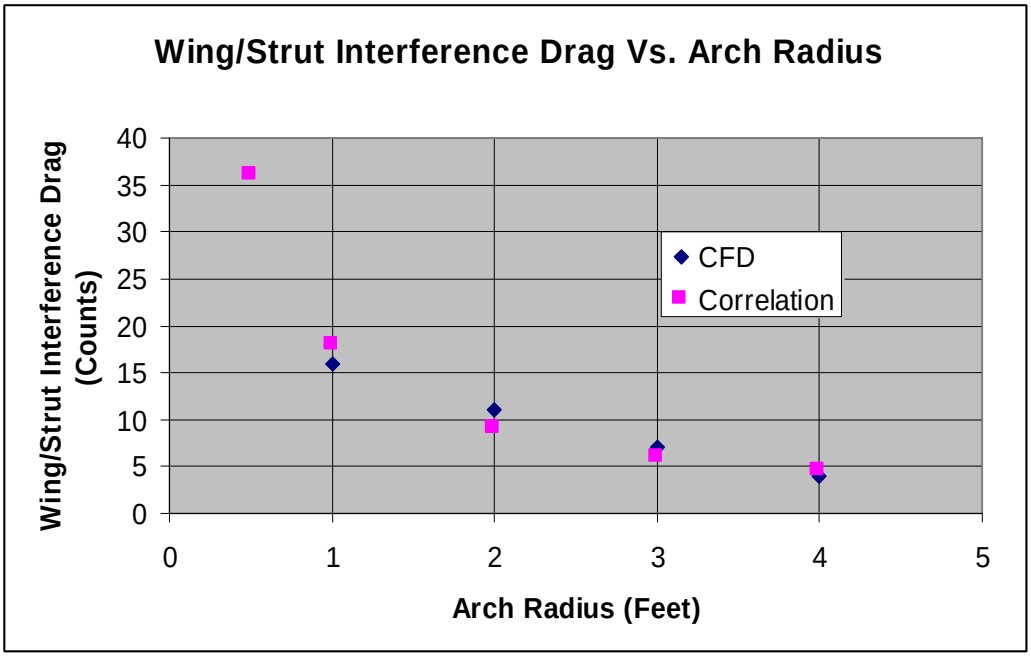

Figure 3.5. Wing/Strut Interference Drag vs. Arch Radius Correlation [Tetrault (1998)].

The wave drag is approximated with the Korn equation, modified to include sweep using simple sweep theory [Grasmeyer (1998A,B), Malone et. al. (1995), Mason (1990)]. This model

estimates the drag divergence Mach number as a function of airfoil technology factor, the thickness to chord ratio, the section lift coefficient, and the sweep angle by:

$$M_{dd} = \frac{\kappa_a}{\cos\Lambda} - \frac{t/c}{\cos^2\Lambda} - \frac{c_l}{10\cdot\cos^3\Lambda}$$

The airfoil technology factor, κ_a, was selected by Lockheed to agree with their original formulation. The wing thickness now uses the new thickness calculation procedure. The critical mach number is:

$$M_{crit} = M_{dd} - \left(\frac{0.1}{80}\right)^{1/3}$$

Finally, the wave drag coefficient of a wing strip is calculated with Lock's formula [Hilton (1952)] as:

$$c_{d_{wave}} = 20(M - M_{crit})^4 \frac{S_{strip}}{S_{ref}}$$

The total wave drag is found by integrating the wave drag of the strips along the wing.

The drag polars output from the Virginia Tech MDO tool and Lockheed's modified FLOPS agree within 1% on average for cantilever wing designs. Figure 3.6 Shows a comparison between Virginia Tech and LMAS drag polars for a 1995 technology level cantilever wing aircraft. Note that LMAS does not have a SBW design for direct comparisons, so all correlations were done with cantilever aircraft. The laminar technology factor, airfoil technology factor and all other aerodynamic constants are the same for all configurations, but the former two vary between 1995 and 2010 technology levels.

Technology factors for the technology analysis may be applied to the induced drag term and the turbulent friction drag of the fuselage and nacelles. The induced drag technology factor is applied to the induced drag directly in AERO.F. The turbulent friction drag technology factor is passed from AERO.F to FDRAG.F, where it is multiplied by the turbulent skin friction term.

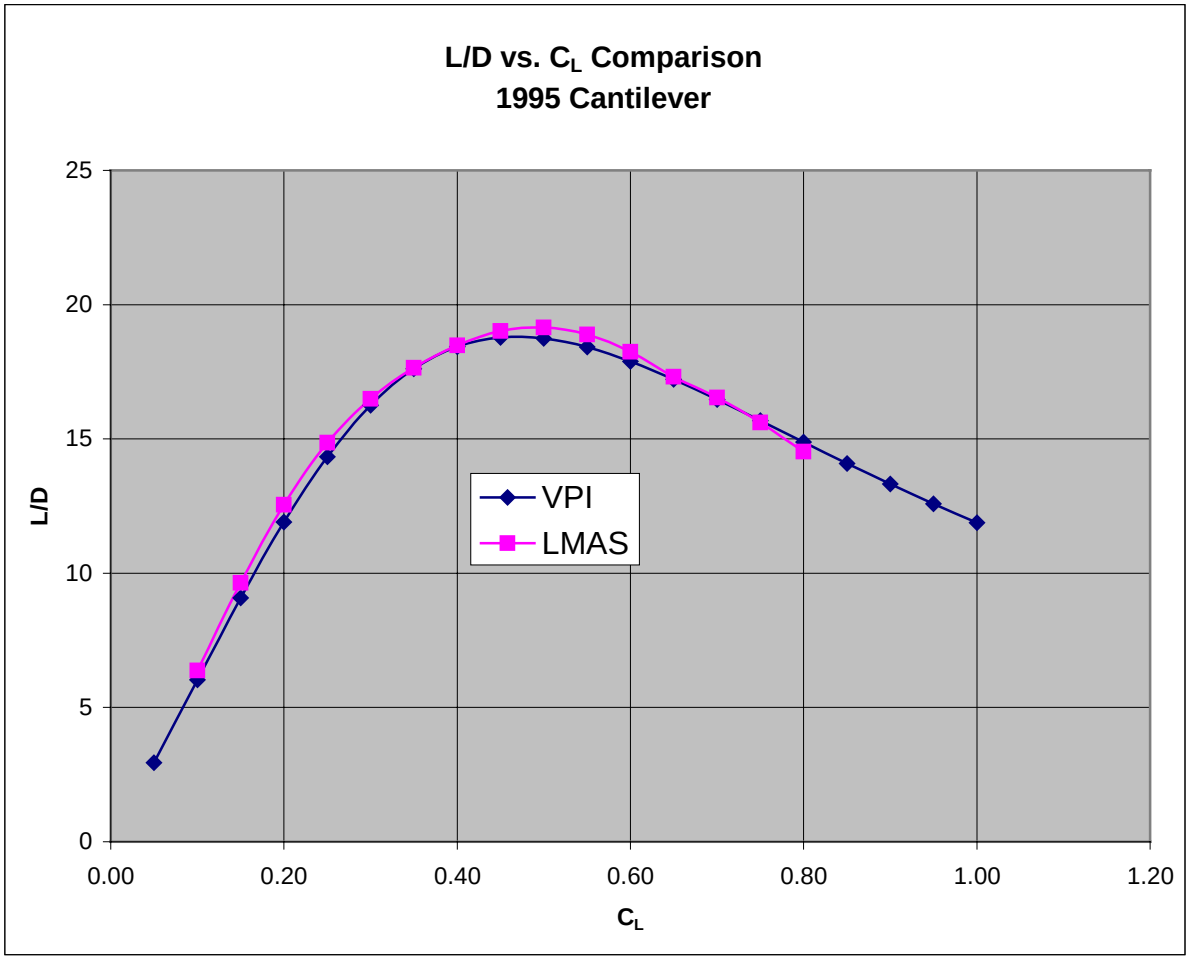

Figure 3.6. Virginia Tech and LMAS Drag Polar Comparison.

3.5 Structures and Weights

The aircraft weight is calculated with several different methods. The majority of the weights equations come from NASA Langley's Flight Optimization System (FLOPS) [McCullers]. Many of the FLOPS equations were replaced with those suggested by LMAS in FLIPS.F. The FLIPS.F and original FLOPS methods do not have the option to analyze the strut-braced wing with the desired fidelity, so a piecewise linear beam model was developed at Virginia Tech to estimate the bending material weight [Naghshineh-Pour et. al. (1998)].

The piecewise linear beam model represents the wing bending material as an idealized double plate model of the upper and lower wing box covers. The vertical offset member discussed in the aerodynamics section was added to the wing/strut intersection to help reduce the interference drag at this intersection. The structural offset length is assumed to be the length of

the aerodynamic offset plus some internal distance within the wing. This offset must take both bending and tension loading. Vertical offset weight increases rapidly with increasing length, but the interference drag decreases. The offset length is now a design variable, and the optimizer selects its optimum value. Fortunately, the vertical offset imposes bending moment relief on the wing at the intersection, and the resulting overall influence on the TOGW is negligible. A 10% weight penalty is applied to the piecewise linear beam model to account for non-optimum loading and manufacturing considerations. An additional 1% bending material weight increase is added to the SBW to address the discontinuity in bending moment at the wing/vertical offset intersection. Figure 3.7 shows the wing weight calculation procedure.

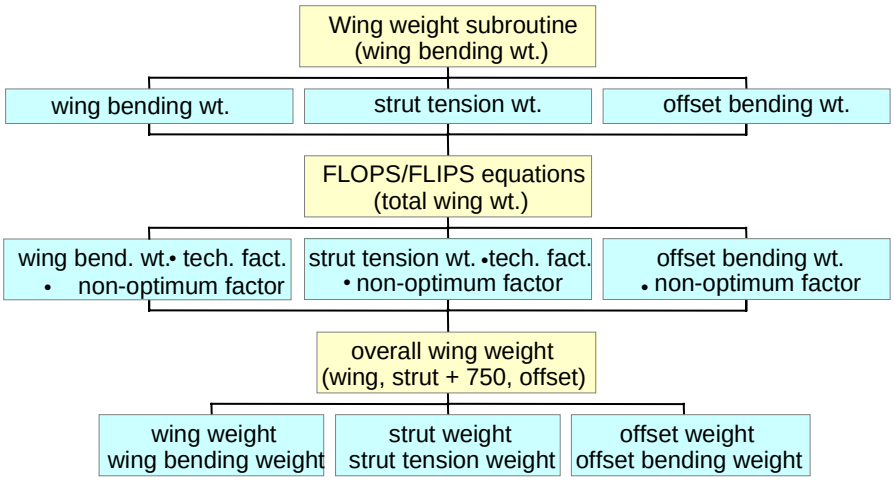

Figure 3.7. Wing Weight Calculation Procedure.

Several modifications have been made to WING.F for the current study. The number of spanwise steps between vortices is decreased from 300 to 30. The taxi load factor was increased from 1.67 to 2.0. A fuel weight distribution error was corrected. A modification was made to the cosine component of the structural wing chord interpolation. The engine load factor of 2.5 was multiplied by 1.5 to account for the safety factor, so the current value is now 3.75. The wing-box chord to wing chord ratio was decreased from 0.5 to 0.45. The minimum gauge thickness was changed from 0.004 to a value specified by LMAS. Aluminum wing allowable stress went from 51,800 psi, the value found in Torenbeek, to a value specified by LMAS. The wing/strut vertical structural offset is now included. The new wing thickness distribution procedure is also now included in WING.F.

Earlier Virginia Tech studies [Grasmeyer (1998A,B), Naghshineh-Pour et. al. (1998)] have shown that the critical structural design case for the single-strut is strut buckling at -1 g loading. To alleviate this stringent requirement, a telescoping sleeve mechanism arrangement is employed such that the strut will engage under positive a load factor, and the wing will essentially act as a cantilever wing under negative loading. LMAS provided a 750-pound weight estimate for the telescoping sleeve mechanism based on landing gear component data. Also, the SBW must contend with the –2 g taxi bump case, where the strut is also inactive.

The wingtip deflection at the taxi bump condition constraint for underwing engines previously only considered the wingtip deflection and not the engine ground strike. Now the sum of the engine diameter, pylon height and downward wing deflection at the engine location give the overall wingtip deflection. The wingtip deflection constraint will be violated if either the wingtip deflection or engine deflection exceed the maximum allowable wingtip deflection value.

Weights calculated in the Virginia Tech TBW code are identical to FLOPS with the exception of nacelle, thrust reverser, landing gear, passenger service, wing, fuselage and tail weights. The above weights are now calculated from proprietary LMAS formulas. Weight technology factors are applied to major structural components and systems to reflect advances in technology levels from composite materials and advanced electronics.

Subroutine FLIPS.F uses a combination of FLOPS weights equations and LMAS equations. The equations themselves are not presented here, but some highlights are described. To account for manufacturing considerations, the cantilever wing bending material weight from WING.F is multiplied by a factor of 1.1. Similarly, SBW wing bending material, strut bending material and strut offset bending material weights from WING.F are multiplied by 1.11 to account for the discontinuous bending moment along the wing at the wing/strut intersection. Systems, landing gear and tail surface weights are calculated first. Then the wing weight, fuselage and zero fuel weights are calculated.

Traditionally, some aircraft weights are implicit functions, and internal iteration loops are required for convergence. However, utilizing the optimizer for zero fuel weight convergence is more efficient and provides smoother gradients. DOT also selects the fuel weight so that the range constraint is not violated. The wing and maximum body and contents weights are also

implicit functions. The fuselage, wing, and zero fuel weight equations have the following functional dependencies.

$$W_{Fuse}(W_{BodyMax,in}, W_{ZF,in}, W_{Fuel})$$
$$W_{Wing}(W_{Wing,in}, W_{ZF,in}, W_{Fuel})$$
$$W_{ZF,Calc}(W_{Wing}, W_{Fuse})$$
$$W_{BodyMax}(W_{Fuse}, W_{ZF,Calc})$$

Earlier versions of FLIPS.F let the maximum body and contents weight and the wing weight be design variables that had to converge with their calculated values. Now a lagging variable method is employed. With this procedure the input wing and maximum body and contents weight inputs are set to their respective output values from the previous iteration. The input values for the first iteration are input from the input file. Convergence of wing and maximum body and contents weights are rapid with the lagging variable method and leads to better conditioning of the optimization problem than if these two variables converge as design variables. The original FLOPS weight subroutine does not rely on such convergence methods for any fuselage or wing weight terms and thus has better problem formulation conditioning.

To find the landing gear weight, the landing gear length is calculated by methods differing from both FLOPS and LMAS weights equations. All SBW landing gear lengths are set to 7 feet to allow for ground clearance at landing and for service vehicles, as specified by LMAS. The main landing gear length for the cantilever wing case has a 4-foot ground clearance, plus the nacelle diameter and pylon height. The four-foot nacelle ground clearance was selected arbitrarily. The nose gear is 70% of the main gear length.

The GE-90 engine reference weight is now lower than previous studies, because this quantity no longer includes the inlet and thrust reverser weights. These are now calculated by proprietary LMAS formulas. The reference engine weight is calculated by an engine scaling factor equal to the ratio of required thrust to reference thrust. The wing bending material weight depends on the weight hanging from the engine pylon. This engine pod weight was modified to allow for the new engine weight accounting system.

3.6 Cost Analysis

The FLOPS cost module is used to calculate the acquisition cost, direct operating cost and indirect operating cost in a similar manner as previous studies by Grasmeyer (1998A,B). The total cost for this formulation is found by:

Total Cost = Acquisition Cost + Direct Operating Cost + Indirect Operating Cost

Originally, the FLOPS cost module used the weights produced by the FLOPS weight module for calculations. Now a subroutine COST passes an array of FLIPS.F weight data to FLOPS, overwrites the FLOPS weights, and then calculates cost based on the new FLIPS.F weights. FLOPS is called in a similar method to what was previously done to retrieve the weights data. Now only the cost information and not the FLOPS weights are returned to the main code from COST.

3.7 Stability and Control Analysis

The horizontal and vertical tail areas are first calculated with a tail volume coefficient sizing method. The user specified tail volume coefficients are now based on LMAS statistical data. Grasmeyer (1998A-C) had the tail geometry fixed to that of the Boeing 777. Tail geometric parameters such as taper ratio, aspect ratio and quarter chord sweep are held constant regardless of tail area, but the parameters vary between T-tail and conventional tails. An option exists to input the tail area rather than calculate it from the tail volume coefficient method, but this was not utilized for this study. The tail moment arm is held constant for a given case. The variable used for the tail moment arm, or the distance from the center of gravity to the aerodynamic center of a tail surface, was previously used to define the distance from the leading edge of the wing to the leading edge of the tail surface. Now the distance between the leading edges is calculated from the tail moment arm and wing and tail geometry. Details of the tail geometry formulation are found in Appendix 1.

A vertical tail sizing routine was developed to account for the one engine inoperative condition [Grasmeyer (1998A-C)]. The engine-out constraint is met by constraining the maximum available yawing moment coefficient to be greater than the yawing moment coefficient required to handle the engine-out requirement. The aircraft must be capable of maintaining straight flight at 1.2 times the stall speed, as specified by FAR requirements. The operable engine is at its maximum available thrust. Vertical tail circulation control is permitted

only on the underwing and wingtip-mounted engine cases, resulting in vertical tail lift coefficient augmentation and greater available yawing moment. The change in vertical tail lift coefficient for the wingtip-mounted engine and underwing engine outboard of the strut SBW cases is set to 1.0.

The engine-out yawing moment coefficient required to maintain straight flight is given by:

$$C_{n_{req}} = \frac{(T_E + D_E) \cdot Y_{Eng}}{q \cdot S_w \cdot b_w}$$

where T_E is the thrust of the good engine, D_E is the drag on the inoperable engine, and Y_E is the lateral distance to the engine. The lateral force of the vertical tail provides most of the yawing moment required to maintain straight flight after an engine failure.

The maximum available yawing moment coefficient is obtained at an equilibrium flight condition with a given bank angle and a given maximum rudder deflection. FAR 25.149 limits the maximum bank angle to 5^o, and some sideslip angle is allowed. The stability and control derivatives are calculated using empirical methods based on DATCOM as modified by Grasmeyer (1998A-C) to account for vertical tail circulation control.

To allow a 5^o aileron deflection margin for maneuvering, the calculated deflection must be less than 20^o-25^o. The calculated available yawing moment coefficient is constrained in the optimization problem to be greater than the required yawing moment coefficient. If the yawing moment constraint is violated, a vertical tail area multiplying factor is applied by the optimizer.

3.8 Propulsion

A GE-90 class high-bypass ratio turbofan engine is used for this design study. An engine deck was obtained from LMAS, and appropriate curves for specific fuel consumption and maximum thrust as a function of altitude and Mach number were found through regression analysis. The general forms of the equations are identical to those found in Mattingly (1987) for high-bypass ratio turbofan engines, but the coefficients and exponents are modified. Figure 3.8 shows the correlation between the specific fuel consumption and thrust at altitude models and a GE-90-like engine deck. The steps in the specific fuel consumption found in Figure 3.8 are caused by sudden increases in Mach number at the beginning of each climb segment for the LMAS flight profile. The engine size is determined by the thrust required to meet the most demanding of several constraints. These constraints are thrust at average cruise altitude, rate of climb at initial

cruise altitude, balanced field length, second segment climb gradient, and missed approach climb gradient. The engine weight is assumed to be linearly proportional to the engine thrust. The engine dimensions vary as the square root of their weight, as is typically done in dynamic scaling of aircraft components. The modified engine dimensions are passed to the aerodynamics and structures routines (neglected in previous Virginia Tech SBW studies). Some concerns have arisen regarding the range through which a GE 90-like engine may be scaled, however no other suitable model is available. The specific fuel consumption model is independent of engine scale. A specific fuel consumption technology factor is applied to reflect advances in engine technology. The formulas for the thrust and specific fuel consumption at altitude are:

$$\frac{T}{T_{SL,Static}} = \left(\left(0.6069 + .5344 \cdot (0.9001 - M)^{2.7981}\right) \cdot \left(\frac{\rho}{\rho_{SL}}\right)^{0.8852} \right)$$

$$sfc = \left(\frac{Temp}{Temp_{SL}}\right)^{0.4704} \left(sfc_{Static} + 0.4021 \cdot M\right)$$

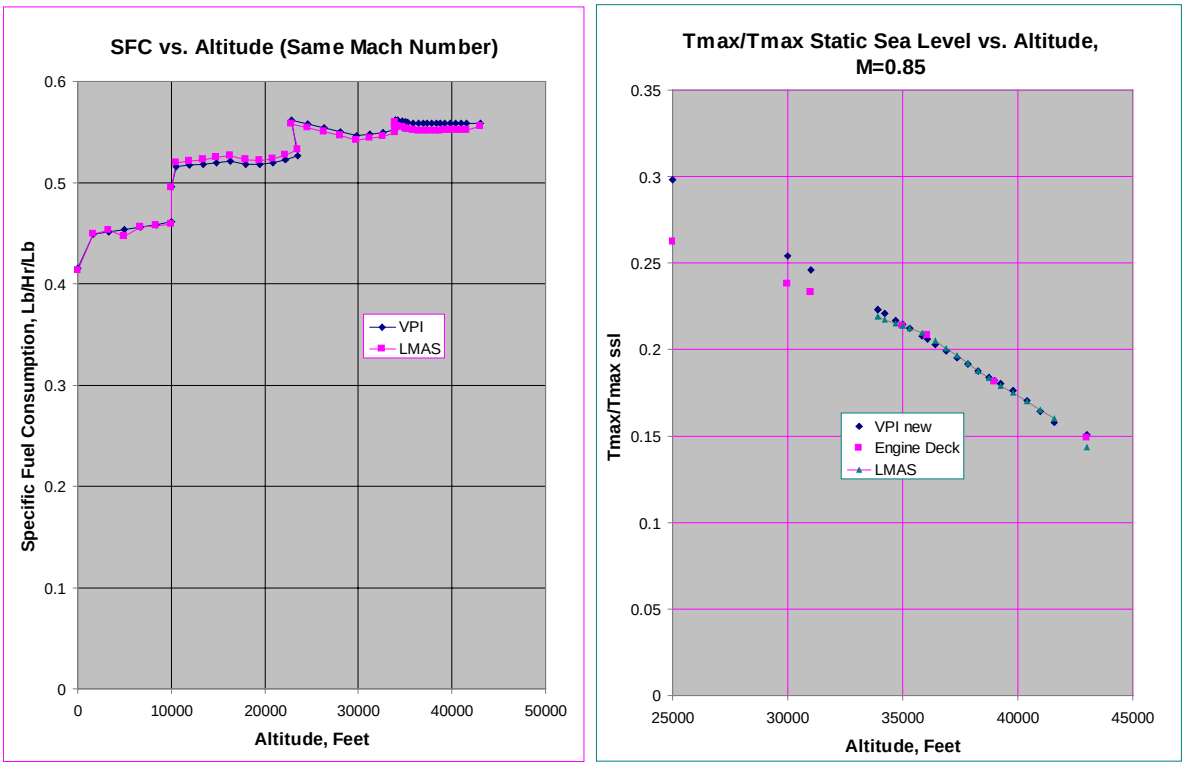

Figure 3.8. Engine Model and Engine Deck Comparison.

3.9 Flight Performance

The calculated range is determined from the Breguet range equation.

$$Range = \frac{(L/D)\cdot V}{sfc} ln\left(\frac{W_i}{W_0}\right) - Reserve$$

The *L/D*, flight velocity and specific fuel consumption are found for the average cruising altitude and fixed Mach number. W_i/W_o is the ratio of initial cruise weight to the zero-fuel weight. The initial cruise weight is 95.6% of the take-off gross weight to account for fuel burned during climb to the initial cruise altitude. A reserve range of 500 nautical miles is used as an approximation to the FAR requirement [Loftin (1980)].

The available rate of climb at the initial cruise altitude is required be greater than 500 feet/second. The average cruise altitude is generally a design variable and is thus known for every iteration. The initial cruise altitude is not known and the following procedure is used to find its value. Mach number and lift coefficient must be constant throughout cruise, and in order for this to be true:

$$\rho \cdot a^2 = \frac{W}{\frac{1}{2}\cdot M^2 \cdot C_L \cdot S_{ref}}$$

where W is the weight at the flight condition and M and C_L are specified. The weight is the initial cruise weight, M is set at 0.85 and C_L is the value from the average cruise condition. The initial altitude is the altitude at which this equation is satisfied for the above conditions. A secant method is employed to solve for the initial cruise altitude by finding the density and sound speed from the STDATM subroutine. If the initial cruise altitude and average cruise altitude are both in the stratosphere, then the temperature is constant and the formula simplifies to:

$$\rho = \frac{W}{\frac{1}{2}\cdot V^2 \cdot C_L \cdot S_{ref}}$$

The initial cruise rate of climb is:

$$R/C_{CruiseInitial} = \left(\frac{T}{W} - \frac{1}{L/D}\right)\cdot M \cdot a$$

with the thrust and weight equal to their values at the initial cruise condition, and the appropriate unit conversions are used. The *L/D* is assumed to be equal to the average cruise *L/D*. The maximum observed *L/D* difference is 2.6%.

3.10 Field Performance

Take-off and landing performance utilizes methods found in Roskam and Lan (1997). The field performance subroutine calculates the second segment climb gradient, the balanced field length, the missed approach climb gradient, and the landing distance. LMAS reviewed the field performance subroutine and decided that it produced results acceptably close to those obtained by their own methods for the 1995 and 2010 technology level cantilever baseline aircraft.

Reference drag polars for the aircraft at take-off and landing were provided by LMAS. Trends are assumed to be the same for both the SBW and cantilever configurations. The actual drag polars utilize corrections based on total aircraft wetted area and wing aspect ratio. The total aircraft wetted area is calculated in AERO.F. It was assumed that, with the level of fidelity of this systems study, the high lift characteristics of the vehicles may be tailored in many ways such that the corrected drag polars can be attained.

A correction factor to the lift dependent drag terms, *f*, is used for the take-off and landing drag polars of wingtip-mounted engine SBW aircraft. The correction factor is found by an interpolation procedure first developed by Grasmeyer (1998A,B) for cruise induced drag. Note that for all cases other than wingtip-mounted engines, $f = 1$. The factor depends strongly on C_L and varies from one flight condition to another. The factor f can be found by the following procedure:

$$f_6 = 1 - 0.35 \cdot C_L$$

$$f_{12} = 1 - 0.20 \cdot C_L$$

$$f = f_6 + (f_{12} - f_6) \cdot \frac{(AR_W - 6)}{(12 - 6)}$$

All calculations are done for hot day conditions, as specified by LMAS, at sea level. LMAS specified that the temperature of the airport be 83 ^{o}F. Density and sound speed corrections were made to the outputs of the standard atmosphere model.

The balanced field length equation found from Roskam is given below.

$$BFL = \frac{0.863}{1 + 2.3 * \Delta\gamma_2}\left(\frac{W_{TO}/S}{\rho \cdot g \cdot C_{L2}} + h_{TO}\right)\left(\frac{1}{\overline{T}/W_{TO} - \mu'} + 2.7\right) + \frac{\Delta S_{TO}}{\sqrt{\rho/\rho_{SL}}}$$

Some of the parameters are:

$$\Delta\gamma_2 = \gamma_2 - \gamma_{2Min}$$

$$h_{TO} = 35\,ft$$

$$\mu' = 0.010 \cdot C_{L\max TO} + 0.02$$

$$\Delta S_{TO} = 655\,ft$$

The second segment climb gradient is the ratio of rate of climb to the forward velocity at full throttle while one engine is inoperative and the gear is retracted. The second segment climb gradient, γ_2, is found by:

$$\gamma_2 = \frac{R/C}{V} = \frac{T-D}{W} = \frac{T}{W} - \frac{1}{(L/D)}$$

The minimum second segment climb gradients for aircraft having 2-4 engines are presented in Table 3.3. The engine thrust at second segment climb is a function of density and Mach number according to a modified version of Mattingly's equation presented in the propulsion section. The mean thrust for the take-off run is determined from the suggested formula in Roskam and Lan (1997):

$$\overline{T} = \frac{3}{4} \cdot \frac{(5 + BPR)}{(4 + BPR)} \cdot T_{static}$$

The maximum take-off lift coefficient is the minimum C_L associated with $V_2 = 1.2V_{stall}$ or the C_L for the tail scrape angle. C_{Lstall} is read in through the input file and is independent of configuration. The tail scrape lift coefficient is:

$$C_{Lscrape} = C_{L\alpha=0} + C_{L\alpha} \cdot (Angle_{scrape} - Margin_{scrape})$$

where $C_{L\alpha=0}$ and $C_{L\alpha}$ are found from LMAS take-off lift curves and drag polars. Currently the tail scrape C_L is the most critical. A 0.5-degree scrape margin is used to match the LMAS C_L.

Roskam and Lan (1997) methods are also used to determine the landing distance. Three legs are defined. The air distance is the distance from clearing the 50 ft. object to the point of wheel touchdown, including the flare distance. The free roll distance is the distance between touch-down and application of brakes. And finally, the brake distance is the distance covered while braking.

The air distance is given by:

$$S_A = \frac{h_f}{\gamma} + \frac{V_F{}^2 \gamma}{2g(n-1)}$$

where h_f is the 50-foot obstacle height, V_F is the velocity at flare, n is the number of g's at flare, and γ is the glide slope. n is assumed to be 1.2. γ is set to the radian conversion of 2-3 degrees

as suggested in Roskam and Lan (1997) since the throttle can be arbitrarily set to match this value. The flare velocity is assumed to be equal to the approach velocity. The lift coefficient is the least of the C_L associated with $V=1.3*V_{stall}$ or the C_L to meet the tail scrape requirement. The drag coefficient is calculated with gear down.

The free roll distance is given by:

$$S_{FR} = t_{FR} \cdot V_{TD}$$

where t_{FR} is the time which the aircraft is in free roll, and V_{TD} is the touch-down velocity which is assumed to be the approach velocity.

The braking distance is found by:

$$S_B = \frac{W}{2g} \cdot \frac{V_{TD}^{\ 2}}{F_m}$$

where F_m is the mean braking force. The first step in calculating the mean braking force is to calculate the static braking force:

$$F_{Static} = \mu_{Brake} \cdot W_{Landing}$$

Next, the initial braking force is:

$$F_{Initial} = \mu_{Brake} \cdot W_{Landing} - \frac{1}{2} \cdot \rho \cdot V_{TD}^2 \cdot \left(\mu_{Brake} \cdot C_{LGround} - C_{DGround}\right)$$

The braking factor is:

$$K_{Brake} = \frac{\left(1 - F_{Initial} / F_{Static}\right)}{Log\left(F_{Static} / F_{Initial}\right)}$$

And finally, the mean braking force is:

$$F_m = K_{Brake} \cdot F_{Static}$$

Corrections must be made to the landing lift curves and landing drag polars in ground effect during the braking segment of landing using equations found in Roskam and Lan (1997). First, the effective aspect ratio in ground effect is:

$$AR_{Weffective} = AR_W \cdot \left(0.2 + 0.7855 \cdot \left(\frac{Clearance}{b_W / 2} \right)^{0.468945} - 0.07164 \cdot \left(\frac{Clearance}{b_W / 2} \right)^{2.0033} \right)$$

The ratio of the lift curve slopes in and out of ground effect is:

$$\frac{C_{L\alpha}}{C_{L\alpha Ground}} = \frac{AR_W}{AR_{Weffective}} \cdot \frac{2 + \sqrt{AR_{Weffective}^2 \left(1 + \frac{TAN^2\left(\Lambda_{W,c/2}\right)}{1 - M_{Landing}^2}\right) + 4}}{2 + \sqrt{AR_W^2 \cdot \left(1 + \frac{TAN^2\left(\Lambda_{W,c/2}\right)}{1 - M_{Landing}^2}\right) + 4}}$$

The effective angle of attack in ground effect is:

$$\alpha_{GroundEffect} = \left(0.6 \cdot t/c_{inboard} + 0.4 \cdot t/c_{outboard}\right) \cdot \left(3.5655 \cdot \left(\frac{\bar{c}}{Clearance}\right) - 0.177 \cdot \left(\frac{\bar{c}}{Clearance}\right)^2\right)$$

Now the lift coefficient in ground effect becomes:

$$C_{LGround} = \frac{C_L}{C_{L\alpha}/C_{L\alpha Ground}} - \frac{C_{L\alpha}}{C_{L\alpha}/C_{L\alpha Ground}} \cdot \alpha_{GroundEffect}$$

The ground roll drag coefficient is:

$$C_{DGround} = C_{DoApproach} + \frac{f}{\pi \cdot AR_W} \cdot \left(C_L^2 + \left(\frac{1}{f_{Approach}} - 1\right) \cdot \left(C_{LBreak,Approach} - C_L\right)^2\right) - \frac{f \cdot \sigma' \cdot C_{LGround}^2}{\pi \cdot AR_W}$$

where f is the wingtip-mounted engine lift dependent drag factor. The ground effect factor for the drag polar, σ', is given by:

$$\sigma' = \frac{\left(1 - \frac{1.32 \cdot Clearance}{b_W}\right)}{\left(1.05 + \frac{7.4 \cdot Clearance}{b_W}\right)}$$

Note that ground effect is not considered at take-off. The balanced field length equation does not require aerodynamic information for conditions other than second segment climb.

The missed approach climb gradient is calculated in the same way as the second segment climb gradient with few exceptions. First, the weight of the aircraft at landing is assumed to be 73% of the take-off gross weight, as specified by LMAS. Second, all engines are operational. Third, the landing drag polar is used, which is distinct from the take-off drag polar. Minimum missed approach climb gradients for aircraft having 2-4 engines are presented in Table 3.3. The FAR minimum missed approach climb gradient constraint and landing distance constraint are never violated in this study.

Table 3.8. Minimum Second Segment and Missed Approach Climb Gradients.

Number of Engines	Minimum Second Segment Climb Gradient	Minimum Missed Approach Climb Gradient
2	0.024	0.021
3	0.027	0.024
4	0.030	0.027

The drag polars take the general form:

$$C_D = C_{Dm} + f \cdot k \cdot (C_L - C_{Lm})^2 + f \cdot k_{Break} \cdot (C_L - C_{LBreak})^2$$

Where

$$k = \frac{1}{\pi \cdot AR_W \cdot e} \qquad \text{and} \qquad k_{Break} = \frac{1}{\pi \cdot AR_W \cdot e_{Break}}$$

when $C_L > C_{LBreak,}$ and $k_{Break}=0$ otherwise. The factors e and e_{Break} are read in from the input file. The minimum drag coefficient, C_{Dm}, is found by:

$$C_{Dm} = C_{DmFactor} \cdot \frac{S_{Wet}}{S_{ref}}$$

where $C_{DmFactor}$ is read in from the input file. All factors are based on LMAS drag polars for aircraft take-off and landing configurations.

The wing aspect ratio used for the take-off and landing drag polars, AR_W, takes a different form than the wing aspect ratio used for wing weight estimation. The wing aspect ratio used by FLIPS.F is the square of the wingspan divided by the reference area. The reference area is the wing area minus the Yehudi flap area. AR_W is the square of the wingspan divided by the wing planform area. The drag polar correlation made with LMAS data is unaffected because the LMAS drag polars were for single taper wings without Yehudi flaps. The reason for using a different aspect ratio for these drag polars (k and k_{break} terms) is that the reference area based aspect ratio becomes very large for the cantilever wing. In this case the wing root chord is restricted if the wingtip chord and wing break chord are both small. This is because the reference area is the area enclosed by the leading and trailing edges of the outboard panel and their inboard projections. The balanced field length and second segment climb constraints are so difficult to meet that the cantilever wing aircraft would manipulate this geometry specification to give wings with very narrow outboard panel chords. Obviously, this is an artificial effect, because aircraft do not reduce the wing break chord to meet field performance requirements.

Chapter 4

Results

4.1 Summary

The results of this study include minimum take-off gross weight and minimum fuel weight designs at various technology levels and range requirements. The cases are arranged in three parts: point optima (Figure 4-1a-c), sensitivity analysis, and range investigations. A total of 75 cases are presented.

Figure 4-1a is a matrix of the 14 primary cases of interest. The columns are arranged by configuration and the rows by mission. . Each element in the matrix is a half-wing planform of an optimum design. The configurations from left to right are the cantilever, T-Tail SBW with fuselage-mounted engines, SBW with wingtip-mounted engines, and the SBW with underwing engines outboard of the strut. The missions from top to bottom are the 2010 technology full mission minimum TOGW, 2010 technology full mission minimum fuel, 2010 technology economic mission minimum TOGW, and 1995 technology full mission minimum TOGW. Each element in Figure 4-1a will be described in greater detail later. Figure 4.1b shows how a given configuration can change with various missions. Vicki Johnson (1990) presented her cost optima results in a similar format. Figure 4.1c demonstrates how varied the final planform of a given mission are for the configurations.

Note that a color-coding representation of the various configurations has been introduced in Figure 4.1a-c. The cantilever wing is black, T-tail fuselage mounted engine SBW is red, the wingtip-mounted engine SBW is blue and the underwing-engine SBW is green. This color convention is used in figures and tables from this point forward.

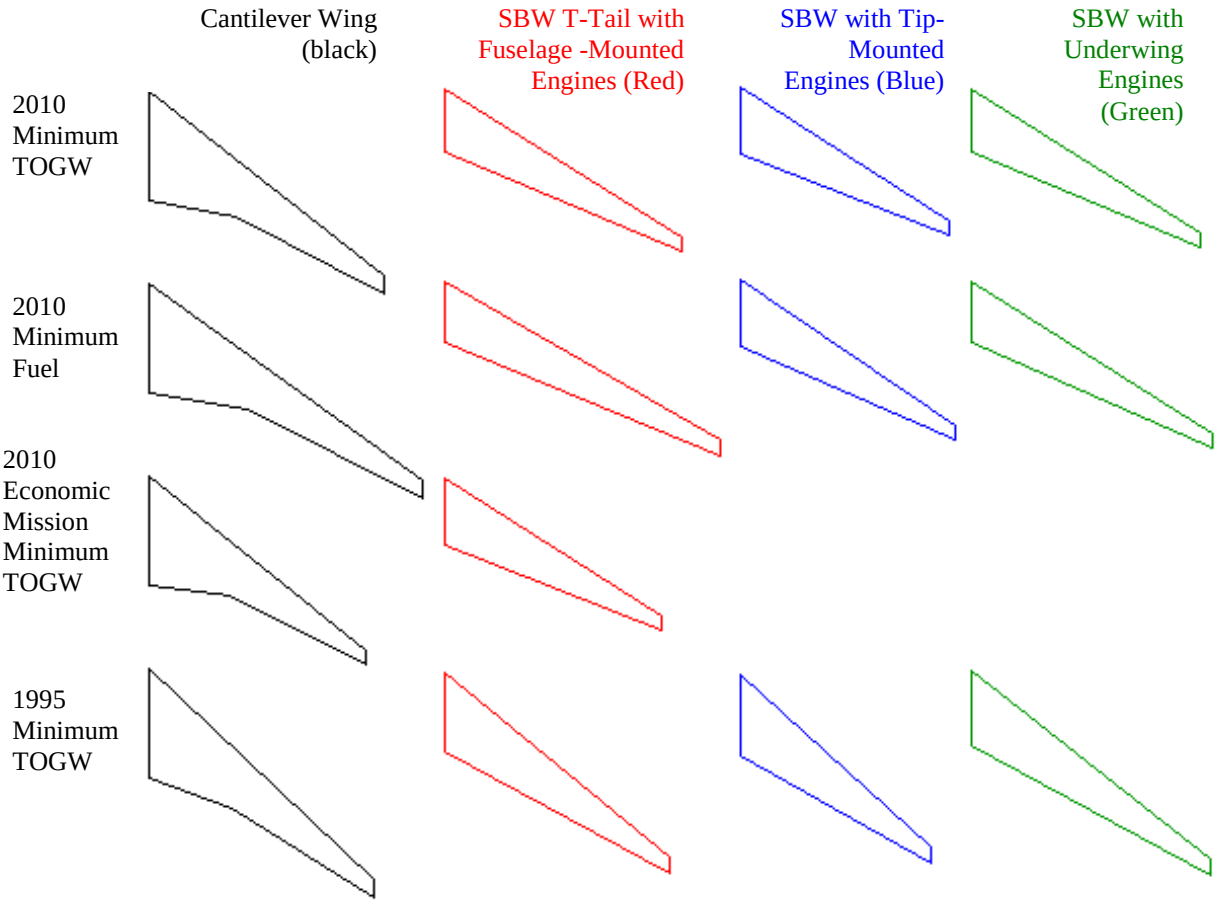

a) Study Matrix.

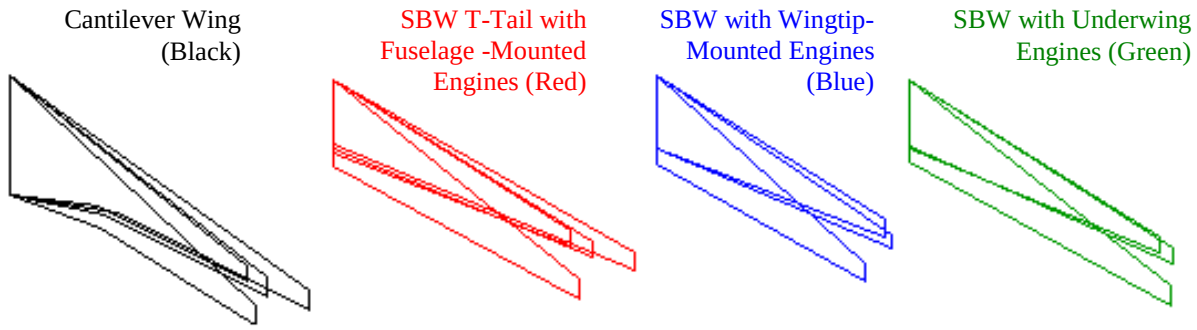

b) Variations within a Single Configuration for Different Objective Functions.

Figure 4.1. Wing Planforms for Different Configurations and Objective Functions.

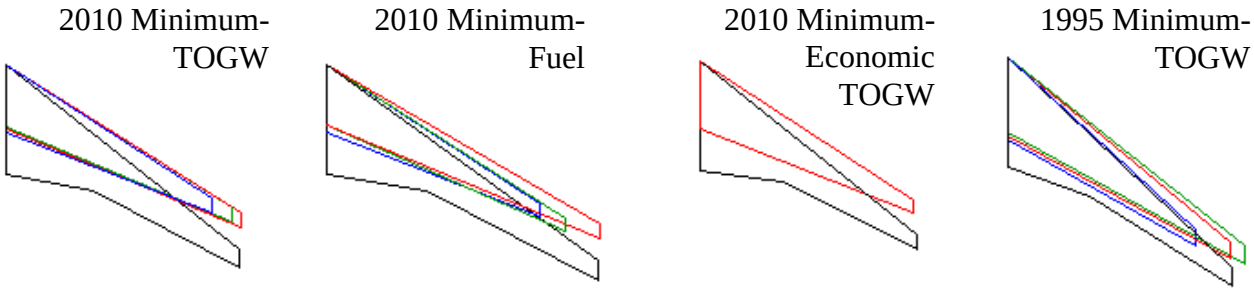

c) Variations within a Single Objective Function for Different Configurations.

Figure 4.1. Continued.

4.2 Minimum Take-Off Gross Weight Optima

Table 4.1 lists the results of the minimum-TOGW cantilever, fuselage-mounted engine T-Tail SBW, wingtip-mounted engine SBW and underwing engine SBW with the engines mounted either inboard or outboard of the strut. Figures 4.2a-c show the graphical output of the four main cases. The SBW is superior to the cantilever configuration for the minimum-TOGW objective function. While the SBW has between 9.2-17.4% decrease in TOGW for minimum TOGW designs, the savings in fuel consumption are even more impressive. A SBW has between 14.3-21.8% lower fuel burn than a cantilever configuration when optimized for minimum-TOGW, and between 16.2-19.3% lower fuel weight when both are optimized for minimum fuel weight.

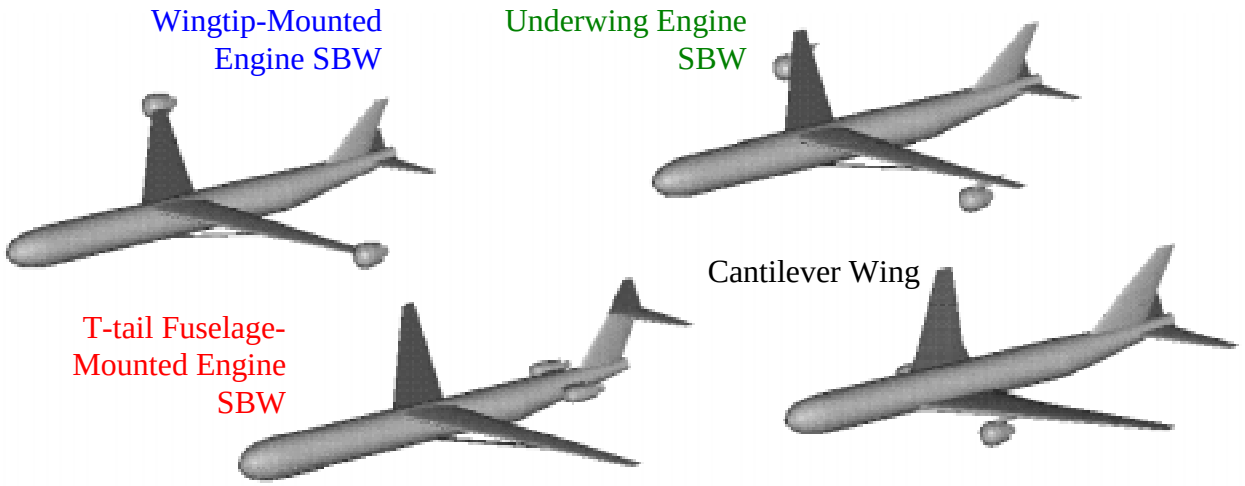

a) Isometric Views.

Figure 4.2. 2010 Minimum-TOGW Designs.

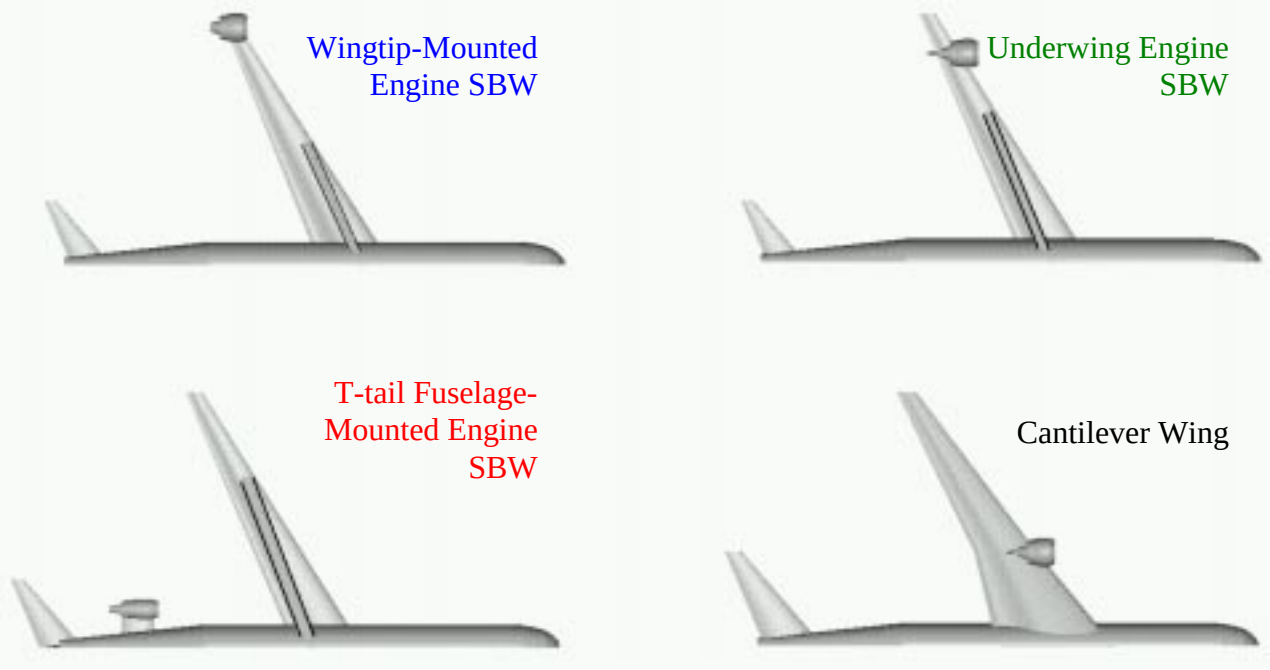

b) Planview from Below.

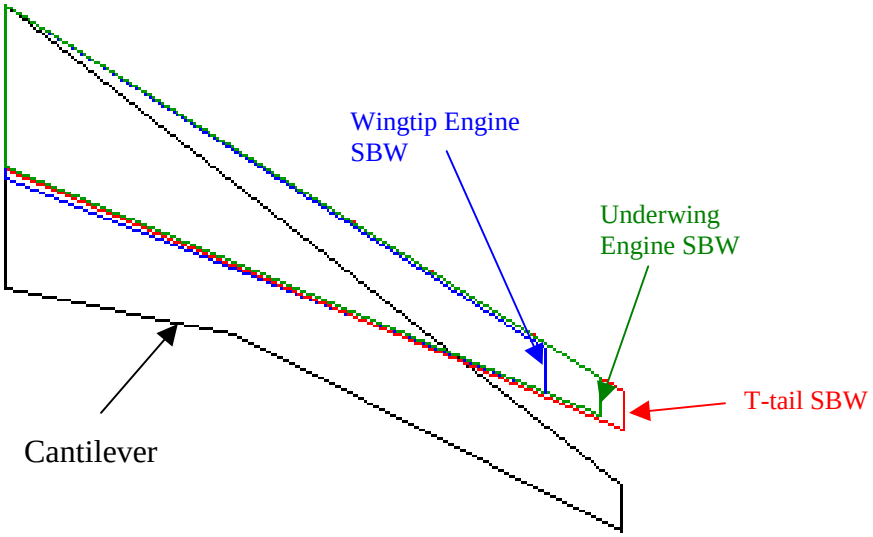

c) Wing Planform Comparison.

Figure 4.2. Continued.

Table 4.1. 2010 Minimum-TOGW Designs.

Cantilever Wing-Eng.	SBW T-Tail	SBW Tip Engines	SBW Underwing	
225.3	226.0	198.6	220.1	Span (ft)
52.0	30.2	31.8	29.4	Root Chord (ft)
5307	4205	3907	3970	S_w (ft^2)
9.57	12.15	10.10	12.20	AR
15.14%	14.28%	14.36%	14.00%	Root t/c
10.55%	6.58%	7.56%	7.15%	Break t/c
7.40%	6.56%	6.85%	7.37%	Tip t/c
34.2	29.9	30.2	29.8	Wing $\Lambda_{1/4}$ (deg)
	20.5	23.5	21.6	Strut $\Lambda_{1/4}$ (deg)
	68.8%	56.8%	62.4%	η Strut
37.0%		100.0%	83.8%	η Engine
75793	59463	51851	56562	T_{max} (lbs)
42052	40429	40736	40097	Cruise Altitude (ft)
23.38	25.33	25.25	25.30	L/D
63706	59581	41854	50287	Wing Wt. (lbs)
47266	42473	25213	33335	Bending Matl (lbs)
186295	159629	145618	151342	Fuel Wt. (lbs)
540230	**490312**	**446294**	**464556**	TOGW (lbs)
1563.24	1507.06	1461.97	1480.44	Total Cost ($M)
87.49	82.69	76.70	79.01	Acquisition Cost ($M)
583.68	538.49	504.86	518.75	DOC ($M)
892.07	885.88	880.41	882.68	IOC ($M)
	9.2%	17.4%	14.0%	% TOGW Improvement
	14.3%	21.8%	18.8%	% Fuel Improvement
	21.5%	31.6%	25.4%	% Thrust Reduction
	3.6%	6.5%	5.3%	% Cost Reduction
ACTIVE	ACTIVE	ACTIVE	ACTIVE	Shock Cl Constraint
ACTIVE	ACTIVE		ACTIVE	2nd Segment Climb
	ACTIVE	ACTIVE	ACTIVE	Balanced Field Length
				Initial Cruise ROC
		ACTIVE	ACTIVE	Wingtip Deflection
ACTIVE				Engine Out
				Approach Velocity
				Fuel Volume

Some trends can be observed from these results which will be found in most cases to follow. In general, the T-tail fuselage-mounted engine SBW has nearly the same span as the cantilever wing configuration. The underwing engine SBW cases have less span than either the T-tail fuselage-mounted engine SBW or the cantilever wing due to the wingtip deflection constraint. Similarly, the wingtip deflection constraint limits the span of the wingtip-mounted engine SBW

such that it has the least span of all arrangements. The configurations, from lightest to heaviest, are the wingtip-mounted engine SBW, underwing engine SBW, T-tail fuselage-mounted engine SBW and cantilever wing. At a 7500 nautical mile range, the same order applies for fuel weight, moving from least to most fuel burned. Figure 4.2c shows the wings of the four main configurations for the 2010 minimum-TOGW cases. Note that there is a break in the trailing edge of the cantilever wing, and the SBW cases generally have much less sweep and less wing area.

As discussed in Chapter 1, the SBW sweep reduction is largely due to a reduction in *t/c* (5.2-7.5% lower for 2010 minimum-TOGW SBW cases), which reduces transonic wave drag. The *t/c* reduction allows the SBW wing to have less sweep than a cantilever wing for the same amount of wave drag. The sweep reduction promotes natural laminar flow. It also decreases the wing structural weight. The combination of these effects drives the SBW wing sweep to lower values than for the cantilever wing configuration (usually around 4^o less sweep).

4.3 Minimum-Fuel Optima

Table 4.2 lists the results of the minimum-fuel cases, and Figures 4.3a-c show the corresponding graphical outputs. These aircraft have greater wingspans to increase the *L/D* and for flight at higher altitudes. The cantilever wing uses 4.62% less fuel, the minimum-fuel T-tail SBW uses 6.76% less fuel than its minimum-TOGW counterpart, the wingtip-mounted engine SBW uses 2.19% less fuel and the underwing engine SBW uses 2.41% less fuel. The fuel reduction for the wingtip-mounted engine and the underwing engine SBW cases are relatively small because the wingtip deflection constraint limits the wingspan. The minimum-fuel-SBW TOGWs are 9.7-19.9% lower than an equivalent cantilever design. The cantilever wing configuration *L/D* increases from 23.4 to 26.4 going from the minimum-TOGW to the minimum fuel objective function, from 25.3 to 29.2 for the T-tail fuselage mounted engine SBW, from 25.3 to 26.1 for the wingtip-mounted engine case and from 25.3 to 26.3 for the underwing engine SBW. The *L/D* increase for the wingtip-mounted engine and underwing engine SBW configurations from changing the objective function from TOGW to fuel weight is very small, because the wingspan experiences little change. Improved aerodynamic efficiency for all configurations except for wingtip-mounted engine and underwing engine cases is achieved by increasing the wing span, but this incurs a cost in structural weight. The increase in TOGW when the objective function is

changed from TOGW to fuel weight is 16,915 pounds for the T-tail SBW and 21,663 pounds for the cantilever wing. TOGW changes for the underwing engine SBW and wingtip engine SBW cases are small.

Fuel burn is likely to be an increasingly important factor in aircraft design from two perspectives. First, as the Earth's petroleum resources are depleted, the cost of aviation fuel will rise. Any reduction in fuel demand will be welcome if the fuel price becomes a larger part of transport life cycle cost. Second, strict emissions regulations stemming from environmental concerns will limit the amount of pollutant discharge permitted by an aircraft. Beyond engine design, reducing the overall amount of fuel consumed for a given flight profile by improved configuration design will also reduce the total amount of emissions.

Airport noise pollution can limit the types of aircraft permitted to use certain urban airfields and impose operational restrictions on those that do. Simply speaking, minimizing engine size can also be expected to reduce the noise generated if the engine is of similar design. Minimum-TOGW SBW engine thrust is reduced by 21.5-31.6% over the equivalent cantilever design. Perhaps the noise pollution at an airport can be reduced by a similar amount.

Table 4.2. Minimum Fuel Optimum Designs.

Cantilever Min Fuel	SBW T-Tail Min F	SBW Tip Eng Min F	SBW Wing Eng	
260.9	262.1	204.3	230.6	Span (ft)
52.0	28.4	32.0	29.1	Root Chord (ft)
5793	4723	3933	4113	S_w (ft^2)
11.75	14.54	10.61	12.92	AR
12.97%	12.20%	14.07%	13.78%	Root t/c
9.27E-02	6.22%	7.52%	7.12%	Outboard t/c
5.21E-02	5.95%	6.88%	7.52%	Outboard t/c
32.5	28.3	31.7	30.5	Wing $\Lambda_{1/4}$ (deg)
	22.0	24.3	22.3	Strut $\Lambda_{1/4}$ (deg)
	65.9%	53.8%	60.2%	η Strut
37.0%		100.0%	82.9%	η Engine
71032	56304	52285	54973	T_{max} (lbs)
43783	42723	40765	40518	Cruise Altitude (ft)
26.37	29.23	26.08	26.34	L/D
92991	85558	47120	56488	Wing Wt. (lbs)
78456	68276	30914	39593	Bending Matl (lbs)
177692	**148838**	**143425**	**147695**	Fuel Wt. (lbs)
561893	507227	449926	466858	TOGW (lbs)
1578.38	1518.53	1464.85	1481.49	Total Cost ($M)
92.66	87.54	77.76	80.12	Acquisition Cost ($M)
590.96	543.02	506.22	518.41	DOC ($M)
894.76	887.98	880.87	882.96	IOC ($M)
	9.7%	19.9%	16.9%	% TOGW Improvement
	16.2%	19.3%	16.9%	% Fuel Improvement
	20.7%	26.4%	22.6%	% Thrust Reduction
	3.8%	7.2%	6.1%	% Cost Reduction
ACTIVE	ACTIVE	ACTIVE	ACTIVE	Shock CI Constraint
ACTIVE				2nd Segment Climb
	ACTIVE	ACTIVE	ACTIVE	Balanced Field Length
	ACTIVE			Initial Cruise ROC
		ACTIVE	ACTIVE	Wingtip Deflection
				Engine Out
				Approach Velocity
				Fuel Volume

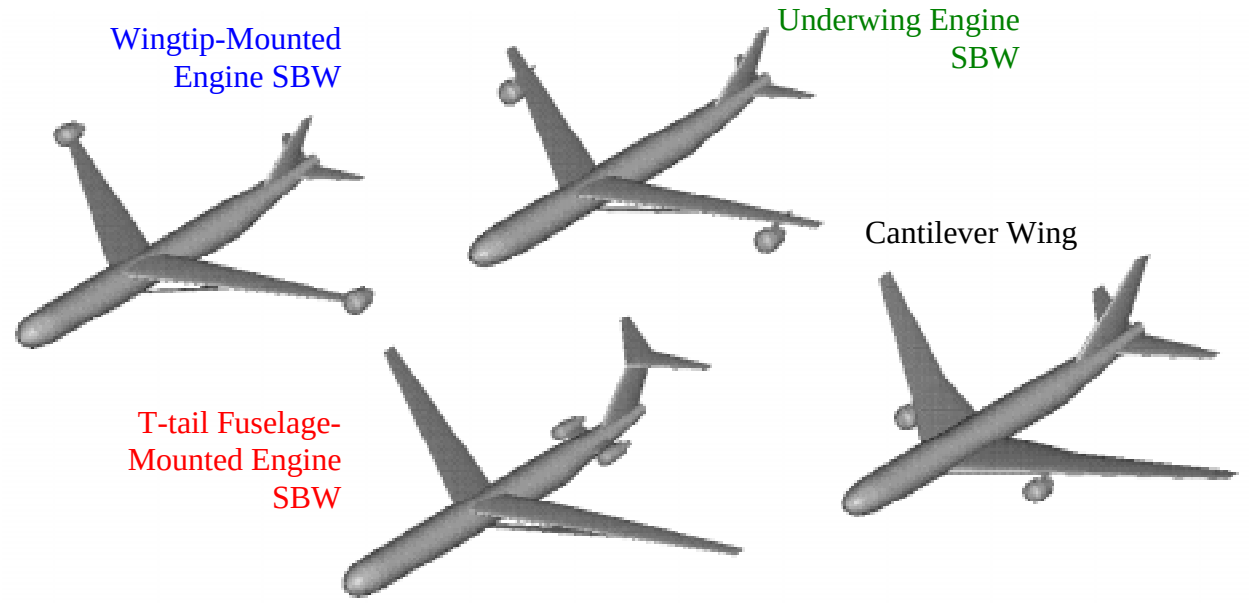

a) Isometric View.

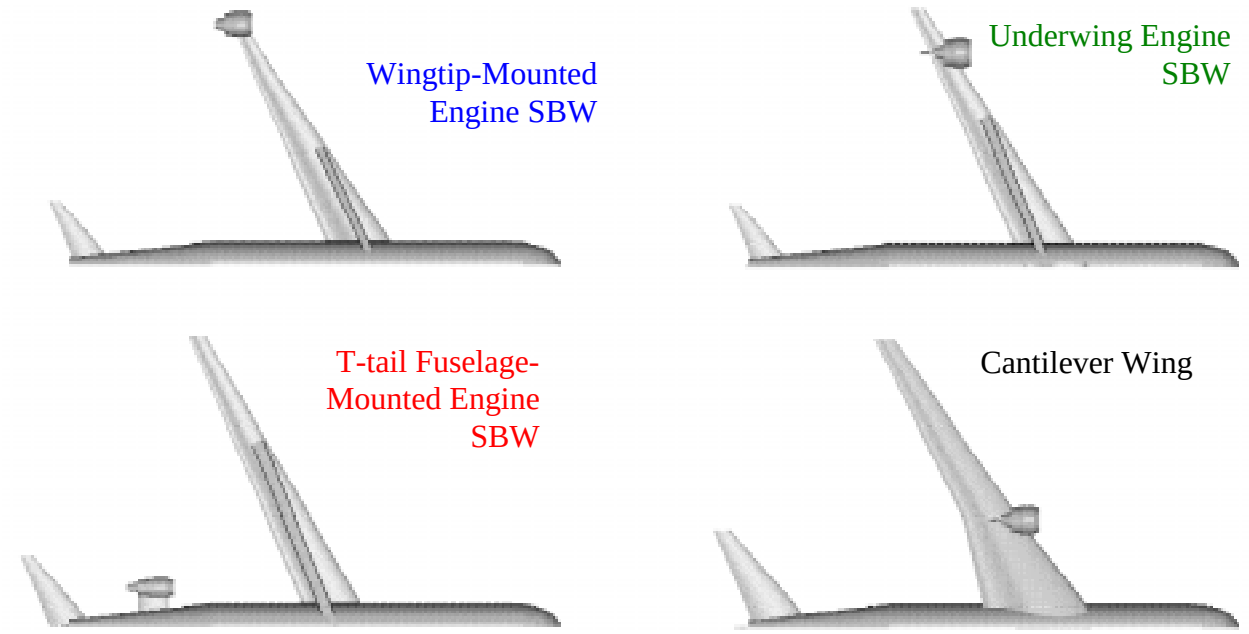

b) Planview from Below.

Figure 4.3. 2010 Minimum-Fuel Designs.

Figure 4.3c shows the overlay of the four 2010 minimum-fuel optima. Again, the cantilever wing has a break in the trailing edge, greater sweep and more area than the SBW designs. Similar wingspan trends are found in the minimum-fuel and minimum TOGW cases. The T-tail

SBW has the largest wingspan, the cantilever concept is slightly less, and then the underwing engine SBW, followed by the wingtip-mounted engine SBW.

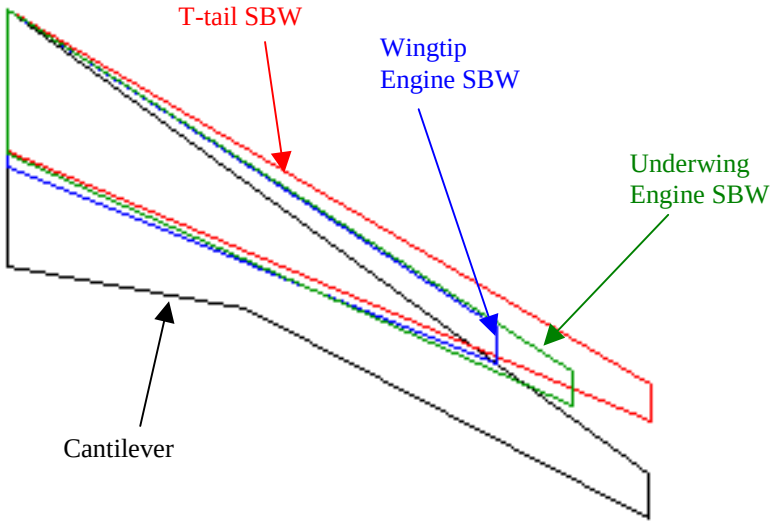

c) Wing Planform Comparison.

Figure 4.3. Continued.

4.4 Economic Mission Analysis

Table 4.3 shows the results of the economic mission analysis. It is important to realize that while the economic mission aircraft is optimized for the minimum economic mission TOGW, the aircraft must also be capable of performing the full mission. Only the cantilever wing and T-tail fuselage-mounted SBW cases are considered. The economic mission analysis did not yield any strikingly different results except for the unexpected similarity in aircraft TOGW when optimized for either the full 7500 nautical mile mission or the 4000 nautical mile economic mission (see Table 4.3). The economic mission and full mission optima have little in common for a given configuration except for the similar TOGW at a design condition. The economic mission aircraft have 16.9-20.5 feet less span (see Figure 4.4), cruise at lower altitudes, and have a lower L/D than their full mission equivalents for both the SBW and cantilever cases. By decreasing the wing span at a reduced passenger and fuel load, the wing bending material weight is less and so is the resulting economic TOGW. Apparently, the *L/D* decrease associated with the span reduction at the full mission scenario adversely affects the full mission TOGW for the minimum economic TOGW optimum. The TOGW at the 7500 nautical mile range is negligibly increased (0.8-1.3%) for those vehicles optimized for the economic mission compared to those

optimized for the full mission. The economic mission TOGW is slightly lower for the full mission optimized cantilever wing case, but the difference is very slight. In other words, the weights at the economic mission condition for the cantilever wing economic mission optimum and the full mission optimum are about the same within the fidelity level of the analysis.

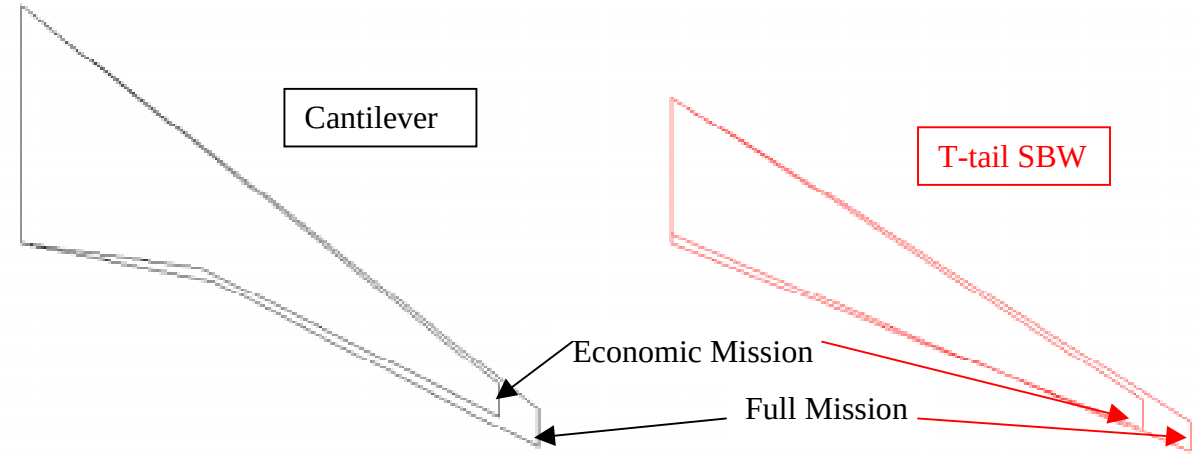

Figure 4.4. Economic Mission Minimum-TOGW and Full Mission Minimum-TOGW Wings.

Table4.3. Economic Mission Results.

Cantilever Wing-Eng.	Cantilever Econ Mission	SBW T-Tail	SBW T-Tail Econ	
225.3	208.4	226.0	205.5	Span (ft)
52.0	52.0	30.2	32.1	Root Chord (ft)
5307	4611	4205	3948	S_w (ft^2)
9.57	9.42	12.15	10.70	AR
15.1%	15.3%	14.3%	14.4%	Root t/c
10.6%	10.8%	6.6%	7.2%	Outboard t/c
7.4%	7.0%	6.6%	6.6%	Outboard t/c
34.2	34.5	29.9	30.2	Wing $\Lambda_{1/4}$ (deg)
		20.5	20.3	Strut $\Lambda_{1/4}$ (deg)
		68.8%	69.0%	η Strut
37.0%	37.0%			η Engine
75793	80909	59463	64846	T_{max} (lbs)
42052	38151	40429	38182	Cruise Altitude (ft)
23.38	21.90	25.33	23.27	L/D
63706	57360	59581	50244	Wing Wt. (lbs)
47266	41585	42473	33536	Bending Matl (lbs)
186295	197896	159629	171022	Fuel Wt. (lbs)
540230	547499	**490312**	494374	TOGW (lbs)
	-0.2%		0.7%	% Econ TOGW Improv.
421276	**422124**	384220	**381707**	Econ TOGW
ACTIVE	ACTIVE	ACTIVE	ACTIVE	Shock CI Constraint
ACTIVE	ACTIVE	ACTIVE	ACTIVE	2nd Segment Climb
		ACTIVE	ACTIVE	Balanced Field Length
				Initial Cruise ROC
				Wingtip Deflection
ACTIVE	ACTIVE			Engine Out
				Approach Velocity
				Fuel Volume

4.5 Range Investigations

Figures 4.5 and 4.6 show the effects of range on TOGW and fuel weight. In each graph, minimum TOGW is the objective function. The SBW becomes increasingly desirable as the design range increases. The T-tail fuselage-mounted engine SBW TOGW reduction relative to the cantilever configuration steadily improves from 6.0% at a 4,000 nautical mile range up to 12.9% at 11,000 nautical miles. Similarly, the TOGW for the wingtip-mounted engine SBW steadily improves from 11.8-23.7% from 4,000 to 11,000 nautical miles, and the underwing engine SBW improves from 9.5-19.2% over the same range span. The T-tail SBW fuel weight savings fluctuates within about 11.3-16.8%, but it generally improves as the design range increases. The wingtip-mounted engine SBW fuel weight savings generally improves with range with values ranging from 17.6-25.8%. Similar trends are found for the underwing engine SBW with values ranging from 16.0-24.6%. The wingtip-mounted engine SBW is superior at all ranges in TOGW, but the underwing engine SBW burns less fuel as range increases. This shows that much of the wingtip-mounted engine SBW TOGW reduction is due to low structural weight rather than fuel consumption benefits relative to the underwing engine SBW case. Maximum fuel weight is set at 400,000 pounds. The T-tail SBW maximum range is 13,304 nautical miles at this fuel weight, whereas the cantilever configuration can only reach 11,906 nautical miles, or the SBW has 11.7% greater maximum range. To orient the reader, an aircraft can reach any destination on Earth with a 12,000-nautical mile range. The maximum range of the underwing engine SBW is 17.4% greater than the cantilever wing at the same maximum fuel weight. The wingtip-mounted engine SBW can not attain the same range as the other cases because the wingtip deflection severely limits the wingspan. The underwing engine SBW can move the engines inboard to meet the wingtip deflection constraint. At the maximum range condition, the underwing engine SBW engine location actually moves slightly inboard of the strut. In general, the SBW can either have a reduced fuel weight for a given range or an increased range for a given fuel weight relative to the cantilever configuration. Range case data tables can be found in the Appendix 2.

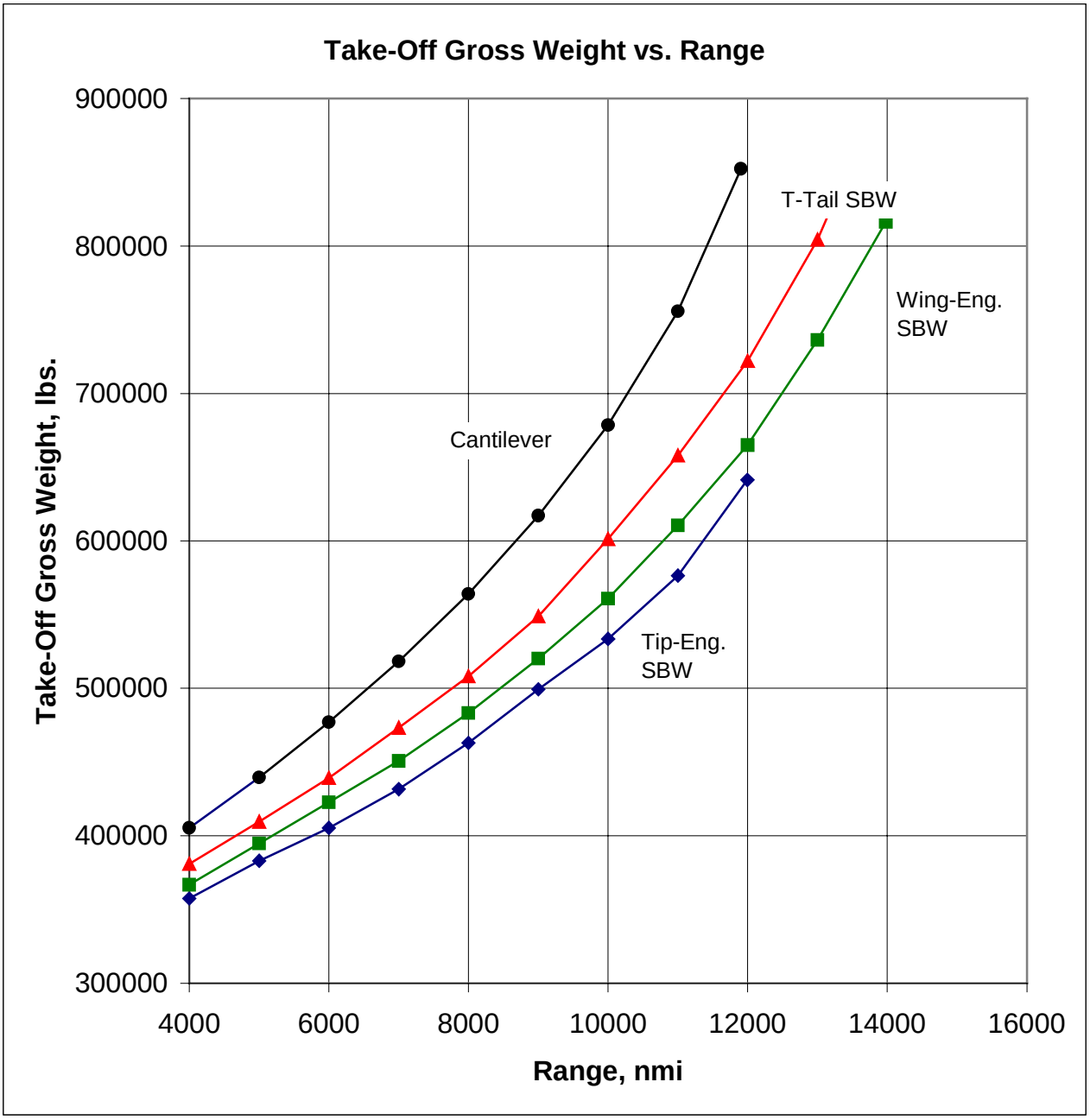

Figure 4.5. Effect of Range on TOGW for All Configurations at Minimum-TOGW.

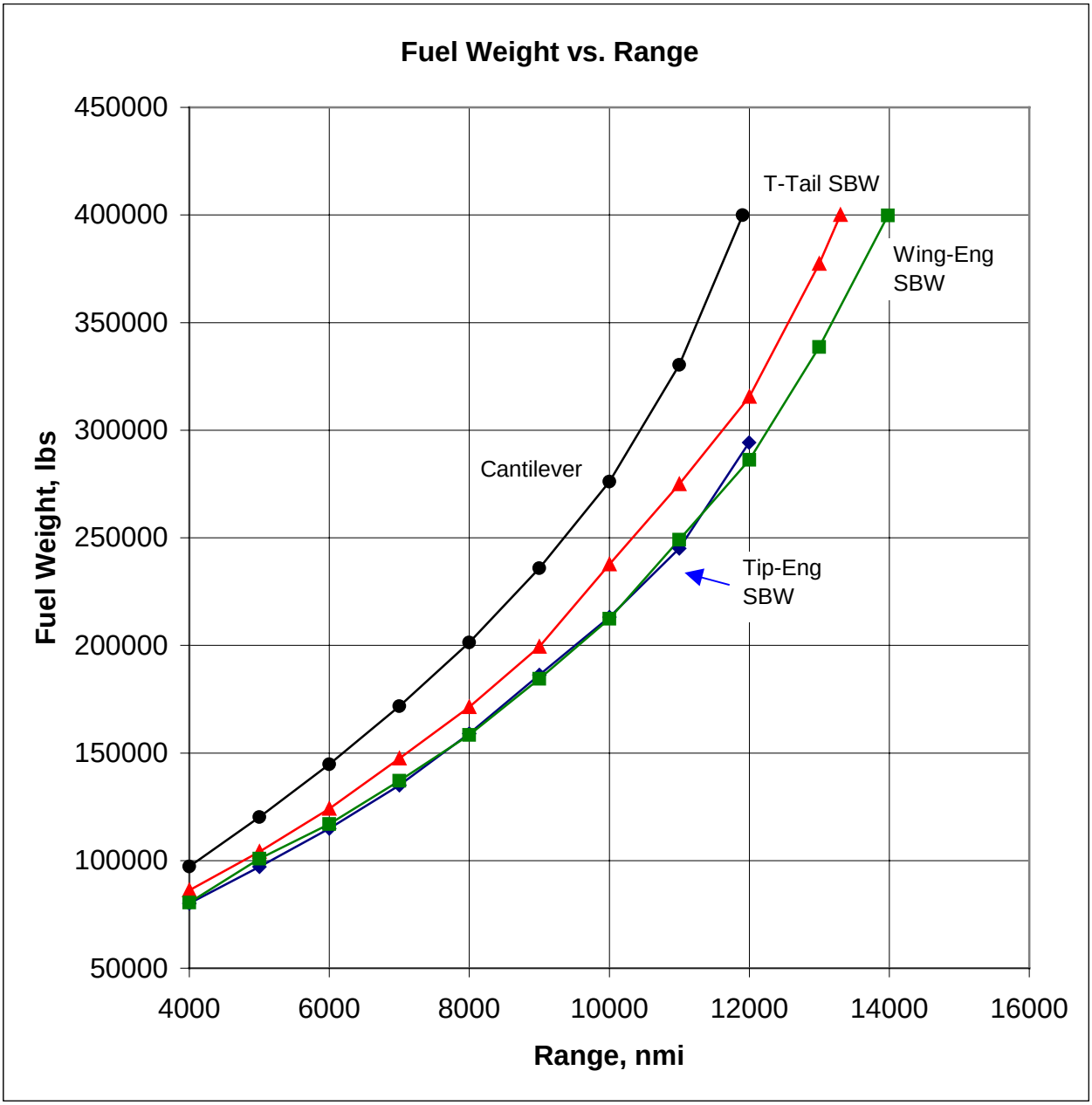

Figure 4.6. Effect of Range on Fuel Weight for All Configurations at Minimum-TOGW.

4.6 Technology Impact Study

The first step in performing the technology impact study is to find 1995 minimum-TOGW optima for all configurations. All weights technology factors are set to 1.0, no natural laminar flow is allowed, the wave drag airfoil technology factor is reduced and the tail volume coefficient is increased. Figures 4.7a-c show the graphical output of the 1995 minimum-TOGW

designs. Note that the wing sweep is greatly increased over the 2010 technology equivalents. SBW wing quarter chord sweeps increase by 6-7 degrees, and the cantilever wing sweep increases by about 5.5 degrees at the 1995 technology level. The sweep is increased to reduce the transonic wave drag, which is more critical with the lower airfoil technology factor. Also, there is no aerodynamic benefit in having low sweep when natural laminar flow is not permitted.

Figure 4.7c shows an overlay of the four 1995 minimum-TOGW wings. Like other cases, the T-tail SBW and cantilever wing have approximately the same wingspan, and the wingtip-mounted engine SBW has the least wingspan. Unlike earlier cases though, the underwing engine SBW has the greatest wingspan. This span increase helps increase the L/D by reducing the induced drag. The associated structural penalties are offset by the ripple-through effect of the fuel reduction due to increased aerodynamic efficiency. The 1995 technology level wingtip-mounted engine SBW wingspan is reduced by about 16.4 feet to meet the wingtip-deflection constraint with the higher engine weight.

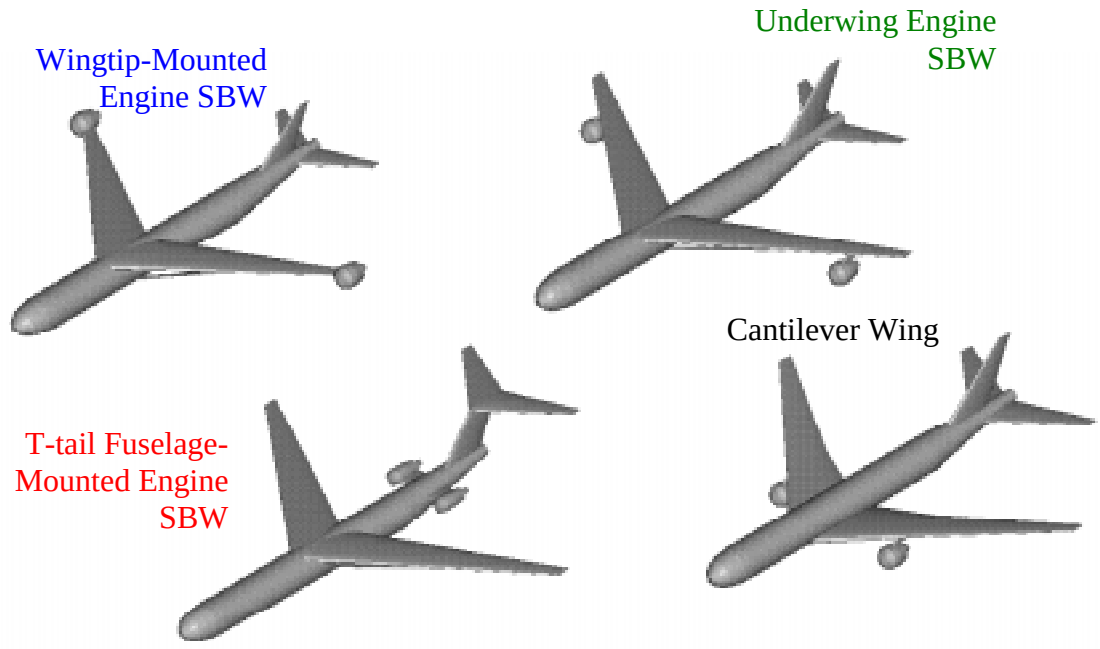

a) Isometric View.

Figure 4.7. 1995 Minimum TOGW Designs.

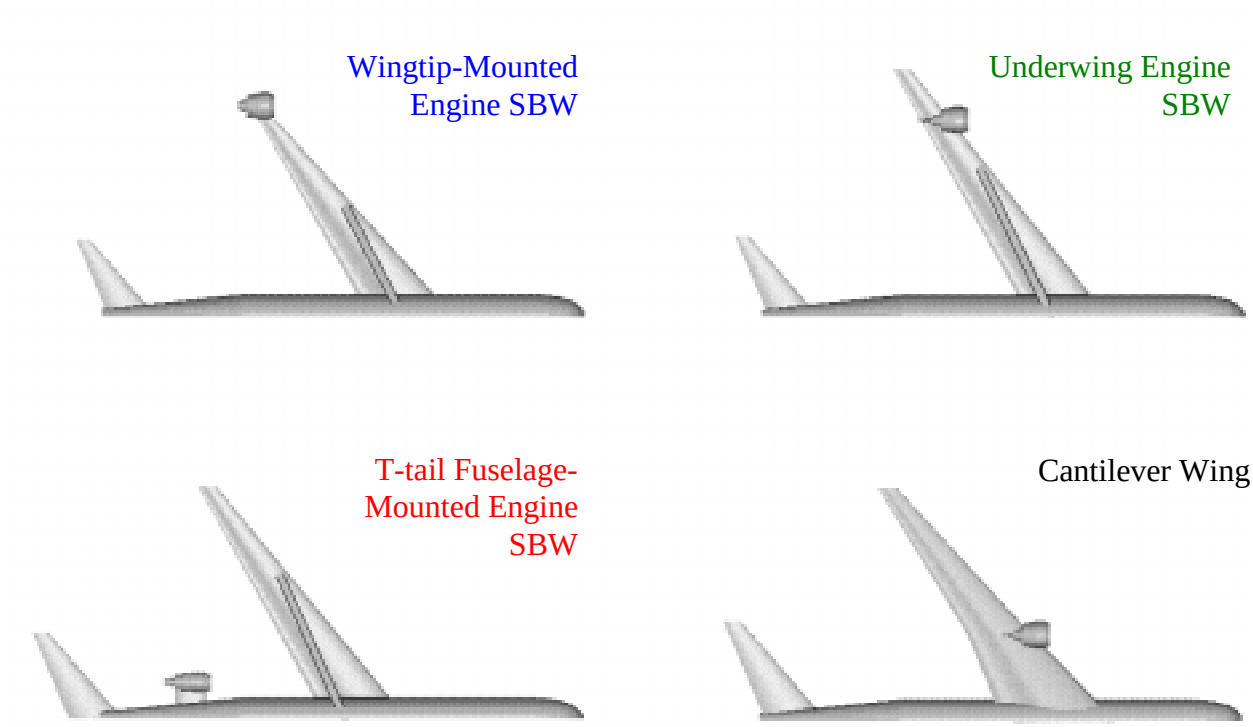

b) Planview from Below.

Figure 4.7. Continued.

Figures 4.8-4.11 show the results of the technology impact study. The top of the left figure is the 1995 technology level aircraft and the bottom is the 2010 technology level aircraft. Each step represents the resulting change in TOGW when a technology group is applied to the 1995 technology level aircraft. The sum of the TOGW changes of the technology groups when applied individually is on the left of the figure, and the overall change in TOGW between 1995 and 2010 technology level is presented on the right of the figure. The right figures show the TOGW and selected weight components of each aircraft.

The technology impact study shows that SBW configurations are more sensitive to improvements in natural laminar flow than the cantilever wing configuration. The sum of the changes made in each technology group is less than the total difference between the 1995 and 2010 SBW designs for all cases, showing that there is generally no overall synergism in the technology group application. The cantilever wing configuration is more responsive to all technology groups except for natural laminar flow than any of the SBW cases, suggesting that the cantilever wing aircraft will benefit more from development of these technologies than the SBW. However, the SBW is superior to the cantilever wing in TOGW and fuel consumption for

all technology levels investigated here. Technology impact study data tables can be found in Appendix 3.

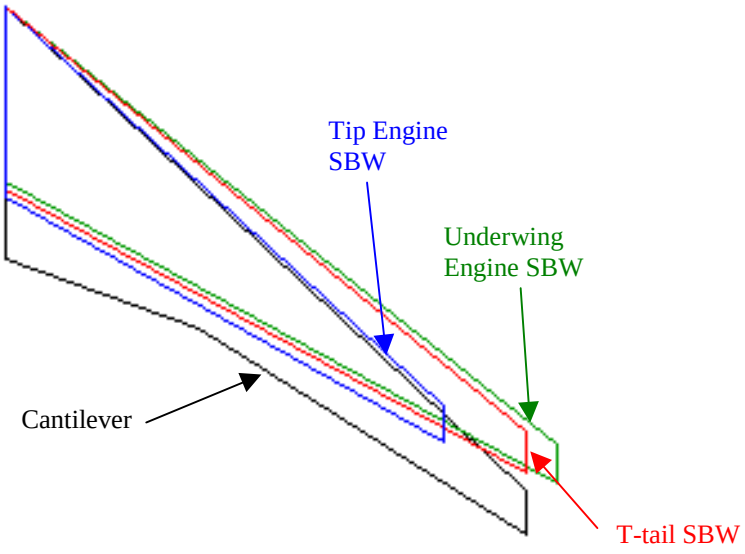

c) Wing Planform Comparison.

Figure 4.7. Continued.

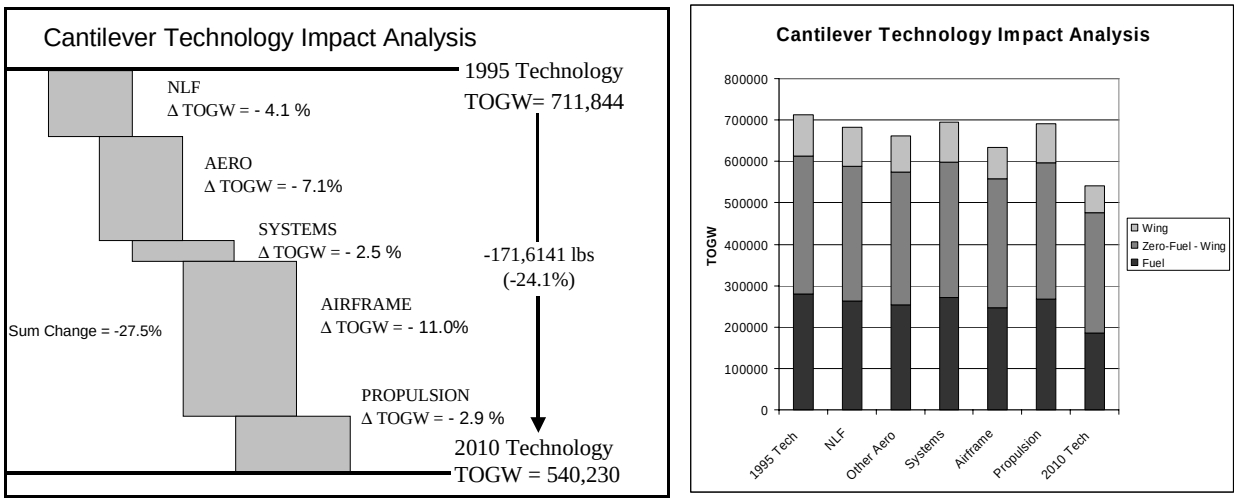

Figure 4.8. Cantilever Sensitivity Analysis.

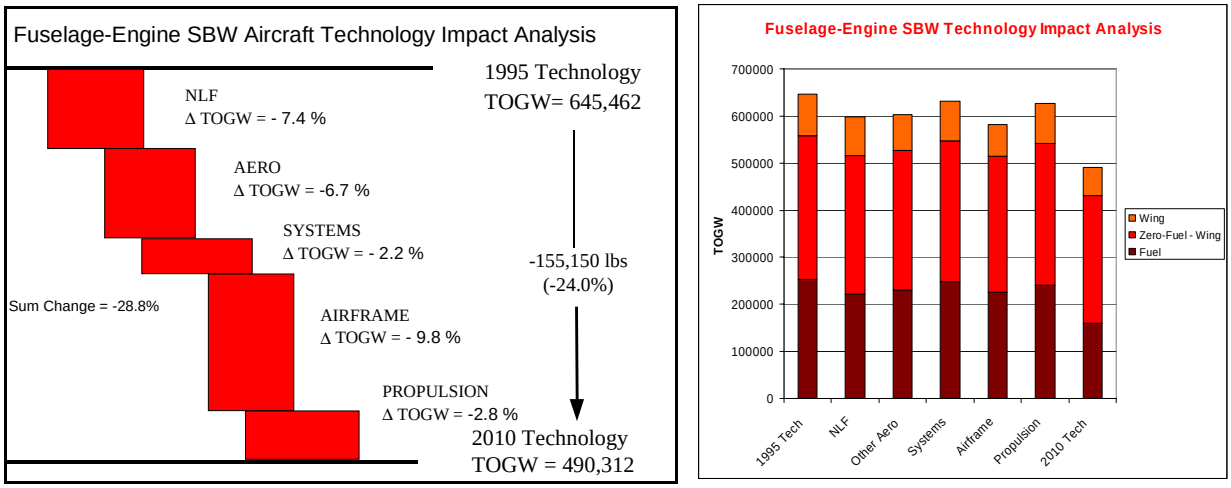

Figure 4.9. T-Tail SBW Sensitivity Analysis.

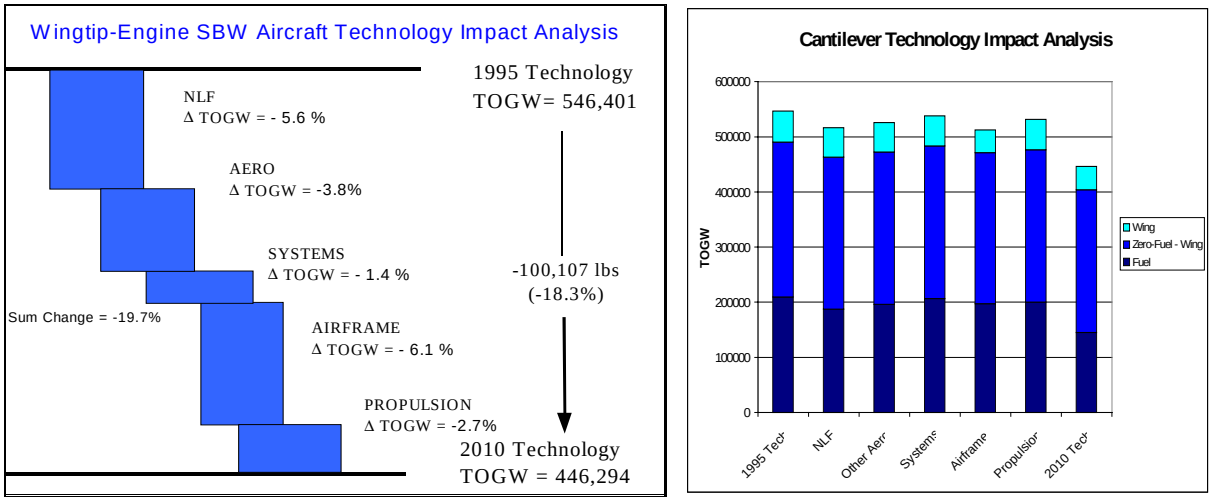

Figure 4.10. Tip-Mounted Engine SBW Sensitivity Analysis.

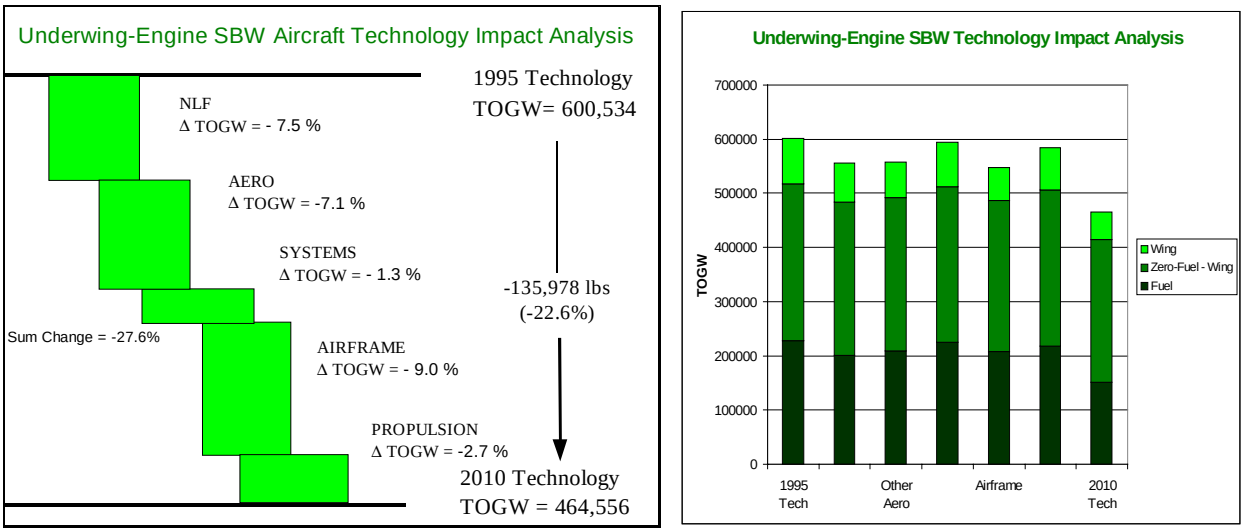

Figure 4.11. Underwing-Engine SBW Sensitivity Analysis.

4.7 Cost Analysis

The FLOPS cost module [McCullers] was used to determine the acquisition cost, direct operating cost and indirect operating cost of all vehicles. The acquisition and direct operating costs are less for the SBW cases than for the cantilever wing cases. The acquisition cost is a function of zero fuel weight. Typical acquisition cost reductions of the SBW designs range from 5.5-16.0%, with the wingtip-mounted engine SBW offering the greatest improvement. Direct operating cost is a function of fuel weight, so naturally the SBW cases offer improvements. SBW direct operating cost improvements over the cantilever wing configuration range from 8.1-14.3%, again with the wingtip-mounted engine case offering the greatest benefits. The indirect operating cost is a weaker function of TOGW, and the SBW has 0.8-1.6% improvement in this area. With this formulation, the total aircraft cost is the sum of the acquisition cost, direct operating cost and indirect operating cost. The total aircraft cost reductions for the SBW cases range from 3.8-7.2%. The SBW cost reductions are not as impressive as the fuel consumption and TOGW, because the costs are also strong functions of the number of passengers and other parameters that do not vary.

4.8 General Configuration Comparisons

The tip-mounted engine SBW is lighter than the fuselage mounted engine SBW because of engine inertia relief on the wing and induced drag reduction at take-off and cruise. Field performance constraints largely dictate the engine size, so any drag reduction produces large benefits. Although the tip-mounted engine vehicle is the lightest of the SBW cases, this configuration raises important issues. LMAS noted that the resultant net thrust and vertical tail lift at the engine-out condition would be at a 45-degree angle to the flight path. Obviously, this is not a practical flight condition. Even when circulation control is allowed, the engine-out constraint imposes severe limitations on the wing span, so the relative benefits are reduced as the TOGW increases.

The underwing engine SBW is a compromise between the wingtip-mounted engine SBW and the fuselage-mounted engine SBW. By not forcing the engines to remain at the tip, the wing can extend beyond the engines freely without running into the engine-out constraint. Because the height of the pylon plus the diameter of the nacelle is considered in the wingtip deflection constraint, it is often more difficult to satisfy than on the wingtip-mounted engine case. This constraint often forces the engines inboard towards the strut.

An underwing engine SBW case with the engines inboard of the strut is generally heavier than if the engines were located outboard of the strut. Engines provide inertia relief to the wing and are more effective for reducing the bending moment at the wing root as they move farther outboard. Thus, it is not surprising to see that the inboard engine case is heavier than the outboard engine case. The inboard engine case does offer the advantage of not requiring circulation control on the vertical tail, and may be a more viable candidate design solution. This configuration still offers advantages over the T-tail fuselage-mounted engine SBW. The T-tail fuselage-mounted engine case has no inertia relief on the wing due to the engine placement. Problems arise when engine/strut interference is considered, because the engine exhaust will blow on the strut when the underwing engine is located inboard of the strut. As a result, this case is not given further consideration.

One can learn much about an optimum design by noting the active constraints. In every optima presented here, the section lift coefficient limit constraint is active. This indicates that the aircraft do not fly at the altitude for best *L/D* and are thus penalized. Typically, the engines are sized based on balanced field length, second segment climb or rate of climb at initial cruise

altitude. The wingtip-mounted SBW engine sizing is dictated by the balanced field length and sometimes by rate of climb at initial cruise altitude. This is because the field performance requirements are greatly relaxed by the induced drag reductions from the tip engines. Other cases generally have the engines sized based on balanced field length and second segment climb.

One of the early concerns regarding the SBW configuration is the large increase in wingspan compared to cantilever wings seen in previous studies [Grasmeyer (1998A,B)]. More refined modeling of the wing structure and added realism brought about through work with LMAS has lessened the earlier trend. Indeed, now the T-tail SBW has about the same span as the cantilever configuration for the minimum TOGW and minimum fuel designs. The underwing engine SBW span is either slightly more or less than the cantilever wing, depending on the case. Part of the reason for the reduced underwing engine SBW span reduction is that the engine deflection is now part of the wingtip deflection constraint, making it much harder to satisfy. The optimum wingspans fall within the FAA 80-meter gate box limitation for all designs.

Chapter 5

Conclusions

Virginia Tech transport studies have shown the potential of the SBW over the traditional cantilever configuration. After much added realism by a major airframe manufacturer, the MDO analysis shows that the SBW still demonstrates major improvements over the cantilever wing configuration. Significant reductions in TOGW and cost were found, but the greatest virtues of the SBW may be its improved fuel consumption and smaller engine size. The SBW TOGW is reduced 9.2-17.4% for minimum-TOGW designs. The minimum-fuel optimum SBW aircraft burn 16.2-19.3% less fuel than an equivalent cantilever wing aircraft. Minimum-TOGW SBW aircraft engines are 21.5-31.6% smaller than a similar cantilever wing engine. These results indicate that the SBW will be more economically viable, reduce the consumption of natural resources, limit pollutant discharge and reduce noise pollution for urban airports. Advantages of the SBW increase with range, suggesting that this configuration may be ideal for larger, long-range transports.

The SBW exhibits a strong sensitivity to natural laminar flow technology. This implies that greater emphasis should be placed on laminar flow than on other systems and technologies in the development of the SBW. An investment in natural laminar flow technologies will give a greater return for the SBW than the cantilever wing configuration. Although the cantilever wing configuration shows more sensitivity to all other technology groups, the SBW is still lighter for every case.

The cooperative relationship with LMAS focussed on adding realism to the SBW design effort for direct comparisons with the cantilever design. Realism often takes the form of weight penalties and expanded performance analysis, which inevitably detracts from SBW theoretical potential. Presently efforts are underway to identify technologies and strut/truss arrangements to exploit the strengths of the strut. In other words, limiting the SBW design arrangements so that the aircraft takes the appearance of a cantilever wing with a strut may not be the most appropriate approach to realize the full potential of the SBW. Some possible design modifications are discussed in the recommendations section.

Finally, the SBW is likely to have a more favorable reaction from the public and aircrews than other competing configurations, especially for those who suffer from a fear of flying.

Affirmative passenger and aircrew acceptance is probable because other than the addition of a visually innocuous strut and a high wing, there is little to distinguish the SBW from the existing airliner fleet. Radical appearances of the blended-wing-body, joined wing, twin-fuselage, C-wing or other candidate configurations may cause apprehension in many flying patrons.

Chapter 6

Recommendations

One can envision a number of extensions to the general SBW layout studied here, with some ideas more daring than others. Such concepts include variations of analysis, configuration, or mission. This limited study demonstrates only a few of the advantages of the strut-braced wing.

Configuration changes may allow the SBW to exhibit further benefits. The strut vertical offset thickness has been assumed as identical to that of the strut. However, the strut offset must take much greater bending loads. Imposing drag penalties as a function of offset thickness but also allowing the thickness to vary will likely yield lower total weights.

One possible way to counter the engine-out problem for the tip-mounted engine configuration would be to add a more powerful engine on the centerline (Figure 6.1). If one of the tip engines fail, the other can be shut off and the centerline engine would provide the necessary thrust for the critical cases. This may raise unique dilemmas when attempting to certify this configuration because it is essentially a two engine aircraft from an engine failure point of view, but there are physically three engines. The FAA would have to decide if the vehicle should meet the two or three-engine requirements.

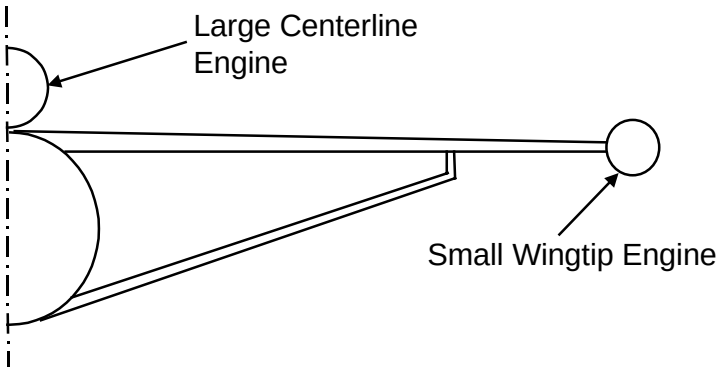

Figure 6.1. SBW with Large Centerline Engine and Small Wingtip Engines.

An arch strut, first suggested by Dr. Joseph Schetz, will eliminate many complex and heavy moving parts by allowing the strut to bend. By eliminating the threat of strut buckling, the demanding -2 G taxi bump case will no longer place such critical demands on the strut.

The vertical distance between the strut and the wing at the fuselage plays a significant role

in strut effectiveness. As the vertical separation increases, a smaller component of the strut force causes compression on the main wing. This lessens the wing skin thickness required to counteract buckling, and reduced the overall wing weight. A double-deck fuselage would greatly increase the vertical separation of the wing and strut at the fuselage. Other means of achieving a greater separation include using a parasol wing (Figures 6.2-6.3) or attaching the strut to downward-protruding landing gear pods (Figure 6.3). These arrangements may facilitate underwing engines inboard of the strut/wing intersection without unwanted exhaust interference effects with the strut.

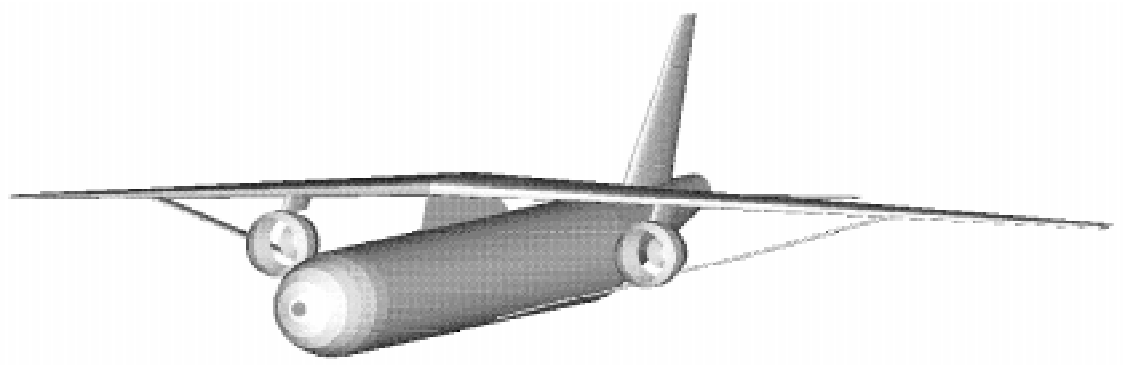

Figure 6.2. Parasol SBW Layout.

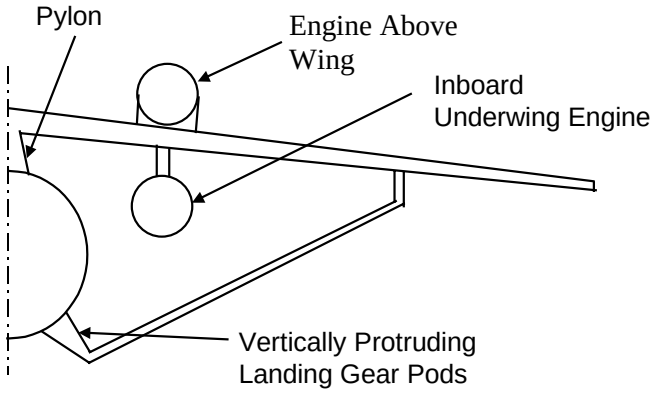

Figure 6.3. Parasol SBW with Landing Gear Pod Extensions.

Locating engines above the wings (Figure 6.3) can add inertia relief without interfering with the strut. Blowing over the upper wing surface will help decrease the take-off distance. Furthermore, inboard engines will not demand exotic schemes like vertical tail blowing to meet the engine-out constraint.

Perhaps the most fanciful of strut variations is to make the SBW a hydrofoil flying boat

(Figure 6.4). The FAA may be concerned that the SBW aircraft cabin may flood more quickly with its high-wing after a water landing than a low wing cantilever configuration. Virtue may be found in addressing this concern. Landing gear pods could extend out from the fuselage to act as sponsons, while the strut then extends up towards the wing. The fuselage and strut are partially submerged while the aircraft is at rest in the water. The strut is effectively a hydrofoil, lifting the aircraft out of the water as it accelerates. Retractable steps may be necessary to break rear fuselage suction. Imagine a luxury airliner flying from one port of call to the next in the nostalgic tradition of the Pan Am clippers of old. McMasters (1999) developed a similar concept for a C-wing configuration. Such a vehicle could also be used for cargo or utility for island nations or in major ports.

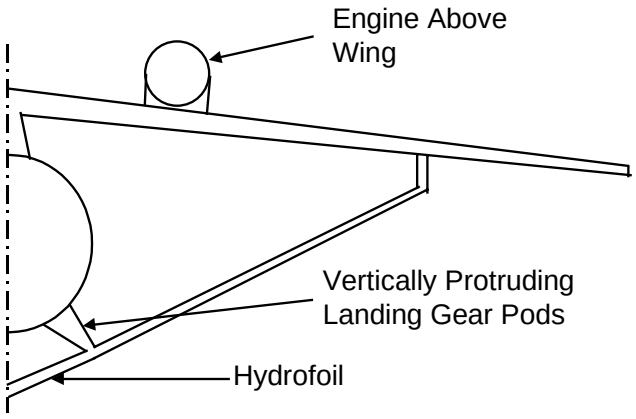

Figure 6.4. Hydrofoil SBW Configuration.

References

Braslow, A.L., Maddalon, D.V., Bartlett, D.W., Wagner, R.D., and Collier, F.S., "Applied Aspects of Laminar-Flow Technology," *Viscous Drag Reduction in Boundary Layers*, AIAA, Washington D.C., 1990, pp. 47-48.

Dollyhigh, S.M., Monta, W.J., and Sangiorgio, G., "Longintudinal Aerodynamic Characteristics at Mach 0.60 to 2.86 of a Fighter Configuration with Strut-Braced Wing," NASA-TP-1102, December 1977.

Grasmeyer, J.M., "Multidisciplinary Design Optimization of a Strut-Braced Wing Aircraft", MS Thesis, Virginia Polytechnic Institute & State University, April 1998A.

Grasmeyer, J.M., Naghshineh_Pour, A., Tetrault, P.-A., Grossman, B., Haftka, R.T., Kapania, R.K., Mason, W.H., and Schetz, J.A., "Multidisciplinary Design Optimization of a Strut-Braced Wing Aircraft with Tip-Mounted Engines", MAD 98-01-01, 1998B.

Grasmeyer, J., "Stability and Control Derivative Estimation and Engine-Out Analysis", VPI-AOE-254, January 1998C.

Grasmeyer, J., "A Discrete Vortex Method for Calculating the Minimum Induced Drag and Optimimum Load Distribution of Aircraft Configurations with Noncoplanar Surfaces," VPI-AOE-242, January 1997.

Hilton, W.F., *High Speed Aerodynamics*, Longmans, Green & Co., London, 1952.

Hoerner, S.F., *Fluid Dynamic Drag*, published by Mrs. Hoerner, 1965. Current address: P.O. Box 65283, Vancouver, WA 98665, pp. 8-1 – 8-20.

Jobe, C.E., Kulfan, R.M., and Vachal, J.D., "Wing Planforms for Large Military Transports," AIAA-78-1470, 1978.

Johnson, Vicki, "Minimizing Life Cycle Cost for Subsonic Commercial Aircraft", *Journal of Aircraft*, Vol. 27, No. 2, February 1990, pp. 139-145.

Kulfan, R.M., and Vachal, J.D., "Wing Planform Geometry Effects on Large Subsonic Military Transport Airplanes," Boeing Commercial Airplane Company, AFFDL-TR-78-16, February 1978.

Liebeck, R.H., Page, M.A. and Rawdon, B.K., "Blended-Wing-Body Subsonic Commercial Transport," AIAA Paper 98-0438, January 1998.

Loftin, L.K., *Subsonic Aircraft: Evolution and the Matching of Size to Performance*, NASA RP 1060, Hampton, VA, 1980, pp. 152-153.

Malone, B. and Mason, W.H., "Multidisciplinary Optimization in Aircraft Design Using Analytic Technology Models," *Journal of Aircraft*, Vol. 32, No. 2, March-April 1995, pp. 431-438.

Martin, K.C., and Kopec, B.A., "A Structural and Aerodynamic Investigation of a Strut-Braced Wing Transport Aircraft Concept", LG98ER0431, November 1998.

Mason, W.H., *FRICTION Code Documentation*, available on the World Wide Web at: http://www.aoe.vt.edu/aoe/faculty/Mason_f/CatxtAppD5.pdf

Mason, W.H., "Analytic Models for Technology Integration in Aircraft Design," AIAA-90-3262, September, 1990.

Mattingly, J.D., Heiser, W.H., and Daley, D.H., *Aircraft Engine Design, AIAA*, Washington, D.C., 1987, pp. 36.

McCullers, L.A., *FLOPS User's Guide*, Release 5.81. Text file included with the FLOPS code, NASA Langley Research Center.

McMasters, J.H., and Kroo, I.M., "Advanced Configurations for Very Large Transport Airplanes", *Aircraft Design* Vol. 1, No. 4, 1999, pp. 217-242.

Miranda, L.R., and Brennan, J.E., "Aerodynamic Effects of Wingtip-Mounted Propellers and Turbines," AIAA-86-1802, 1986.

Naghshineh-Pour, A.H., Kapania, R., and Haftka, R., "Preliminary Structural Analysis of a Strut-Braced Wing", VPI-AOE-256, June 1998.

Park, P.H., "The Effect on Block Fuel Consumption of a Strutted vs. Cantilever Wing for a Short Haul Transport Including Strut Aerolastic Considerations," AIAA 78-1454, 1978.

Patterson, J.C., and Bartlett, G.R., "Evaluation of Installed Performance of a Wing-Tip-Mounted Pusher Turboprop on a Semispan Wing," NASA Technical Paper 2739, 1987.

Pfenninger, W., "Design Considerations of Large Subsonic Long Range Transport Airplanes with Low Drag Boundary Layer Suction," Northrop Aircraft, Inc., Report NAI-54-800 (BLC-67), November 1954.

Roskam, J., and Lan, C.-T. E. *Airplane Aerodynamics and Performance*, DARCorporation, Lawrence, KS, 1997, pp. 100-104, 435-508.

Smith, P.M., DeYoung, J., Lovell, W.A., Price, J.E., and Washburn, G.F., "A Study of High-Altitude Manned Research Aircraft Employing Strut-Braced Wings of High-Aspect Ratio," NASA CR-159262, February, 1981.

Spearman, M.L, “A High-Capacity Airplane Design Concept Having an Inboard-Wing Bounded by Twin Tip-Mounted Fuselages,” AIAA-97-2276, June 1997.

Tetrault,P.-A., Private Communications, July-October, 1998.

Torenbeek, E., *Synthesis of Subsonic Airplane Design, Delft University Press*, Delft, 1981, pp. 63, 459.

Turriziani, R.V., Lovell, W.A., Martin, G.L., Price, J.E., Swanson, E.E., and Washburn, G.F., “Preliminary Design Characteristics of a Subsonic Business Jet Consept Employing an Aspect Ratio 25 Strut-Braced Wing,” NASA CR-159361, October 1980.

Vanderplaats Research & Development, Inc., *DOT User’s Manual*, Version 4.20, Colorado Springs, CO, 1995.

Wolkovitch, J. “The Joined Wing – An Overview,” AIAA-85-0274, January, 1985.

Appendix 1. Tail Geometry

This appendix details the calculation procedure for finding the distance from the wing leading edge to the leading edge of the two tail surfaces given their tail moment arms used for stability and control analysis. The input variable *dx_htail* and *dx_vtail* no longer represent the distance from the leading edge of the wing to the leading edge of the respective tail surface. Now these variables represent the distance from the aircraft center of gravity to the aerodynamic center of the tail surface in question. Figure A1.1 shows the new convention. The center of gravity is assumed to be at the wing aerodynamic center. So *dx_htail* and *dx_vtail* are tail moment arms used for tail volume coefficient sizing. The tail areas are:

$$S_{HT} = \frac{TVC_{HT} \cdot S_w \cdot MAC_w}{dx\_htail} \quad \text{and} \quad S_{VT} = \frac{TVC_{VT} \cdot S_w \cdot b_w}{dx\_vtail}$$

where S is the planform area of a tail surface, *TVC* is tail volume coefficient, S_w is the wing planform area, MAC_w is the wing aerodynamic chord and b_w is the wing span. The input file has an integer variable tvc_flag to control whether or not to use the tail volume coefficient sizing method or to simply input a constant tail area. If the tail volume coefficient flag is set to 1 in the input file, then the tail volume coefficient method is employed. Otherwise, if it is set to 0, then input tail areas are used.

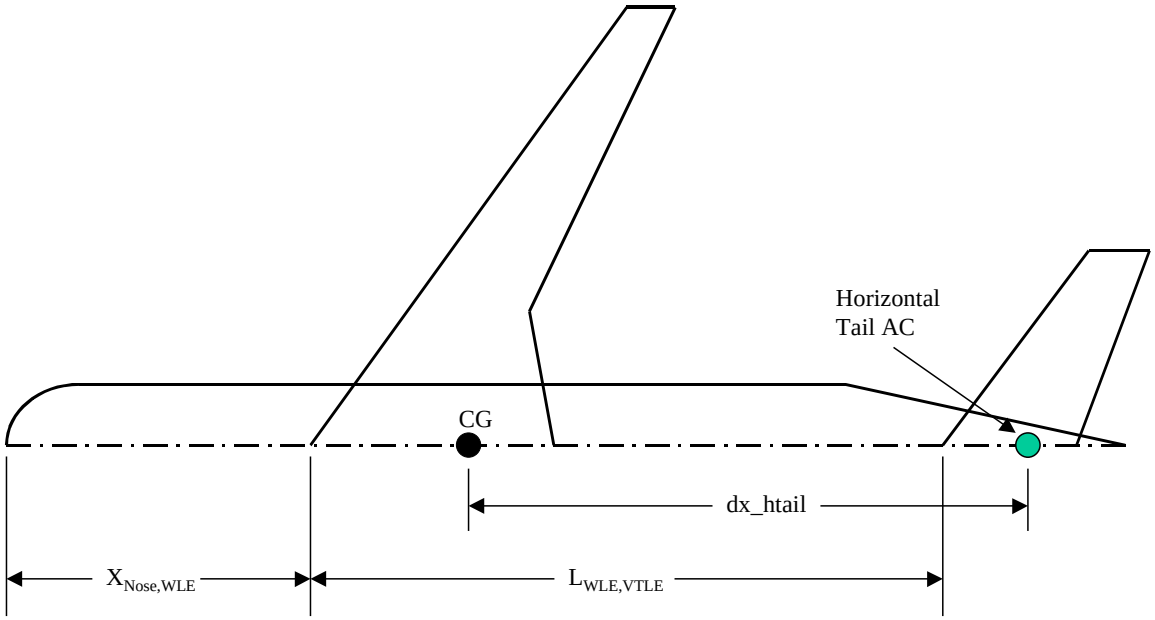

Figure A1.1. Length Definitions.

Previously, the span, root chord and tip chord of the horizontal and vertical tail surfaces, and the rudder span and average chord were input directly. This was the most convenient way to handle the tail geometry if the tail size remains constant. In studies by Grasmeyer (1998A-C), the tail size and geometry were held fixed at the value of the Boeing 777. Because the tail volume coefficient method allows the tail size to vary with the wing geometry, defining tail lengths is no longer convenient. To remedy this, the tail geometry was parameterized in terms of aspect ratio, taper ratio, sweep, and percentage chord and span of the rudder. The lengths are found from the dimensionless parameters and areas by:

$$C_{HTroot} = \frac{2 \cdot \sqrt{\frac{S_{HT}}{AR_{HT}}}}{(1-\lambda_{HT})} \qquad \text{and} \qquad C_{VTroot} = \frac{2 \cdot \sqrt{\frac{S_{VT}}{AR_{VT}}}}{(1-\lambda_{VT})}$$

$$AR_{HT} = \frac{b_{HT}^2}{S_{HT}} \quad \text{and} \quad AR_{VT} = \frac{b_{VT}^2}{S_{VT}}$$

where b_{HT} and b_{VT} are the spans of the respective tail surfaces including their projections into the fuselage.

$$C_{HTtip} = C_{HTroot} \cdot \lambda_{HT} \quad \text{and} \quad C_{VTtip} = C_{VTroot} \cdot \lambda_{VT}$$

$$b_{HT} = \frac{AR_{HT}}{2} \cdot C_{HTroot} \cdot (1 - \lambda_{HT}) \quad \text{and} \quad b_{VT} = \frac{AR_{VT}}{2} \cdot C_{VTroot} \cdot (1 - \lambda_{VT})$$

$$C_{rudder} = \%C_{rudder} \cdot \frac{(C_{VTroot} + C_{VTtip})}{2}$$

$$b_{rudder} = \%b_{rudder} \cdot b_{VT}$$

Once the lengths are calculated, they are used in the same way as before for the stability and control analysis and for drag calculations. Since the variables *dx_htail* and *dx_vtail* no longer represent the distance from the wing leading edge to the leading edge of the respective tail surfaces, this value must be found for the DXF file generator. Figure A1.2 shows the wing geometry and terms used to define the wing.

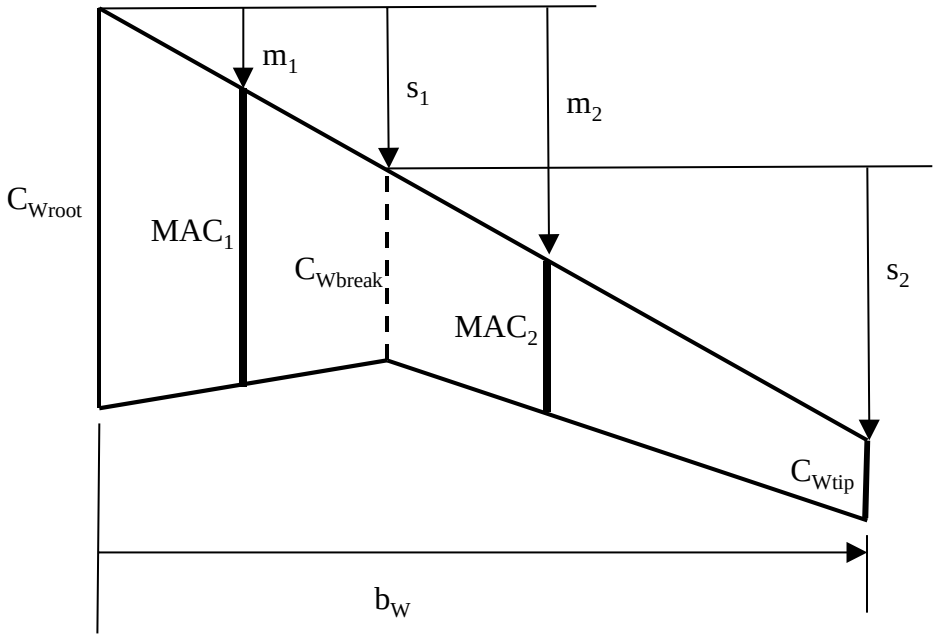

Figure A1.2. Wing Geometry for Tail Length Calculations.

The first step in this procedure is to find the mean aerodynamic chords (MAC) of the inboard and outboard wing panels.

$$MAC_1 = \frac{2}{3}\left(C_{Wroot} + C_{Wbreak} - \frac{C_{Wroot} \cdot C_{Wbreak}}{C_{Wroot} - C_{Wbreak}} \right) \quad \text{and} \quad MAC_2 = \frac{2}{3}\left(C_{Wbreak} + C_{Wtip} - \frac{C_{Wbreakt} \cdot C_{Wtip}}{C_{Wbreak} - C_{Wtip}} \right)$$

Then the leading edge sweep of the leading edge is found, assuming that the leading edge sweep for the inboard panel is the same as the outboard panel.

$$\Lambda_{W,LE} = TAN^{-1}\left(\frac{2}{b_W}\left(-\frac{1}{4}C_{Wtip} + \frac{1}{4}C_{Wbreak} + \frac{b_W}{2}TAN\left(\Lambda_{W,c/4}\right) \right) \right)$$

The streamwise-distance from the leading edge of the segment root to the leading edge of the segment tip is:

$$s_1 = \frac{b_W}{2} \cdot \eta_{break} \cdot TAN\left(\Lambda_{W,LE}\right) \quad \text{and} \quad s_2 = \frac{b_W}{2} \cdot \left(1 - \eta_{break}\right) \cdot TAN\left(\Lambda_{W,LE}\right)$$

Now, the streamwise-distance from the leading edge of the wing root chord to the leading edge of the mean aerodynamic chord of each segment can be found by:

$$m_1 = s_1 \cdot \frac{\left(C_{Wroot} + 2 \cdot C_{Wbreak}\right)}{3} \cdot \left(C_{Wroot} + C_{Wbreak}\right) \quad \text{and}$$

$$m_2 = s_1 + s_2 \cdot \frac{\left(C_{Wbreak} + 2 \cdot C_{Wtip}\right)}{3} \cdot \left(C_{Wbreak} + C_{Wtip}\right)$$

The areas of each segment are:

$$S_{W1} = \frac{b_W}{4} \cdot \eta_{break} \cdot \left(C_{Wroot} + C_{Wbreak}\right) \quad \text{and} \quad S_{W2} = \frac{b_W}{4} \cdot \left(1 - \eta_{break}\right) \cdot \left(C_{Wbreak} + C_{Wtip}\right)$$

Now the overall MAC and distance from the leading edge of the root chord to the leading edge of the MAC are calculated as the area weighted average of the components:

$$MAC_W = \frac{\left(MAC_1 \cdot SW_1 + MAC_2 \cdot SW_2\right)}{\left(SW_1 + SW_2\right)}$$

$$m_W = \frac{\left(m_1 \cdot SW_1 + m_2 \cdot SW_2\right)}{\left(SW_1 + SW_2\right)}$$

The same general procedure is duplicated for the tails. Calculations are simplified, because the each tail surface consists of only one component. The procedure for calculating the MAC and distance form the root leading edge to the mean aerodynamic chord of each tail surface is as follows:

$$MAC_{HT} = \frac{2}{3} \cdot \left(C_{HTroot} + C_{HTtip} + \frac{C_{HTroot} \cdot C_{HTtip}}{C_{HTroot} + C_{HTtip}} \right)$$

$$MAC_{VT} = \frac{2}{3} \cdot \left(C_{VTroot} + C_{VTtip} + \frac{C_{VTroot} \cdot C_{VTtip}}{C_{VTroot} + C_{VTtip}} \right)$$

$$\Lambda_{HT,LE} = TAN^{-1}\left(\frac{2}{b_{HT}} \cdot \left(-\frac{1}{4} C_{HTtip} + \frac{1}{4} C_{HTroot} + \frac{b_{HT}}{2} \cdot TAN\left(\Lambda_{HT,c/4}\right) \right) \right)$$

$$\Lambda_{VT,LE} = TAN^{-1}\left(\frac{1}{b_{VT}} \cdot \left(-\frac{1}{4} C_{VTtip} + \frac{1}{4} C_{VTroot} + b_{VT} \cdot TAN\left(\Lambda_{VT,c/4}\right) \right) \right)$$

$$m_{HT} = \frac{b_{HT}}{2} \cdot TAN\left(\Lambda_{HT,LE}\right) \cdot \frac{\left(C_{HTroot} + 2 \cdot C_{HTtip}\right)}{3 \cdot \left(C_{HTroot} + C_{HTtip}\right)}$$

$$m_{VT} = b_{VT} \cdot TAN\left(\Lambda_{VT,LE}\right) \cdot \frac{\left(C_{VTroot} + 2 \cdot C_{VTtip}\right)}{3 \cdot \left(C_{VTroot} + C_{VTtip}\right)}$$

Finally, the distance from the leading edge of the wing to the leading edge of the each tail surface now becomes:

$$L_{WLE,HTLE} = dx\_htail + m_W + \frac{1}{4}MAC_W - m_{HT} - \frac{1}{4}MAC_{HT}$$

$$L_{WLE,VTLE} = dx\_vtail + m_W + \frac{1}{4}MAC_W - m_{VT} - \frac{1}{4}MAC_{VT}$$

For a conventional tail, the horizontal root trailing edge is farther aft than the vertical tail root trailing edge, and there is a nominal separation of 3 feet from the aft end of the fuselage. The corresponding distance between the nose of the aircraft and the leading edge of the wing root for a conventional tail is:

$$X_{Nose,WLE} = L_{Fuselage} - 3 - C_{HTroot} - L_{WLE,HTLE}$$

For a T-tail aircraft, a similar argument applies except the vertical tail root trailing edge is a nominal distance of 3 feet from the aft end of the fuselage. The distance from the nose of the aircraft to the wing root leading edge now becomes:

$$X_{Nose,WLE} = L_{Fuselage} - 3 - C_{VTroot} - L_{WLE,VTLE}$$

The values $X_{Nose,WLE}$, $L_{WLE,HTLE}$, and $L_{WLE,VTLE}$ are passed to DXF.F and calculations proceed as before. One new modification is that T-tail flag is now passed to DXF.F and the leading edge of the root chord of the horizontal tail is automatically attached to the tip chord leading edge of the vertical tail, regardless of the *dx_htail* value.

Appendix 2. Range Analysis

These tables summarize the results of minimum-TOGW optima designed to fly at the specified ranges. Each of the four configurations have separate tables.

Table A2.1. Cantilever Wing Range Effects.

Cant 4000	Cant 5000	Cant 6000	Cant 7000	Cant 8000	Cant 9000	Cant 10000	Cant 11000	Cant Max	
4000	5000	6000	7000	8000	9000	10000	11000	**11906**	Range (nmi)
196.4	202.4	211.2	220.2	231.0	239.8	248.9	249.4	250.2	Span (ft)
52.0	52.0	52.0	52.0	52.0	52.0	52.0	52.0	52.0	Root Chord (ft)
4343	4498	4757	5121	5534	5746	6223	6160	6480	Sw (ft^2)
8.88	9.10	9.37	9.47	9.64	10.01	9.96	10.09	9.66	AR
15.61%	15.17%	15.12%	15.04%	15.14%	14.99%	15.01%	14.87%	14.69%	Root t/c
10.75%	10.58%	10.63%	10.48%	10.62%	10.61%	10.62%	10.62%	9.83%	Outboard t/c
5.49%	5.28%	5.00%	5.02%	5.21%	5.36%	5.01%	5.25%	6.20%	Outboard t/c
34.1	34.0	34.1	33.8	34.1	34.2	33.9	34.2	33.4	Wing L1/4 (deg)
60655	64883	68917	73499	78184	83986	91426	103085	118178	Tmax (lbs)
42573	41919	41814	42094	42127	41058	41188	38992	36987	Cruise Altitude (ft)
21.69	22.13	22.68	23.17	23.68	24.03	24.29	23.97	23.30	L/D
41461	46610	53031	59970	68424	78424	88661	98142	108286	Wing Wt. (lbs)
27223	31882	37653	43901	51539	61269	70703	80205	90005	Bending Matl (lbs)
97179	120225	144765	171752	201312	235901	276144	330385	399848	Fuel Wt. (lbs)
405310	**439630**	**477044**	**518210**	**563994**	**617150**	**678548**	**755682**	852366	TOGW (lbs)
78.07	80.43	83.09	85.98	89.22	92.70	96.74	100.82	105.57	Acquisition Cost ($M)
543.38	550.63	561.32	575.50	592.71	614.34	641.19	677.05	857.95	DOC ($M)
941.93	920.42	906.02	895.97	888.84	883.97	880.82	879.57	930.78	IOC ($M)
ACTIVE	ACTIVE	ACTIVE	ACTIVE	ACTIVE	ACTIVE	ACTIVE	ACTIVE	ACTIVE	Shock Cl Constraint
ACTIVE	ACTIVE	ACTIVE	ACTIVE	ACTIVE	ACTIVE	ACTIVE	ACTIVE	ACTIVE	2nd Segment Climb
								ACTIVE	Balanced Field Length
	ACTIVE	ACTIVE	ACTIVE	ACTIVE	ACTIVE	ACTIVE	ACTIVE	ACTIVE	Engine Out
								ACTIVE	Approach Velocity
									Fuel Volume

Table A2.2. T-Tail SBW Range Effects.

SBW-fuse 4000	SBW-fuse 5000	SBW-fuse 6000	SBW-fuse 7000	SBW-fuse 8000	SBW-fuse 9000	SBW-fuse 10000	SBW-fuse 11000	SBW-fuse 12000	SBW-fuse 13000	SBW-fuse Max	
4000	5000	6000	7000	8000	9000	10000	11000	12000	13000	**13304**	Range (nmi)
198.8	208.5	215.0	220.9	228.1	234.3	233.6	244.9	261.2	257.9	262.5	Span (ft)
27.3	28.3	28.2	30.1	30.4	32.0	34.6	36.9	38.7	42.0	43.3	Root Chord (ft)
3334	3648	3763	4137	4344	4683	4983	5495	6126	6509	6807	S_w (ft^2)
11.86	11.92	12.29	11.80	11.97	11.73	10.95	10.91	11.14	10.22	10.12	AR
13.94%	13.78%	13.71%	13.78%	13.80%	13.88%	13.60%	13.10%	13.20%	13.23%	13.21%	Root t/c
7.54%	7.13%	7.12%	6.95%	7.15%	7.17%	6.75%	7.09%	7.14%	6.83%	6.68%	Outboard t/c
6.86%	6.53%	6.79%	6.36%	6.72%	6.65%	5.69%	6.58%	6.92%	6.25%	6.08%	Outboard t/c
27.5	28.7	29.1	29.9	30.2	31.1	31.0	30.1	31.0	31.1	30.6	Wing $\Lambda_{1/4}$ (deg)
20.7	20.6	21.0	20.8	21.1	21.2	21.6	22.6	22.9	22.1	21.8	Strut $\Lambda_{1/4}$ (deg)
66.1%	67.2%	67.4%	68.7%	68.4%	68.5%	68.6%	63.2%	67.2%	66.0%	66.7%	η Strut
48134	50840	53778	58187	61843	66897	75658	82100	88492	103686	108450	T_{max} (lbs)
40025	40697	40263	40951	40859	40943	40415	40540	40881	41571	41656	Cruise Altitude (ft)
23.50	24.47	25.01	25.23	25.64	25.80	25.30	25.61	26.07	25.34	25.22	L/D
41236	47042	52298	56970	62689	68530	73411	83976	97297	103034	108225	Wing Wt. (lbs)
6493	7343	8019	9023	9912	11107	12413	12612	15855	15227	15688	Strut Wt. (lbs)
2231	2540	2835	3247	3478	3801	4646	5614	6333	7025	7109	Offset Wt. (lbs)
27104	31950	36805	40184	45501	50321	53544	63953	75851	79733	84097	Bending Matl (lbs)
86202	104107	124129	147456	171325	199396	237726	274929	315517	377323	399999	Fuel Wt. (lbs)
380952	**409516**	**439224**	**473298**	**508164**	**548776**	**601136**	**657972**	**721974**	**804260**	837288	TOGW (lbs)
11.3%	13.4%	14.3%	14.1%	14.9%	15.5%	13.9%	16.8%				% Fuel Reduction
6.0%	6.8%	7.9%	8.7%	9.9%	11.1%	11.4%	12.9%				% TOGW Reduction
75.14	77.46	79.43	81.73	83.92	86.44	89.20	92.99	97.39	101.24	103.01	Acquisition Cost ($M)
512.07	515.17	521.51	533.11	544.32	560.02	584.19	608.56	636.00	674.93	759.17	DOC ($M)
936.54	914.97	900.24	890.03	882.32	876.83	873.52	871.14	869.73	869.87	895.99	IOC ($M)
ACTIVE	ACTIVE	ACTIVE	ACTIVE	ACTIVE	ACTIVE	ACTIVE	ACTIVE	ACTIVE	ACTIVE	ACTIVE	Shock CI Constraint
ACTIVE	ACTIVE	ACTIVE	ACTIVE	ACTIVE	ACTIVE	ACTIVE	ACTIVE				2nd Segment Climb
				ACTIVE	ACTIVE	ACTIVE	ACTIVE	ACTIVE	ACTIVE	ACTIVE	Balanced Field Length
											Engine Out
											Approach Velocity
											Fuel Volume

Table A2.3. Tip Engine SBW Range Effects.

SBW-tip 4000	SBW-tip 5000	SBW-tip 6000	SBW-tip 7000	SBW-tip 8000	SBW-tip 9000	SBW-tip 10000	SBW-tip 11000	SBW-tip 12000	SBWtip maxr	
4000	5000	6000	7000	8000	9000	10000	11000	12000	**12114**	Range (nmi)
178.6	191.1	191.9	195.8	198.5	198.5	198.4	209.0	222.0	215.2	Span (ft)
30.2	30.9	30.8	31.6	33.6	35.7	36.1	40.4	47.9	51.2	Root Chord (ft)
3305	3640	3643	3812	4049	4176	4349	4966	6043	6413	S_w (ft^2)
9.65	10.03	10.11	10.06	9.73	9.44	9.05	8.79	8.16	7.22	AR
14.39%	14.37%	14.33%	14.34%	14.31%	14.14%	14.24%	13.97%	13.70%	13.62%	Root t/c
7.34%	7.55%	7.46%	7.51%	7.49%	7.29%	7.37%	7.04%	6.80%	6.80%	Outboard t/c
6.85%	6.87%	6.85%	6.83%	6.85%	6.76%	6.82%	6.90%	6.67%	6.40%	Outboard t/c
28.9	30.0	30.0	30.1	30.6	31.4	31.4	32.0	32.3	32.6	Wing $\Lambda_{1/4}$ (deg)
23.6	23.5	23.6	23.5	23.6	24.1	23.8	25.5	25.9	25.2	Strut $\Lambda_{1/4}$ (deg)
56.2%	56.6%	56.6%	56.6%	56.8%	55.5%	56.3%	56.5%	57.0%	57.9%	η Strut
45000	46292	47626	49813	53814	60390	66005	67753	69668	73316	T_{max} (lbs)
40708	40708	40708	40708	40357	39557	40557	40257	40257	39057	Cruise Altitude (ft)
23.84	24.55	24.91	25.10	24.99	24.88	24.94	24.98	24.26	22.75	L/D
30879	35660	37578	40260	42667	45642	47014	52999	60860	59913	Wing Wt. (lbs)
4125	4918	4873	5021	5235	4807	5260	6112	6873	6630	Strut Wt. (lbs)
3113	3837	3834	3976	4181	4186	4406	5078	5566	5969	Offset Wt. (lbs)
16695	20301	21961	24014	25580	28026	28499	32902	37963	35638	Bending Matl (lbs)
80057	97131	114874	134991	158957	186235	213127	245034	294200	326248	Fuel Wt. (lbs)
357540	**383050**	**405305**	**431677**	**462911**	**499382**	**533471**	**576456**	**641327**	677111	TOGW (lbs)
17.6%	19.2%	20.6%	21.4%	21.0%	21.1%	22.8%	25.8%			% Fuel Reduction
11.8%	12.9%	15.0%	16.7%	17.9%	19.1%	21.4%	23.7%			% TOGW Reduction
71.48	73.45	74.44	75.84	77.46	79.34	80.87	83.35	86.98	87.93	Acquisition Cost ($M)
490.32	492.56	494.14	500.44	511.38	525.80	537.57	554.51	585.55	627.26	DOC ($M)
931.36	910.19	895.06	884.52	877.03	871.67	867.11	864.11	863.36	872.78	IOC ($M)
ACTIVE		ACTIVE	ACTIVE	ACTIVE	ACTIVE		ACTIVE	ACTIVE	ACTIVE	Shock CI Constraint
										2nd Segment Climb
			ACTIVE	ACTIVE	ACTIVE	ACTIVE	ACTIVE	ACTIVE	ACTIVE	Balanced Field Length
	ACTIVE	ACTIVE	ACTIVE	ACTIVE	ACTIVE	ACTIVE	ACTIVE			Wingtip Deflection
						ACTIVE	ACTIVE	ACTIVE	ACTIVE	Engine Out
										Approach Velocity
ACTIVE	ACTIVE	ACTIVE							ACTIVE	Initial Cruise ROC

Table A2.4. Underwing Engine SBW Range Effects.

SBW-wing 4000	SBW-wing 5000	SBW-wing 6000	SBW-wing 7000	SBW-wing 8000	SBW-wing 9000	SBW-wing 10000	SBW-wing 11000	SBW-wing 12000	SBW-wing 13000	SBW-wing maxr	
4000	5000	6000	7000	8000	9000	10000	11000	12000	13000	**13979**	Range (nmi)
204.5	207.8	224.5	229.9	236.8	242.3	249.6	249.9	259.9	262.3	262.5	Span (ft)
28.1	30.2	29.5	29.4	29.8	31.4	32.8	34.8	36.8	39.7	42.5	Root Chord (ft)
3447	3778	4022	4117	4312	4651	4989	5304	5795	6258	6712	S_w (ft^2)
12.13	11.43	12.53	12.83	13.01	12.63	12.49	11.78	11.65	11.00	10.27	AR
13.07%	13.31%	12.95%	12.88%	12.76%	12.79%	12.79%	12.84%	12.81%	12.84%	12.89%	Root t/c
6.59%	7.55%	6.73%	6.47%	6.38%	6.47%	6.89%	6.86%	6.86%	6.89%	7.46%	Outboard t/c
8.49%	9.05%	8.39%	8.25%	8.18%	8.12%	8.41%	8.25%	8.32%	8.21%	8.43%	Outboard t/c
27.0	28.4	27.4	27.0	27.5	27.6	28.8	29.3	29.8	30.3	31.4	Wing $\Lambda_{1/4}$ (deg)
24.9	25.9	25.3	25.1	25.3	25.6	26.3	26.0	26.2	26.2	26.6	Strut $\Lambda_{1/4}$ (deg)
62.9%	59.2%	63.8%	64.4%	63.2%	62.8%	61.6%	63.9%	64.3%	65.5%	63.3%	η Strut
86.6%	87.5%	82.9%	82.5%	80.7%	79.5%	79.5%	72.4%	72.5%	67.5%	60.7%	η Engine
45208	49335	51172	52913	56209	60796	65416	73022	79275	90162	103557	T_{max} (lbs)
40728	41282	41987	41622	41444	41715	41672	41425	41510	41042	40519	Cruise Altitude (ft)
24.50	24.26	25.74	26.09	26.66	26.70	26.92	26.50	26.66	26.11	25.47	L/D
38381	40276	48720	53247	59849	64850	71711	76620	85929	93477	100744	Wing Wt. (lbs)
5419	6091	7844	7811	8908	10141	9786	12120	13159	14486	14607	Strut Wt. (lbs)
2263	2620	2810	2648	3161	3866	3890	4929	5597	6500	6666	Offset Wt. (lbs)
23714	24525	32417	36669	42753	46945	53006	56997	65162	71401	77267	Bending Matl (lbs)
80520	100938	116978	137046	158367	184422	212310	249139	286181	338617	399824	Fuel Wt. (lbs)
366842	**394693**	**422759**	**450678**	**483205**	**520031**	**560812**	**610516**	**664945**	**736297**	816265	TOGW (lbs)
17.1%	16.0%	19.2%	20.2%	21.3%	21.8%	23.1%	24.6%				% Fuel Reduction
9.5%	10.2%	11.4%	13.0%	14.3%	15.7%	17.4%	19.2%				% TOGW Reduction
73.25	75.06	77.49	79.08	81.30	83.52	86.06	88.61	91.98	95.61	98.84	Acquisition Cost ($M)
496.57	503.48	506.98	513.44	523.50	537.60	553.40	575.30	598.23	631.16	833.68	DOC ($M)
933.40	912.29	897.72	887.03	879.40	873.83	869.70	867.05	865.21	864.88	926.32	IOC ($M)
ACTIVE	ACTIVE	ACTIVE	ACTIVE	ACTIVE	ACTIVE	ACTIVE	ACTIVE	ACTIVE	ACTIVE	ACTIVE	Shock CI Constraint
	ACTIVE		ACTIVE	ACTIVE	ACTIVE	ACTIVE	ACTIVE	ACTIVE	ACTIVE	ACTIVE	2nd Segment Climb
				ACTIVE		ACTIVE	ACTIVE	ACTIVE	ACTIVE	ACTIVE	Balanced Field Length
	ACTIVE		ACTIVE	ACTIVE	ACTIVE						Wingtip Deflection
									ACTIVE	ACTIVE	Engine Out
											Approach Velocity
ACTIVE	ACTIVE	ACTIVE									Initial Cruise ROC
										ACTIVE	Fuel Volume

Appendix 3. Technology Impact Study Results

These tables summarize the results of the technology impact study of minimum-TOGW optima with various technologies. Results for each of the four configurations are presented in separate tables.

Table A3.1 Cantilever Wing Sensitivity Analysis.

1995 Conv Wing Eng.	1995 Conv NLF	1995 Conv Aero	1995 Conv Airframe	1995 Conv Propulsion	1995 Conv Systems	2010 Conv Wing-Eng.	Tot Change **-171614** Sum Change **-27.5%**
7500.1	7496.5	7500.1	7500.1	7500.0	7500.1	7499.8	Range
214.9	211.5	217.9	215.2	210.4	213.9	225.3	Span (ft)
52.0	52.0	52.0	52.0	52.0	52.0	52.0	Root Chord (ft)
8.8	8.3	8.6	8.2	8.5	8.6	8.5	Root Chord (ft)
5413	5213	5198	4959	5254	5415	5307	S_w (ft^2)
8.53	8.58	9.13	9.34	8.43	8.45	9.57	AR
15.61%	15.27%	16.36%	15.26%	15.39%	15.65%	15.14%	Root t/c
10.65%	10.32%	11.73%	10.83%	10.28%	10.61%	10.55%	Break t/c
6.20%	5.78%	6.66%	5.52%	5.75%	5.25%	7.40%	Tip t/c
39.8	39.0	36.7	40.4	39.3	39.8	34.2	Wing $\Lambda_{1/4}$ (deg)
37.0%	37.0%	37.0%	37.0%	37.0%	37.0%	37.0%	η Engine
108861	104599	98437	94274	106772	105789	75793	T_{max} (lbs)
35640	35598	37253	36112	35519	35943	42052	Cruise Altitude (ft)
19.94	20.68	20.83	20.39	19.79	20.15	23.38	L/D
98791	93734	87267	75388	94109	96260	63706	Wing Wt. (lbs)
280900	262535	253180	246252	268265	271935	186295	Fuel Wt. (lbs)
430948	420028	408324	387600	422738	422209	353928	Zero Fuel Wt. (lbs)
711844	**682770**	**661501**	**633848**	**691004**	**694142**	**540230**	TOGW (lbs)
1745.56	1714.78	1693.33	1666.17	1723.94	1722.98	1563.24	Total Cost ($M)
102.51	100.54	98.56	94.81	101.02	99.55	87.49	Acquisition Cost ($M)
729.68	704.50	687.65	667.66	712.13	712.26	583.68	DOC ($M)
913.37	909.74	907.12	903.69	910.78	911.17	892.07	IOC ($M)
	-4.1%	-7.1%	-11.0%	-2.9%	-2.5%	-24.1%	% TOGW Reduction
	-1.8%	-3.0%	-4.5%	-1.2%	-1.3%	-10.4%	% Fuel Reduction
ACTIVE	ACTIVE	ACTIVE	ACTIVE	ACTIVE	ACTIVE	ACTIVE	Shock Cl Constraint
ACTIVE	ACTIVE	ACTIVE	ACTIVE	ACTIVE	ACTIVE	ACTIVE	2nd Segment Climb
							Balanced Field Length
							Wingtip Deflection
ACTIVE	ACTIVE	ACTIVE	ACTIVE	ACTIVE	ACTIVE	ACTIVE	Engine Out
ACTIVE	ACTIVE			ACTIVE			Approach Velocity
							Initial Cruise ROC
							Fuel Volume

Table A3.2. T-Tail Fuselage-Mounted Engine Sensitivity Analysis.

T-Tail SBW 1995	T-Tail SBW NLF	T-Tail SBW AERO	T-Tail SBW Airframe	T-Tail SBW Propulsion	T-Tail SBW Systems	T-Tail SBW 2010	Tot Change -155150 Sum Change -28.80%
7500.0	7499.5	7499.2	7499.5	7498.9	7497.8	7499.9	Range
214.4	210.9	208.4	212.7	211.8	212.2	226.0	Span (ft)
37.7	36.3	35.9	35.1	37.1	37.5	30.2	Root Chord (ft)
8.1	7.3	8.1	7.6	7.9	7.8	7.0	Tip Chord (ft)
4910	4598	4581	4541	4770	4805	4205	Sw (ft^2)
9.37	9.68	9.48	9.96	9.41	9.37	12.15	AR
13.68%	13.36%	14.19%	13.65%	13.74%	13.64%	14.28%	Root t/c
7.07%	6.61%	7.13%	6.72%	6.82%	6.85%	6.58%	Break t/c
7.48%	6.93%	7.55%	7.43%	7.39%	7.33%	6.56%	Tip t/c
36.9	35.6	32.9	37.1	36.4	36.6	29.9	Wing $\Lambda_{1/4}$ (deg)
23.7	24.5	21.6	26.4	24.6	24.4	20.5	Strut $\Lambda_{1/4}$ (deg)
65.5%	67.6%	67.5%	66.1%	64.5%	68.8%	68.8%	η Strut
89515	81836	83553	78461	86991	87404	59463	Tmax (lbs)
36700	36576	37851	37046	36628	36648	40429	Cruise Altitude (ft)
20.10	21.89	20.88	20.48	20.07	20.10	25.30	L/D
88200	81346	75472	67152	85143	84196	59581	Wing Wt. (lbs)
50794	46012	41735	48129	48876	47679	42500	Bending Matl (lbs)
253141	220879	230181	225527	241120	247624	159629	Fuel Wt. (lbs)
392000	377036	372286	356850	386141	383556	330683	Zero Fuel Wt. (lbs)
645000	**597922**	**602480**	**582378**	**627268**	**631176**	**490312**	TOGW (lbs)
1675.30	1624.60	1631.86	1611.11	1656.17	1656.34	1507.31	Total Cost ($M)
95.30	92.40	91.70	88.90	94.10	92.30	82.70	Acquisition Cost ($M)
675.00	633.00	640.00	625.00	659.00	661.00	538.00	DOC ($M)
905.00	899.00	900.00	897.00	903.00	903.00	886.00	IOC ($M)
	7.3%	6.6%	9.7%	2.7%	2.1%	24.0%	% TOGW Reduction
	12.7%	9.1%	10.9%	4.7%	2.2%	36.9%	% Fuel Reduction
ACTIVE	ACTIVE	ACTIVE	ACTIVE	ACTIVE	ACTIVE	ACTIVE	Shock Cl Constraint
ACTIVE	ACTIVE	ACTIVE	ACTIVE	ACTIVE	ACTIVE	ACTIVE	2nd Segment Climb
ACTIVE	ACTIVE	ACTIVE	ACTIVE	ACTIVE	ACTIVE	ACTIVE	Balanced Field Length
							Wingtip Deflection
							Engine Out
ACTIVE		ACTIVE		ACTIVE	ACTIVE		Approach Velocity
							Initial Cruise ROC
							Fuel Volume

Table A3.3. Wingtip-Mounted Engine SBW Sensitivity Analysis.

Tip SBW 1995	Tip SBW NLF	Tip SBW AERO	Tip SBW Airframe	Tip SBW Propulsion	Tip SBW Systems	Tip SBW 2010	Tot Change -100107 Sum Change **19.7%**
7499.7	7496.1	7499.9	7495.5	7499.6	7499.9	7499.7	Range
182.2	181.9	182.6	176.5	183.0	181.1	198.6	Span (ft)
38.8	38.1	38.4	37.1	40.8	38.7	31.8	Root Chord (ft)
7.6	7.0	7.2	7.4	6.8	7.3	7.5	Tip Chord (ft)
4221	4099	4165	3931	4360	4171	3907	S_w (ft^2)
7.86	8.07	8.01	7.93	7.68	7.87	10.10	AR
14.17%	14.09%	14.37%	14.16%	14.14%	14.23%	14.36%	Root t/c
7.71%	7.17%	7.78%	7.81%	7.03%	7.77%	7.56%	Break t/c
7.49%	6.99%	7.39%	7.55%	6.97%	7.58%	6.85%	Tip t/c
39.2	38.2	36.7	39.9	39.5	39.7	30.2	Wing $\Lambda_{1/4}$ (deg)
26.5	26.9	25.2	26.3	27.6	26.9	23.5	Strut $\Lambda_{1/4}$ (deg)
58.7%	58.6%	58.5%	58.0%	63.9%	57.3%	56.8%	η Strut
100.0%	100.0%	100.0%	100.0%	100.0%	100.0%	100.0%	η Engine
71302	65587	66961	67511	65621	70164	51851	T_{max} (lbs)
38540	38376	38650	38513	38567	38301	40736	Cruise Altitude (ft)
20.68	22.38	21.53	20.57	20.65	20.81	25.25	L/D
55668	53356	52426	42179	54596	55190	41854	Wing Wt. (lbs)
25462	24475	23606	23555	24543	25279	25213	Bending Matl (lbs)
210173	187580	196448	197894	200271	206309	145618	Fuel Wt. (lbs)
336228	328318	329010	314928	331191	332432	300676	Zero-Fuel Wt. (lbs)
546401	**515984**	**525459**	**512826**	**531463**	**538821**	**446294**	TOGW (lbs)
1574.13	1540.89	1551.70	1540.12	1558.07	1562.00	1462.46	Total Cost ($M)
84.84	83.30	83.49	80.74	84.02	82.80	76.70	Acquisition Cost ($M)
596.45	568.37	577.87	570.59	582.99	587.28	504.86	DOC ($M)
892.84	889.05	890.24	888.67	890.98	891.89	880.41	IOC ($M)
	5.6%	3.8%	6.1%	2.7%	1.4%	18.3%	% TOGW Reduction
	10.7%	6.5%	5.8%	4.7%	1.8%	30.7%	% Fuel Reduction
ACTIVE	ACTIVE	ACTIVE	ACTIVE	ACTIVE	ACTIVE	ACTIVE	Shock CI Constraint
							2nd Segment Climb
ACTIVE	ACTIVE	ACTIVE	ACTIVE	ACTIVE	ACTIVE	ACTIVE	Balanced Field Length
ACTIVE	ACTIVE		ACTIVE	ACTIVE		ACTIVE	Wingtip Deflection
ACTIVE	ACTIVE	ACTIVE	ACTIVE	ACTIVE	ACTIVE		Engine Out
			ACTIVE				Approach Velocity
							Initial Cruise ROC
							Fuel Volume

Table A3.4. Underwing Engine SBW Sensitivity Analysis.

Wing SBW 1995	Wing SBW NLF	Wing SBW AERO	Wing SBW Airframe	Wing SBW Propulsion	Wing SBW Systems	Wing SBW 2010	Tot Change -135978 Sum Change **27.6%**
7498.2	7498.0	7499.9	7498.9	7498.5	7497.3	7499.3	Range
227.1	217.1	212.7	217.9	223.0	226.8	220.1	Span (ft)
36.0	34.7	33.8	33.8	35.7	35.9	29.4	Root Chord (ft)
7.9	7.7	7.6	7.5	7.9	7.9	6.6	Tip Chord (ft)
4981	4601	4412	4501	4860	4969	3970	S_w (ft^2)
10.36	10.25	10.26	10.54	10.23	10.35	12.20	AR
13.81%	13.89%	14.22%	13.60%	13.81%	13.82%	14.00%	Root t/c
7.26%	7.50%	7.00%	6.62%	7.21%	7.29%	7.15%	Break t/c
7.64%	8.08%	7.32%	7.21%	7.65%	7.66%	7.37%	Tip t/c
36.2	35.4	31.1	36.1	36.1	36.3	29.8	Wing $\Lambda_{1/4}$ (deg)
24.9	27.0	24.3	25.3	25.3	24.9	21.6	Strut $\Lambda_{1/4}$ (deg)
63.7%	62.5%	64.1%	62.7%	63.2%	63.7%	62.4%	η Strut
79.5%	82.6%	83.9%	80.7%	80.7%	79.5%	83.8%	η Engine
77745	72939	73927	70892	76285	76530	56562	T_{max} (lbs)
38536	38481	38891	38446	38561	38682	40097	Cruise Altitude (ft)
21.03	22.57	21.48	21.00	20.90	21.17	25.30	L/D
82685	71738	65728	60285	78471	82048	50287	Wing Wt. (lbs)
45999	38202	34038	40883	42893	45638	33335	Bending Matl (lbs)
228225	200881	208875	207958	218235	224112	151342	Fuel Wt. (lbs)
372222	354888	348929	338608	365947	368511	313214	Zero-Fuel Wt. (lbs)
600534	**555770**	**557802**	**546574**	**584174**	**592442**	**464556**	TOGW (lbs)
1627.49	1580.68	1584.22	1573.58	1610.57	1614.87	1480.44	Total Cost ($M)
91.40	88.16	87.07	85.28	90.24	89.30	79.01	Acquisition Cost ($M)
636.54	598.53	602.89	595.45	622.80	626.99	518.75	DOC ($M)
899.55	894.00	894.25	892.86	897.53	898.57	882.68	IOC ($M)
	7.5%	7.1%	9.0%	2.7%	1.3%	22.6%	% TOGW Reduction
	12.0%	8.5%	8.9%	4.4%	1.8%	33.7%	% Fuel Reduction
ACTIVE	ACTIVE	ACTIVE	ACTIVE	ACTIVE	ACTIVE	ACTIVE	Shock CI Constraint
ACTIVE	ACTIVE	ACTIVE	ACTIVE	ACTIVE	ACTIVE	ACTIVE	2nd Segment Climb
		ACTIVE				ACTIVE	Balanced Field Length
ACTIVE	ACTIVE	ACTIVE		ACTIVE		ACTIVE	Wingtip Deflection
							Engine Out
							Approach Velocity
							Initial Cruise ROC
							Fuel Volume